DEVELOPING NEW METHODOLOGIES FOR ANTI-FOULING POLYMERIC NETWORK SYNTHESES, ORTHOGONAL MODIFICATIONS, AND APPLICATIONS IN MARINE ENVIRONMENT

A Dissertation

by

KELLIE SEETHO

Submitted to the Office of Graduate and Professional Studies of
Texas A&M University
in partial fulfillment of the requirements for the degree of

DOCTOR OF PHILOSOPHY

Chair of Committee,	Karen L. Wooley
Committee Members,	James D. Batteas
	David E. Bergbreiter
	Melissa A. Grunlan
Head of Department,	Francois P. Gabbai

May 2016

Major Subject: Chemistry

ABSTRACT

Biofouling on ship hulls and other surfaces calls for immediate attention as fouling organisms increase both friction and weight of vessels, resulting in wasted fuel consumption, travel time, and cleaning resources. There are currently many efforts to develop polymeric networks as anti-fouling coatings to replace traditional anti-fouling paints, which contain toxic compounds. This dissertation focuses on the development of new methodologies for anti-fouling polymeric network syntheses, orthogonal modifications, characterization and anti-fouling properties for marine anti-fouling applications.

A terpolymer network based on hyperbranched fluoropolymers crosslinked with poly(ethylene glycol) and polydimethylsiloxane that displayed improved fouling releasing properties was generated. Methodologies and experiments were designed and performed to investigate the stability and crosslinking efficiency of the network when the crosslinking polymers were increased. The concept of using a three-component system was retained while changing each component. A ternary network of silsesquioxanes, an amphiphilic fluorinated compound and sulfobetaines was generated by thiol-ene click chemistry and to form coatings. The anti-fouling performances of the coatings were then tested against various marine fouling organisms.

A facile, two-step modification to generate an amphiphilic zwitterionic copolymer from a commodity copolymer was also explored. A copolymer containing hydrophobic units and reactive units was synthesized and subsequently modified to produce an

amphiphilic, zwitterionic polymer. The amphiphilic zwitterionic polymer was covalently attached onto silanized glass with different crosslinking extents to form amphiphilic crosslinked networks. The surface properties of the resultant polymer coating can be easily tuned by varying the extent of cross-linking in the network. Anti-fouling studies of bovine serum albumin and *Ulva* zoospores suggest that this system displayed potential as an anti-fouling material.

Lastly, the thermal and mechanical properties of zwitterionic *vs*. blended ionic polymers were investigated. Different charged polymers were prepared by functionalizing poly[(allyl glycidyl ether)-*b*-(ethylene oxide)-*b*-(allyl glycidyl ether)] (P(AGE-*b*-EO-*b*-AGE)) with different charged thiols through highly efficient photo-initiated thiol-ene chemistry. Equimolar amounts of polymers with positive charged side chains and negative charged side chains were then mixed together and compared to polymers with zwitterionic side chains that possess similar charge densities. The bulk polymers were characterized by thermogravimetric analysis, differential scanning calorimetry, and dynamic mechanical thermal analysis to study the effect of the nature of ionic interactions of the charged polymers.

DEDICATION

To my mother, Florence Wijaya

ACKNOWLEDGEMENTS

I would first like to thank my Ph.D. advisor, Professor Karen L. Wooley, for her guidance, support, and advice throughout my Ph.D. study at Texas A&M University. She has believed in my abilities and given me the freedom to use my abilities to explore the fields of polymer science for use in anti-fouling applications. In the past five years, she has instilled confidence in me and taught me to think critically which has helped mold me into the independent researcher, presenter and collaborator that I am today. She has also supported me on many development opportunities such as internship programs, conference presentations, and instrumentation trainings. Her work ethics, determination and perseverance have influenced me to want to be successful like her. Without her, I would not been able to accomplish what I have accomplished today. I can truly say that I have much more confidence in myself today than when I first started graduate school.

I would also like to thank my committee members, Professor James D. Batteas, Professor David. E. Bergbreiter, and Professor Melissa A. Grunlan for their time, support, guidance and advice throughout the course of this research.

This work would not have been completed without the help of my external collaborators. Therefore, I would like to thank all my collaborators who have brought in their expertise and contributed to the work. The collaborators who have contributed to this work include Professor John Finlay, Dr. Nick Aldred, Dr. Sofia Franco and Professor Tony Clare at Newcastle University, Professor Craig Hawker and Dr. Nathaniel Lynd at

University of California, Santa Barbara, and Dr. Edgar Martinez at Beckman Coulter Particle Characterization Laboratory.

I would also like to thank Willliam Seward and Ronald Page at Texas A&M University for fabricating the custom Delrin® and aluminum molds. I greatly appreciate the Materials Characterization Facility at Texas A&M University for XPS instrumentation access and training.

I would like to acknowledge the support of the Office of Naval Research, Grant No. N00014-10-1-0527, N00014-14-1-0082, and the Welch Foundation through the W. T. Doherty-Welch Chair in Chemistry, Grant No. A-0001 in my graduate research career.

Within the Wooley group, I would like to recognize Dr. Jeffery Raymond, Dr. Shiyi Zhang, Dr. Jiong Zou, Dr. Guorong Sun and Dr. Kevin Pollack. I appreciate their mentorship, advice and guidance in my research and have learned many useful research skills and techniques from these talented scientists. I would like to thank my undergraduate researcher, Mr. Eric Vavra, who not only helped me in my research, but also taught me how to be a mentor. I would also like to thank all the past and present members of the Wooley group, Mr. Johnson Asi, Dr. Celine Besset, Dr. Yannick Borguet, Dr. Sangho Cho, Mr. Daniel Dobbins, Ms. Mei Dong, Dr. Andrew Dove, Ms. Sussana Elkassih, Dr. Mahmoud Elsabahy, Mr. Jingwei Fan, Ms. Simcha Felder, Ms. Jeniree Flores, Dr. Christopher Fidge, Dr. Marco Giles, Ms. Amelia Gonzales, Dr. Tiffany Gustafson, Mr. Xun He, Mr. Gyu Seong Heo, Ms. Jesscia Huang, Dr. Ashley Jahnke, Ms. Nari Kang, Ms. Sarosh Khan, Mr. Chris Komatsu, Ms. Samantha Kristufek, Dr. Nam Lee, Mr. Eric Leonhardt, Dr. Ang Li, Mr. Richen Li, Dr. Soon-Mi Lim, Dr. Young Lim, Mr.

Yen Nan Lin, Dr. Yun Lin, Ms. Lauren Link, Mr. Alex Lonnecker, Ms. Casey McDonald, Mr. Andy Moutray, Dr. Koichiro Mikami, Ms. Audrey Nelson, Mr. Tan Nguyen, Dr. Amandine Noel, Dr. Adriana Pavia-Sanders, Ms. Jennifer Summerhill, Mrs. Stephanie Pollack, Mrs. Danielle Policarpio, Mr. Kenton Rauwerdink, Mr. Joel Russell, Dr. Sandani Samarajeewa, Dr. Ritu Shrestha, Mr. Justin Smolen, Ms. Yue Song, Ms. Jennifer Streff, Mr. Matthew Svach, Dr. Lu Su, Ms. Judy Taylor, Mr. Timothy Tsao, Mr. Bryan Tucker, Ms. Ginny Vance, Ms. Mariela Vasquez, Ms. Brook Versaw, Mr. Kevin Wacker, Ms. Sarah Ward, Mr. Hai Wang, Mrs. Chao Yang, Dr. Scott Zawko, Mr. Ryan Zentay, and Dr. Fuwu Zhang for being such great peers and making the lab environment so enjoyable to be in.

Lastly, I would like to thank my family, Ms. Florence Wijaya, Mr. Charles Lei, Mrs. Carmen Lei, Mr. Evan Lei, and Ms. Olivia Lei for their continued support and encouragement. Specifically, I would like to thank my mother Ms. Florence Wijaya, who has loved and raised my sister and me single-handedly. She has truly been with me through every moment and supported me throughout my life.

NOMENCLATURE

AGE	Allyl glycidyl ether
AF	Anti-fouling
AFM	Atomic force microscopy
AFSM	Amphiphilic fluorinated small molecule
ATR-FTIR	Attenuated total reflectance-Fourier transform infrared spectroscopy
ATR-SCVCP	Atom transfer radical-self condensing vinyl copolymerization
BHT	Butylated hydroxytoluene
BSA	Bovine serum albumin
CA	Contact angle
CAA	2-Carboxy ethyl acrylate
COP	Chloro-2-oxo-1,3,2-dioxaphospholane
DCM	Dichloromethane
DIPEA	*N*,*N*-Diisopropylethylamine
DMF	*N*,*N*-Dimethylformamide
DMPA	2,2-Dimethoxy-2-phenylacetophenone
DSC	Differential scanning calorimetry
DMTA	Dynamic mechanical thermal analysis
GPC	Gel permeation chromatography
HBFP	Hyperbranched fluoropolymers

HRMS	High-resolution mass spectrometry
IMO	International Maritime Organization
NMR	Nuclear magnetic resonance
PBS	Phosphate buffer saline
PDMS	Polydimethylsiloxane
PEG	Poly(ethylene glycol)
PFS	2,3,4,5,6-Pentafluorostyrene
PMMA	Polymethyl methacrylate
POSS	Thiopropyl T8/T10 silsesquioxane
RFU	Relative fluorescence units
SA	Sulfonate
SAA	Poly(styrene-*co*-allyl alcohol)
SAP	Poly(styrene-*co*-allyl phospholane)
SEM	Scanning electron microscopy
TBT	Tributyltin
TEA	Triethylamine
TGA	Thermogravimetric analysis
THF	Tetrahydrofuran
TMA	Trimethylammonium chloride
TMBD	N,N,N’,N’-tetramethyl-1,4-butanediamine
TrEG	Triethylene glycol
UV	Ultraviolet

UV-vis	Ultraviolet-visible
XPS	X-ray photoelectron spectroscopy

TABLE OF CONTENTS

LIST OF FIGURES

LIST OF TABLES

CHAPTER I

INTRODUCTION

1.1 Introduction

The ability to resist the adsorption of biomolecules and microorganisms is critical in both marine and biomedical applications.[1-5] After thorough investigations, certain polymeric materials such as silicone elastomers, fluoropolymers, PEGylated (poly(ethylene glycol)-conjugated) polymers and zwitterionic polymers have shown to display unique properties that contribute to the effectiveness of fouling resistance.[4,6-22] Silicone elastomers, polydimethylsiloxane (PDMS) in particular, exhibit low surface energy, inertness, stability, and modulus allowing the attached fouling organism to detach easily by hydrodynamic forces.[23,24] Fluoropolymers have low surface energy, low wettability and high chemical stability that help deter fouling.[10-14] PEGylated polymers have also shown great anti-fouling properties as a hydration layer forms around PEG through hydrogen bonds, which requires disruption from proteins that is both energetically and kinetically unfavorable.[4,14-18] An alternate class of hydrophilic polymers that shows promising protein anti-fouling properties is zwitterionic polymers, which are inspired by blood cell membranes.[3,4,19,25-28] Unlike PEGylated polymers, zwitterionic polymers such as phosphorylcholine, carboxybetaine and sulfobetaine produce the hydration layer through electrostatic interactions in addition to hydrogen bonding.[3,4,19,26-28] The hydrogen bonding interactions of water molecules with

zwitterions have also been reported to be stronger than the hydrogen bonding interactions of water molecules with other hydrophilic materials.[29]

In the aquatic environment, fouling occurs when marine microorganisms form biofilms on surfaces such as ship hulls and allows for larger marine organisms, such as diatoms and barnacles, to attach onto the biofilms and proliferate.[21,30] Accumulation of marine fouling organisms on hulls not only increases the weight of the vessel, but also increases hydrodynamic drag, thus decreasing the vessel's speed and maneuverability and resulting in higher fuel consumption and traveling time.[22,31] Furthermore, the need to clean the fouling organisms off ship hulls and also increases the added cost due to fouling.[32] The US Navy alone, which accounts for less than half a percent of the world's shipping industry, spent additional $180M-$260M USD per year as a result of fouling.[22] Fouling organisms also pose a significant threat to the environment as they cling onto ship hulls and travel into foreign waters where they can create ecological imbalances in populations.[33-36] For example, Yamaguchi and coworkers have found fourteen previously unrecorded barnacle species on two international ship hulls in the port of Osaka Bay.[33,34] In order to reduce fuel consumption, hull cleaning costs, and the invasion of non-indigenous species, tributyltin (TBT) was added into marine paints as the first strategy to combat biofouling in the 1960s.[37] Although these coatings are successful at resisting fouling, the TBT is considered to be one of the most toxic chemicals to be deliberately introduced into the marine environment and has been banned by the International Maritime Organization (IMO).[38-40] Cuprous oxides were then used as a substitute for TBT. However, cuprous oxides are still toxic and shown to

be less effective as an anti-fouling agent than TBT.[41] This lack of effective alternatives to TBT calls for immediate attention to find solutions to combat biofouling in a more efficient and environmentally benign approach.

A grand challenge in anti-fouling in the marine environment is that different marine organisms have been shown to foul differently on different polymeric materials as marine organisms, depending on the species, foul on a surface by secreting either hydrophobic or hydrophilic glycoprotein adhesives.[14,15,42,43] Soft fouler green marine algae have been demonstrated to foul more on hydrophilic PEGylated surfaces than on hydrophobic fluorinated surfaces, while hard fouler *Navicula* diatoms displayed the opposite trend and fouled more on hydrophobic fluorinated surfaces than on hydrophilic PEGylated surfaces.[14,15,43] Amphiphilic copolymer coatings that combine both fluoropolymers and PEGylated polymers resulted in weak adhesion of both *Ulva* and *Navicula*.[14] Thus, multi-component polymer systems have generated much interest for anti-fouling applications in the marine environment as the system combines the anti-fouling properties of each component and displays chemical heterogeneities.[14,44,45]

Our group has designed and synthesized hyperbranched fluoropolymers (HBFP) which, when deposited with complementarily-reactive diamino-PEG on a substrate, gives rise to an amphiphilic crosslinked network that displays topological, topographical and chemical heterogeneities over both nanoscale and microscale, due to the covalent, kinetic trapping of the two physically-incompatible polymers.[46-48] With chemical heterogeneity and topographical and topological features on the order of nanoscale and microscale, it is less likely for fouling organisms and their secreted hydrophobic or

hydrophilic proteins to find a suitable region on the HBFP-PEG surface to adhere strongly to.[48] The crosslinking mechanism of HBFP with PEG involves nucleophilic substitution of bromoalkyl end groups of HBFP that was generated from atom transfer radical-self condensing vinyl copolymerization (ATR-SCVCP) with difunctional amino terminated end groups of PEG. This crosslinking mechanism allows for the tuning of the HBFP-PEG network with varying wt% of PEG relative to HBFP to achieve optimal anti-fouling properties. For example, the resistance against the settlement of hydrophobic biomacromolecule, bovine serum albumin (BSA) and an amphiphilic biomacromolecule, lipopolysaccharides from *Escherichia coli* (LPSE) was studied on a series of HBFP-PEG networks with varying wt% of PEG.[46] The studies showed that BSA adhered more onto surfaces with lower wt% of PEG while LPSE adhered more onto surfaces with higher wt% of PEG.[46] These results indicated that a surface which presents optimal nanoscale heterogeneity in terms of chemical composition, topology and topography can resist proteins that adhere to hydrophobic or hydrophilic surfaces, and that biofoulers can discriminate between surface domains of different wettability and of a specific size in the micrometer range.[46,47]

For additional heterogeneity and improved mechanical properties in HBFP-PEG networks, a third component, PDMS, was incorporated into the current HBFP-PEG system to form HBFP-PEG-PDMS terpolymer networks.[49,50] The HBFP-PEG-PDMS terpolymer networks have shown to have improved fouling release of diatoms than HBFP-PEG networks.[49,50] Significant advances in the preparation of the HBFP-PEG-

PDMS terpolymer networks have also been made as the coatings can be prepared rapidly with less materials required by airbrush application.

This dissertation focuses on the development of new methodologies for anti-fouling polymeric network syntheses, orthogonal modifications, characterization and anti-fouling properties for marine anti-fouling applications. Chapters 2, 3 and 4 involve the investigations in amphiphilic networks for anti-fouling in the marine environment. Specifically, Chapter 2 discusses the stability and crosslinking efficiency of increasing the amount of PEG contents in the HBFP-PEG-PDMS terpolymer system. Chapter 3 focuses on the anti-fouling properties of a new ternary network in which multifunctional silsesquioxane (POSS) is crosslinked with an amphiphilic fluorinated small molecule (AFSM) and zwitterionic small molecule (ZSM) *via* thiol-ene "click" chemistry. The overall goal of this work is to generate an amphiphilic ternary anti-fouling coating that combines the properties of POSS, amphiphilic fluoro- and oligo(ethylene oxide) compounds, and zwitterionic compound efficiently. Chapter 4 details a method that utilizes facile chemistry to introduce both amphiphilicity and zwitterionicity into a commodity polymer to form a polymer coating, which exhibited great anti-fouling performance. With increasing anti-fouling materials that includes zwitterionic or net neutral mixed charged polymers in various anti-fouling applications, investigations of thermal and mechanical properties of zwitterionic polymers and net neutral mixed charged polymers are reported in Chapter 5 as the polymer properties become of significance when applying to a specific application.

In Chapter 2, the stability and crosslinking ability of HBFP-PEG-PDMS terpolymer networks were further investigated in order to determine if increasing the wt% of linear polymers of PEG and PDMS was feasible. HBFP-PEG-PDMS terpolymer network was generated using 200 wt% PEG relative to HBFP and 50 wt% PDMS relative to HBFP, which requires higher crosslinking sites in comparison to previous HBFP-PEG-PDMS terpolymer networks that were generated using up to 75 wt% PEG relative to HBFP and 75 wt% PDMS relative to HBFP. The HBFP-PEG-PDMS terpolymer coating was prepared on an Interseal® 670 HS epoxy-based undercoat covered microscope glass slide. Scanning electron microscopy (SEM), attenuated total reflectance-fourier transform infrared spectroscopy (ATR-FTIR) and atomic force microscopy (AFM) characterizations were used to confirm the HBFP-PEG-PDMS terpolymer network on the Interseal® 670 HS epoxy-based undercoat covered microscope glass slide. The thicknesses of the HBFP-PEG-PDMS terpolymer network layer and the Interseal® 670 HS epoxy-based undercoat layer were measured using SEM. The stability and crosslinking efficiency of the HBFP-PEG-PDMS terpolymer network were investigated by comparing the HBFP-PEG-PDMS terpolymer network when immersed in synthetic seawater for 0 d, 1 d, and 1 wk. AFM images, static water contact angles and IR spectra of the HBFP-PEG-PDMS terpolymer network after immersion in synthetic seawater for 0 d, 1 d, and 1 wk showed no significant change suggesting that the HBFP-PEG-PDMS terpolymer network was stable during the 1 wk immersion in synthetic seawater. The crosslinking efficiency and stability of the HBFP-PEG-PDMS terpolymer network were also investigated by subjecting the HBFP-PEG-PDMS

terpolymer networks that were immersed in synthetic seawater for 0 d, 1 d and 1 wk to Soxhlet extraction using tetrahydrofuran (THF) as solvent. At the end of the Soxhlet extraction, all HBFP-PEG-PDMS terpolymer networks that were immersed in synthetic seawater for 0 d, 1 d and 1 wk were still intact and only resulted in a 10% mass loss. Lastly, no evidence of the loss of HBFP, PEG, or PDMS was present in the ^{1}H NMR spectra of the extracted contents, indicating that the HBFP could be functionalized with more linear polymers or even small molecules than what had been previously done.

In Chapter 3, a ternary coating was designed involving a multi-functional thiol POSS crosslinked with AFSM and coupled with ZSM *via* thiol-ene click chemistry. Four different types of coatings (A, B, C, D) with varying stoichiometric molar ratios of AFSM and ZSM were generated. The resulting coatings yielded thicknesses that ranged from 0.2 μm to 1.3 μm as determined by SEM images. The anti-fouling and fouling release performances of ternary coatings with and without biofilm layer were investigated with *Ulva linza*, *Navicula incerta*, and *Balanus amphitrite* to test if the presence of a biofilm on the ternary coatings influences the settlement and adhesion of fouling organisms on the ternary coatings. With the presence of biofilm, spore settlement densities of *Ulva linza* were increased in all ternary coatings and control. Spore settlement densities on all ternary coatings were lower than those on glass surfaces but higher than those on PDMS. There was no major difference between anti-fouling performances of ternary coatings and silanized glass against diatoms. As for the results collected from barnacle cyprid assay, the settlement densities on the ternary coatings

were not affected by the presence of the biofilm and were higher than those of silanized glass.

In Chapter 4, a novel strategy that utilizes simple chemistry was designed to modify a commercially-available polymer to form an amphiphilic polymer coating, in which the hydrophilic component is composed of zwitterionic units. The amphiphilic, zwitterionic, anti-fouling polymer coating on silanized microscope glass slide was engineered by a two-step modification of a commodity polymer. The surface properties of the resultant polymer coating can be easily tuned by varying the extent of crosslinking in the network. Nominally 0%, 25%, and 50% crosslinked amphiphilic zwitterionic coatings were prepared and measured by calipers to range from 30 μm to 50 μm. X-ray photoelectron spectroscopy (XPS) was used to confirm the chemistry of the conversion of phosphotriester units into phosphorylcholine units taking place on the surface of the coating. AFM images of the coatings in the dry state presented rough surfaces with randomly distributed topographical features while the images of the coatings in the water-swollen state displayed lower R_{rms} and decrease in surface area, resulting in a smoother surface than their dry counterparts. Both AFM images and static water contact angles of the coatings in both the dry and water-swollen states confirmed that dynamic reorganization had occurred on the surface when immersed in water. Higher anti-fouling efficiency was observed for these surfaces *vs*. an elastomeric polydimethylsiloxane standard (Sylgard® 184) against the adsorption of biomacromolecules and *Ulva* zoospores. This design establishes a platform for the achievement of functionalized

amphiphilic zwitterionic copolymers from relatively inexpensive starting materials *via* simple chemical manipulations.

In Chapter 5, the thermal and mechanical properties of zwitterionic polymers and net neutral mixed charged polymers were investigated. Different charged polymers were prepared by functionalizing poly[(allyl glycidyl ether)-*b*-(ethylene oxide)-*b*-(allyl glycidyl ether)] (P(AGE-*b*-EO-*b*-AGE)) with different charged thiols through highly efficient photo-initiated thiol-ene chemistry. Equimolar amounts of polymers with positive charged side chains and negative charged side chains were then mixed together and compared to polymers with zwitterionic side chains which possess similar charge densities. The bulk polymers were characterized by thermogravimetric analysis (TGA), differential scanning calorimetry (DSC) and dynamic mechanical thermal analysis (DMTA) and the effect of the nature of ionic interactions on the thermal/mechanical properties studied. The zwitterionic polymer exhibits lower crystallinity than the cationic/anionic blended polymer. DMTA traces suggested that zwitterionic units in zwitterionic polymers resulted in higher storage modulus than those of between cationic and anionic units of cationic/anionic blended polymers at temperatures above -27 °C.

CHAPTER II

INVESTIGATIONS OF THE STABILITY AND CROSSLINKING EFFICIENCY OF HYPERBRANCHED FLUOROPOLYMER-POLYDIMETHYLSILOXANE-POLY(ETHYLENE GLYCOL) CROSSLINKED TERPOLYMER NETWORKS [*]

2.1 Introduction

A considerable amount of effort has been invested into the prevention of fouling on ship hulls since the ban of TBT.[39,51] However, the prevention of fouling has proven to be challenging due to the many variables that play a role in fouling such as water region, water temperature, salinity, and marine organism species.[39,52-56] Different marine organisms have been shown to foul differently on different polymeric materials as marine organisms, depending on the species, foul on a surface by secreting either hydrophobic or hydrophilic glycoprotein adhesives.[14,15,42,43] For example, hydrophobic fluorinated surfaces have been demonstrated to resist adsorption of soft fouler green marine algae, *Ulva*, but not of hard fouler *Navicula* diatoms, while hydrophilic PEGylated surfaces show better resistance to the adhesion of diatoms than to the adhesion of *Ulva*.[14,15,43] Amphiphilic copolymer coatings with the combination of both fluoropolymers and PEGylated polymers resulted in a weak adhesion of both *Ulva* and *Navicula*.[14]

---

* In collaboration with Jennifer N. Zigmond, Eric D. Vavra, Kevin A. Pollack, Samantha L. Kristufek, Karen L. Wooley, Departments of Chemistry, Chemical Engineering and Materials Science & Engineering, Texas A&M University

Polymeric materials have been heavily investigated and have been shown to be effective as anti-fouling coatings. Some of the most explored polymers are silicone elastomers, fluoropolymers, PEGylated polymers and zwitterionic polymers.[12-32] Silicone elastomers, PDMS in particular, have been commercialized as non-toxic antibiofouling coatings.[23] These coatings exhibit low surface energy and low modulus allowing the attached fouling organism to detach easily by hydrodynamic forces.[23,24] Another class of polymers that has been studied extensively as anti-biofoulers are fluoropolymers, due to their low surface energy, low wettability and high chemical stability.[10-14] PEGylated polymers have also shown great anti-fouling performance as the hygroscopic PEG forms a hydration layer through hydrogen bonds around the surface which requires disruption from proteins that is both energetically and kinetically unfavorable.[4,14-18]

Our laboratory has designed and synthesized a hyperbranched fluoropolymer HBFP, which has amphiphilic character to enhance anti-biofouling performance while retaining the desired nanoscale surface heterogeneities.[57] An advantage of HBFP is that it possesses bromoalkyl end groups from bromoacetyl and bromobenzyl groups generated during ATR-SCVCP, which can react with amine groups *via* nucleophilic substitution reaction. The ability for the bromoalkyl end groups to undergo nucleophilic substitution reaction with amine groups allows for the HBFP to be coupled and/or crosslinked with small molecules or other polymers that bear amine groups. HBFP was crosslinked with varying amounts of poly(ethylene glycol) bis(3-aminopropyl) terminated. The resultant crosslinked HBFP-PEG networks displayed topological,

topographical and chemical heterogeneity over a variety of scales, which had shown to deter the settlement of both biomacromolecules and marine organisms.[46,48,58-60] We have recently explored introducing a third polymer, poly(dimethylsiloxane) bis(3-aminopropyl) terminated, which is a fouling release polymer, into HBFP-PEG systems to form terpolymer AF HBFP-PEG-PDMS systems.[43,50]

Previous HBFP-PEG-PDMS terpolymer systems which were investigated involve a series of nine HBFP-PEG-PDMS terpolymer networks with varying stoichiometries of HBFP, PEG (25, 50 and 75 wt%, relative to HBFP) and PDMS (25, 50 and 75 wt%, relative to HBFP) components.[43,50] The highest wt% of linear polymers in the series is 150 wt% (75 wt% PEG and 75 wt% PDMS) relative to HBFP, which is by far the network with the highest crosslinking density that we have ever prepared. It is of our continued interest to understand the crosslinking efficiency of HBFP so that networks with higher components could be generated in order to increase chemical complexity while maintaining a stable crosslinked network. Therefore, HBFP-PEG-PDMS terpolymer coatings with a formulation of HBFP, PEG (200 wt% relative to HBFP) and PDMS (50 wt% relative to HBFP) were prepared to test for the crosslinking efficiency of HBFP with PEG and PDMS. The stability and crosslinking efficiency of the coatings were investigated by performing Soxhlet extraction and various characterization techniques such as AFM and IR on the terpolymer networks.

2.2 Experimental Section

Materials

All chemicals and reagents were purchased from Sigma-Aldrich (St. Louis, MO) and used without further purification unless otherwise noted. 2,3,4,5,6-Pentafluorostyrene (PFS) was purchased from Oakwood Chemical (West Columbia, SC) and filtered through neutral alumina to remove inhibitor prior to use. Microscope glass slides (75 mm x 25 mm x 1 mm) were purchased from VWR (Radnor, PA). Synthetic seawater was purchased from Ricca Chemical Company (Arlington, TX). Interseal® 670 HS was purchased from Richmond Supply, Inc. (Augusta, GA). Custom aluminum molds were fabricated at the Texas A&M University machine shop (College Station, TX). Central Pneumatic mini air compressor with airbrush and hose (120 VAC/ 60 Hz, 1/5 HP, 1750 RPM, 30 PSI Working Air Pressure, Air Outlet: 1/8" – 27 NPT, Item 95830) were purchased from Harbor Freight Tools (Los Angeles, CA). Glascribe tungsten carbide tipped pen was purchased from Ted Pella, Inc (Redding, CA).

Nuclear Magnetic Resonance Spectroscopy

^{1}H NMR, ^{13}C NMR NMR and ^{19}F NMR spectra were recorded on a Varian Inova 300 (Varian Inc., Palo Alto, CA) interfaced to a UNIX computer using VnmrJ software. ^{1}H NMR and ^{13}C NMR were analyzed using the solvent signal as an internal reference.

High-resolution Mass Spectrometry

High-resolution Mass Spectrometry (HRMS) for the monomers was conducted on an Applied Biosystems PE SCIEX QSTAR.

Elemental Analysis

Elemental analysis of the polymers was performed at Midwest Microlab, LLC (Indianapolis, IN).

Gel Permeation Chromatography

The molecular weight and molecular weight distribution of polymer was determined by gel permeation chromatography (GPC) with a Waters 1515 isocratic HPLC pump (Waters Corporation, Milford, MA) equipped with a Waters 2414 differential refractomer (Waters Corporation, Milford, MA), and a PD2020 dual-angle (15° and 90°) light scattering detector (Precision Detectors, Inc., Bellingham, MA), and four PL_{gel} polystyrene-*co*-divinylbenzene gel columns (Polymer Laboratories, Inc., Amherst, MA) connected in series: 5 μm Guard (50 × 7.5 mm), 5 μm Mixed C (300 × 7.5 mm), 5 μm 10^4 (300 × 7.5 mm), and 5 μm 500 Å (300 × 7.5 mm) using the Breeze (version 3.30, Waters, Inc.) software. The instrument was opeated using THF as the eluent at a flow rate at 1.00 mL/min at 35 °C. An injection volume of 200 μL of polymer solution (1 mg/mL) was used. Data collection and analyses were performed using Precision Acquire 32 Acquisition program (Precision Detectors, Inc., Bellingham, MA) and Discovery32 software (Precision Detectors, Inc., Bellingham, MA), respectively. A calibration curve was generated by plotting the known molecular weights of a series of broad polydispersity poly(styrene) standards as a function of retention time.

Thermal Analysis

TGA was performed under argon atmosphere using a Mettler-Toledo model TGA/DSC1 Star^e system (Mettler-Toledo, Inc., Columbus, OH), with a heating rate of 10 °C/min. Measurements were analyzed by using Mettler-Toledo STAR^e v. 7.01 software. Glass transition temperatures (T_g) were measured by differential scanning calorimetry (DSC) on a Mettler-Toledo DSC822^e (Mettler-Toledo, Inc., Columbus, OH), with cooling and heating rates of 5 °C/min. Measurements were analyzed using Mettler-Toledo STAR^e v. 7.01 software. The T_g was taken as the midpoint of the inflection tangent, upon the third heating scan.

Attenuated Total Reflectance-Flourier Transform Infrared Spectroscopy

ATR-FTIR spectra were recorded using an IR Prestige 21 system (Shimadzu Corp., Kyoto, Japan) attached with PIKE MIRacle™ ATR and diamond crystal and analysis was performed using IRsolution v. 1.40 software.

Scanning Electron Microscopy

SEM images were imaged using TESCAN VEGA3 SEM. All samples were sputter coated with either a 20 nm layer of gold or a 5 nm layer of 80% platinum/20% palladium. Samples were mounted perpendicular to the secondary electron detector using conductive carbon tape. Six replicates were imaged for each sample and the average and standard deviation of the thickness of the coating were reported.

Static Surface Water Contact Angle

Static contact angle of nanopure water was measured on nine areas per sample using the sessile drop technique on an Attension Theta optical tensiometer (Biolin

Scientific, Stockholm, Sweden) and analysis was performed by fitting drops with a Young-Laplace formula using the Theta Software to calculate the average static contact angles. Three replicate measurements were acquired for each sample and the average and standard deviation of static water contact angle were reported.

Atomic Force Microscopy

AFM images were taken with MFP-3D-BIO AFM system (Asylum Research, Santa Barbara, CA) under ambient conditions in air using standard silicon tips (VISTA probes, T190 - 25, resonance constant: 190 kHz, tip radius: ~ 10 nm, spring constant: 48 N/m). Three replicates were imaged for each sample and the average and standard deviation of the R_{rms} roughness were reported.

Synthesis of 4-[Oxy(tri(ethylene glycol))]-2,3,5,6-tetrafluorostyrene

To a 500 mL three-necked round-bottom flask equipped with a magnetic stir bar was added 60 wt% sodium hydride dispersion in oil (2.33 g, 62.0 mmol). The flask was purged with N_2 and lowered into an ice bath. Into the flask was added dropwise THF (200 mL), followed by an addition of a solution of triethylene glycol (TrEG) (23.2 g, 155 mmol) in THF (50 mL). PFS (10.0 g, 51.5 mmol) was then added dropwise into the solution. The solution was allowed to warm to room temperature and stirred for 16 h. The solution was concentrated *in vacuo* and the resulting oil was dissolved in dichloromethane (100 mL) before being washed with brine (3 x 100 mL). The organic fraction was dried with anhydrous $MgSO_4$, filtered and concentrated *in vacuo*. The product was isolated using flash chromatography with 10% methanol in dicloromethane as the eluent (yield: 63%). ^{1}H NMR (300

MHz, $CDCl_3$, ppm,): δ 6.60 (dd, *J* = 18 Hz and 12 Hz, 1H, ***H***(H)C=CH-R (*cis*)) , 6.00 (d, *J* = 18 Hz, 1H, H_2C=C***H***-R), 5.61 (d, *J* = 12 Hz, 1H, ***H***(H)C=CH-R (*trans*)), 4.36 (t, *J* = 5 Hz, 2H, TFSOC***H₂***CH_2O), 3.82 (t, *J* = 5 Hz, 2H, OCH_2C***H₂***OH), 3.75-3.55 (m, 8H, OEG ***Hs***). ^{13}C NMR (75 MHz, $CDCl_3$, ppm): δ 146.6, 143.3, 142.8, 139.4, 136.3, 122.2, 122.0, 110.8, 74.1, 70.8, 70.7, 70.2, 68.8, and 64.9. ^{19}F NMR (282 MHz, $CDCl_3$, ppm): δ -145 (m, Ar ortho- ***Fs***), -158 (m, Ar meta- ***Fs***). HRMS (m/z): calculated for $C_{14}H_{16}F_4O_4$ $[M+H]^+$ 325.11; found 325.1063. FTIR (cm^{-1}): 3600–3200, 3050–2750, 1680–1590, 1550–1390, 1360, 1290, 1250, 1200–1000, 960, 940, 880, 850.

Synthesis of 4-[Oxy(tri(ethylene glycol)bromoisopropionyl)]-2,3,5,6-tetrafluorostyrene

To a 500 mL three-neck round-bottom flask equipped with a magnetic stir bar containing triethylamine (7.70 mL, 55.5 mmol) in THF (250 mL) was added 4-[oxy(tri(ethylene glycol))]-2,3,5,6-tetrafluorostyrene (5.00 g, 15.4 mmol). The flask was purged with N_2 and lowered into an ice bath. 2-Bromoisopropionyl bromide (4.00 g, 18.5 mmol) was added dropwise into the flask. The solution was allowed to warm to room temperature and stirred for 16 h. The reaction mixture was filtered and concentrated *in vacuo* and dissolved in dichloromethane (250 mL). The solution was washed with deionized water (4 x 250 mL) and the organic layer was dried over $MgSO_4$. The solution was filtered and concentrated *in vacuo*. The product was isolated using flash chromatography with 30% ethyl acetate in hexanes as the eluent (yield: 79%). ^1H NMR (300 MHz, $CDCl_3$, ppm,): δ 6.61 (dd, *J* = 18 Hz and 12 Hz,

1H, ***H***(H)C-CH-R (*cis*)) , 6.02 (d, *J* = 18Hz, 1H, H_2C=C***H***-R), 5.62 (d, *J* = 12 Hz, 1H, ***H***(H)C-CH-R (*trans*)), 4.39 (q, *J* = 7 Hz, 3H, C***H***BrCH_3), 4.37 (t, *J* = 5 Hz, 2H, TFSOC***H_2***CH_2O), 4.31 (t, *J* = 5 Hz, 2H, OCH_2C***H_2***OOC), 3.83 (t, *J* = 5 Hz, 2H, TFSOCH_2C***H_2***O), 3.80-3.60 (m, 6H, OEG ***Hs***), 1.81 (d, *J* = 7 Hz, 3H, CHBrC***H_3***). ^{13}C NMR (75 MHz, $CDCl_3$, ppm): δ 170.9, 146.6, 143.3, 142.8, 139.3, 136.3, 122.2, 122.0, 110.8, 74.1, 70.8, 70.6, 70.1, 68.8, 64.6, 55.6, and 30.5. ^{19}F NMR (282 MHz, $CDCl_3$, ppm): δ -145 (m, Ar ortho- ***Fs***), -158 (m, Ar meta- ***Fs***). HRMS (m/z): calculated for $C_{17}H_{19}BrF_4O_5$ $[M+H]^+$ 459.02; found 459.0430. FTIR (cm^{-1}): 3070–2750, 1740, 1640, 1550–1310, 1220, 1190–1000, 965, 935, 855, 760, 675.

Synthesis of Hyperbranched Fluoropolymers

To a 250 mL flame-dried Schlenk flask containing a magnetic stir bar was added 4-[oxy(tri(ethylene glycol))bromoisopropionyl]-2,3,5,6-tetrafluorostyrene (2.00 g, 4.36 mmol), PFS (1.70, 8.71 mmol), CuBr (62.5 mg, 0.44 mmol), 2,2'-bipyridine (150 mg, 0.96 mmol) and anisole (5 mL). The solution was deoxygenated *via* three freeze-pump-thaw cycles before being backfilled with N_2. The Schlenk flask containing the deoxygenated solution was then lowered into an oil bath set at 65 °C and the reaction was allowed to proceed for 20 h. The polymerization was quenched by submerging the flask in liquid nitrogen and exposing the reaction mixture to air. After the reaction mixture had thawed, the contents were poured into dichloromethane (20 mL). The solution was then passed through an alumina column to remove the catalyst and concentrated *in vacuo*. The polymer was precipitated in cold hexanes (3x) to afford a white powder (47% yield). ^{1}H NMR (300 MHz, $CDCl_3$, ppm): δ 4.45-4.20 (m,

TFSOC***H₂***CH_2O and CH_2C***H₂***OOC), 3.90-3.60 (m, OEG ***Hs***), 2.80-1.50 (m, C***H₂***C***H*** backbone), 1.30=0.85 (br, CC***H₃***). ^{13}C NMR (75 MHz, $CDCl_3$, ppm): δ 176.6, 144.7, 140.7, 137.6, 122.2, 114.7, 74.3, 70.8–70.0, 68.8, 63.6, 41.7–32.1, 30.7–29.7, 24.7. ^{19}F NMR (282 MHz, $CDCl_3$, ppm): δ -143 (br, Ar ortho- ***Fs***), -156 (br, Ar para- ***F***), -161 (br, Ar meta- ***Fs***). FTIR (cm^{-1}): 3050–2790, 1740, 1645, 1575–1400, 1360, 1320–1190, 1185–1010, 955, 860, 785–710. Elemental Analysis: calculated for $C_{1874}H_{1132}F_{946}Br_{34}$: C, 48.03; H, 2.43; F, 38.35; Br, 5.80%. Found: C, 48.22; H, 3.01; F, 30.68; Br, 10.10%. M_w^{GPC} = 46,900 Da, M_n^{GPC} = 28,300 Da, M_w/M_n = 1.66. DSC: T_g = 60 °C. TGA in Ar: 30-200 °C, 0% mass loss; 200-300 °C, 9% mass loss; 300-400 °C, 42% mass loss; 400-500 °C, 78% mass loss; 22% mass remaining above 500°C.

Application of Interseal® 670 HS Epoxy-based Undercoat on Microscope Glass Slides

Component A and component B of Interseal® 670 HS were added into a plastic beaker in an 8:1 ratio and mixed until homogenous to form a viscous epoxy solution. 15 microscope glass slides were placed in a specialty custom aluminum mold to help hold the microscope glass slides in place while the homogenous epoxy was coated on the microscope glass slides *via* a draw down method. The draw down method entails homogeneous epoxy (3 mL) being deposited at the top of each microscope glass slide and a roller being used to roll the epoxy down the microscope glass slides. The Interseal® 670 HS epoxy-based undercoat covered microscope glass slides were cured at room temperature under N_2 for 24 h.

General Procedure for the Application of Terpolymer Coating onto Interseal® 670 HS Epoxy-based Undercoat Covered Microscope Glass Slides

To a 40 mL scintillation vial was added HBFP (72.0 mg, 0.00154 mmol), poly(ethylene glycol) bis(3-aminopropyl) terminated (M_n = 1,500 Da) (144 mg, 0.0960 mmol), poly(dimethylsiloxane) bis(3-aminopropyl) terminated (M_n = 2,000 Da) (36.0 mg, 0.0144 mmol), THF (10 mL) and *N*,*N*-diisopropylethylamine (DIPEA) (28.5 mg, 0.0144 mmol). The mixture was sonicated until all contents were dissolved to form a homogenous terpolymer formulation solution. Double-sided tape was used to adhere the Interseal® 670 HS epoxy covered microscope glass slides on a piece of card board with the epoxy facing up. The terpolymer formulation was applied on the Interseal® 670 HS epoxy-based undercoat covered microscope glass slides using an airbrush applicator with an application pressure of 50 psi from a distance of approximately 15 cm. Multiple airbrush passes were made over the slides with the applicator with a one minute rest between every two passes until the solvent had evaporated. The slides were then cured in an oven at 110 ºC for 45 minutes under N_2 atmosphere.

SEM Sample Preparation of Terpolymer Coating and Interseal® 670 HS Epoxy-based Undercoat on a Microscope Glass Slide

The coated slide of interest was submerged in liquid nitrogen until boiling was no longer observed. The sample was then rapidly removed from the liquid nitrogen with a pair of tweezers and sandwiched perpendicularly between two glass slides with the coated side of the sample facing the bottom glass slide. A Glascribe® tungsten carbide tipped pen was used to score the back of the coated slide using the top glass slide as a

straight edge. A large pair of tweezers was used to gently tap and cleave the scored-off portion of the coated slide from the bulk coated slide. The previous process to this point was repeated until a sample of approximately 1cm x 1cm was obtained. The sample was placed in a light N_2 stream to remove any glass dust and particulates. All samples were sputter coated with either a 20 nm layer of gold or a 5 nm layer of 80% platinum/20% palladium. Samples were mounted perpendicular to the secondary electron detector using conductive carbon tape.

Preparation of Terpolymer Films for AFM, IR, and Static Water Contact Angle

Nine terpolymer films on Interseal® 670 HS epoxy covered microscope glass slides were prepared by airbrush application method. The coatings were divided into three batches (3 coatings/batch). The first, second and third batch were immersed in synthetic seawater for 0 h, 24 h and 1 week, respectively. The coatings were then characterized.

Preparation of Terpolymer Films for Soxhlet Extraction

Terpolymer formulation solution was drop casted on a microscope glass slide and a thick film was formed upon evaporation of the THF solvent. The film was peeled off the microscope glass slide with a pair of tweezers and cut into nine (1 cm x 1 cm) pieces. The nine pieces of films were divided into three batches (3 films/batch). The first, second and third batch were immersed in synthetic seawater for 0 h, 24 h and 1 week, respectively. After being subjected to seawater immersion for the planned duration of time, the films were rinsed with nanopure water and dried using a vacuum oven at room temperature for 24 h.

Soxhlet Extraction of Terpolymer Films

Each batch of films prepared from drop casting was pre-weighed and inserted into 3 separate paper thimbles. Each paper thimble containing one batch of coatings was inserted into a Soxhlet apparatus that was attached to a 500 mL round-bottom flask containing a stir bar and THF (250 mL). A condenser was attached onto the top of the Soxhlet apparatus with water flowing through the condenser. The Soxhlet experiment setup was lowered into an oil bath set at 80 °C until the bottom half of the round-bottom flask was immersed in oil. Aluminum foil was used to surround the top half of the round-bottom flask and the Soxhlet apparatus and the Soxhlet extraction experiment was allowed to take place for 24 h. The films were removed from the paper thimble and dried in a vacuum oven at room temperature for 24 h before being weighed. The solution of extracted contents in THF in the round-bottom flask was concentrated *in vacuo* and the extracted contents were identified with ^{1}H NMR spectroscopy.

2.3 Results and Discussion

Hyperbranched fluoropolymer was synthesized as illustrated in **Figure 2.1**. A precursor molecule was first prepared by reacting PFS with tri(ethylene glycol) *via* nucleophilic aromatic substitution. The precursor was then reacted with 2-bromopropionyl bromide to afford an inimer which was used to initiate the polymerization. The inimier was copolymerized with PFS (67 mol%) using CuBr and 2,2'-bipyridine by ATR-SCVCP to afford HBFP. The afforded HBFP was analyzed with elemental analysis and was found to contain 10% bromine content. The HBFP was crosslinked poly(ethylene glycol) bis(3-aminopropyl) terminated (200 wt% with respect

to HBFP) and poly(dimethylsiloxane) bis(3-aminopropyl) terminated (50 wt% with respect to HBFP) to create terpolymer networks (**Figure 2.2**). Although the bromine content of HBFP as measured by elemental analysis is approximately 10% less than the theoretical calculated bromine content needed to allow for 100% crosslinking of terpolymer coating with 200 wt% PEG and 50 wt% PDMS with respect to HBFP to take place, it is not expected for both terminal amine groups of PEG and PDMS to react with bromoalkyl end groups to form covalent bonds. Therefore, the insufficient amount of bromoalkyl end groups does not pose a serious concern in the crosslinking of the terpolymer networks.

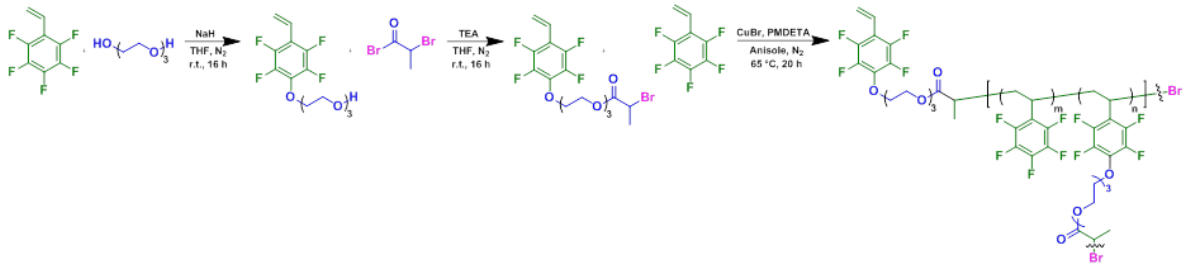

Figure 2.1. (A) Synthesis of inimer. (B) Synthesis of HBFP.

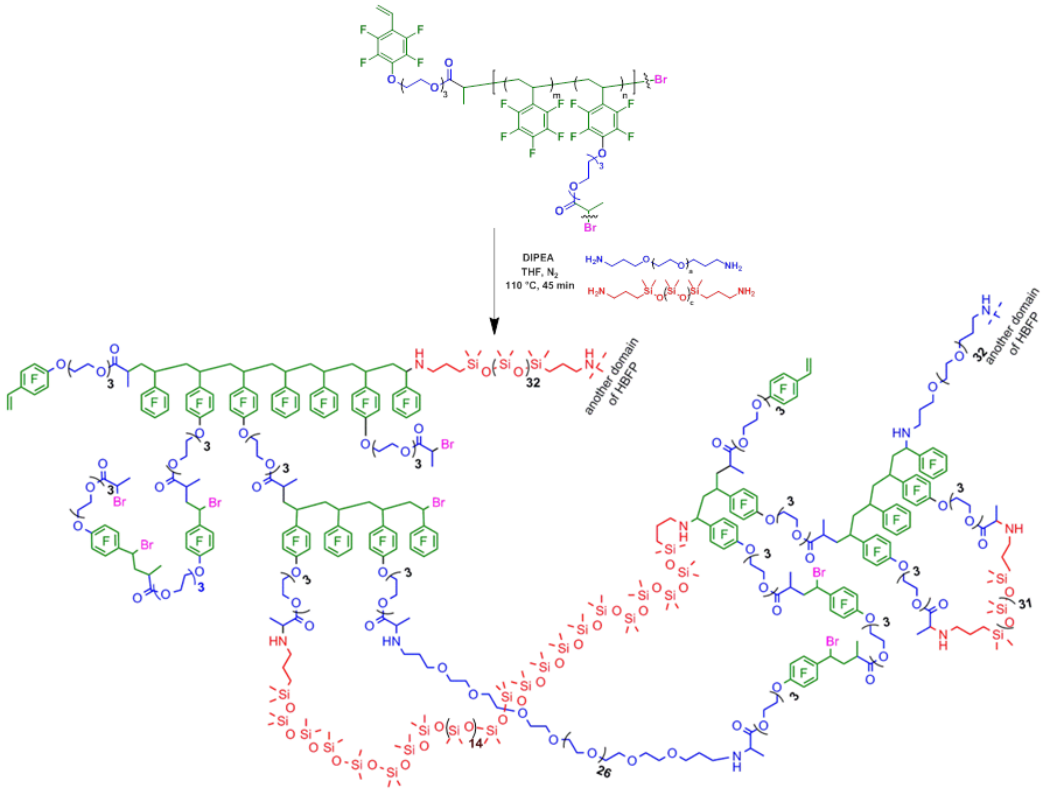

Figure 2.2. Synthesis of HBFP-PEG-PDMS terpolymer crosslinked network.

Previous experiments in the laboratory have shown that HBFP-PEG-PDMS terpolymer coatings delaminate off the substrates when submerged in water, therefore a new method has been developed in our laboratory to prevent delamination.[43] A naval approved epoxy-based undercoat, Interseal® 670 HS, was used to covalently attach to the terpolymer coating to prevent delamination. Interseal® 670 HS epoxy based undercoat was deposited onto microscope glass slides through a draw down method. A formulation of the terpolymer coating with PEG (200 wt% with respect to HBFP) and PDMS (50 wt% with respect to HBFP) was prepared. The formulation was deposited on

the Interseal® 670 HS epoxy-based undercoat covered glass slides by airbrush application method. The overall wt% of each component was calculated and summarized in **Table 2.1**. The overall wt% of HBFP, PEG, and PDMS are 29%, 57%, and 14%, respectively.

Table 2.1. Overall wt% of each component in HBFP-PEG-PDMS terpolymer crosslinked network formed from 100 wt% HBFP, 200 wt% PEG, and 50 wt% PDMS.

	HBFP	**PEG**	**PDMS**
wt%	29	57	14

Microscope glass slides with Interseal® 670 HS epoxy-based undercoat and microscope glass slides with Interseal® 670 HS epoxy-based undercoat and terpolymer coating were cut so that the cross sections could be imaged by SEM (**Figure 2.3**). The thickness of Interseal® 670 HS epoxy-based undercoat and coating was measured using SEM images of the cross sections. The Interseal® 670 HS epoxy-based undercoat could be easily identified on SEM and was measured to be approximately 250 μm (**Table 2.2**). The terpolymer coating was measured to be approximately 1 μm. However, the differentiation of the Interseal® 670 HS epoxy-based undercoat and terpolymer coating was not apparent. Therefore, we have also deposited the terpolymer formulation on a naked microscope glass slide using the same airbrush techniques to formed terpolymer coatings and measured the thickness to be approximately 1 μm which was in agreement

to the measure thickness of the terpolymer coating on the Interseal® 670 HS epoxy-based undercoat.

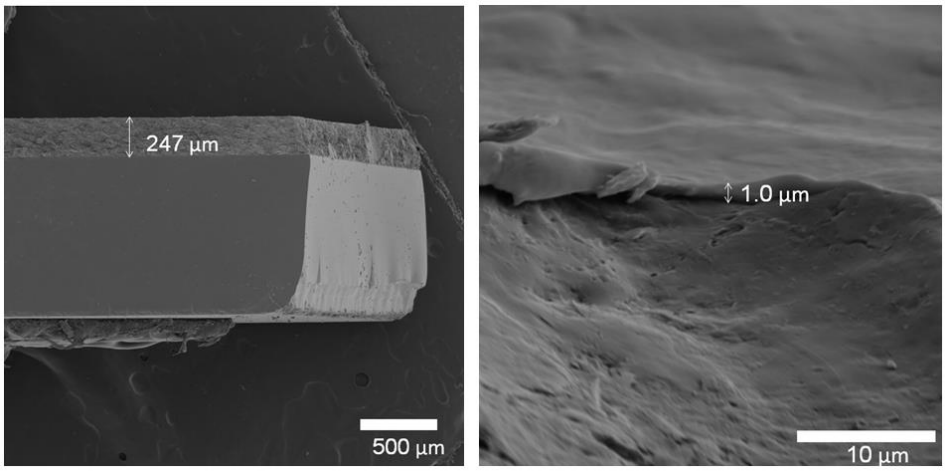

Figure 2.3. SEM image of Interseal® 670 HS epoxy-base undercoat on a microscope glass slide (left) and SEM image of terpolymer coating on Interseal® 670 HS epoxy base undercoat (right).

Table 2.2. Thicknesses of Interseal® 670 HS epoxy-base coating and HBFP-PEG-PDMS terpolymer coating.

Formulation	Thickness (µm)
Interseal® 670 HS epoxy-based undercoat	250 ± 2
HBFP-PEG-PDMS terpolymer coating	1.1 ± 0.4

The crosslinking efficiency and stability of the HBFP-PEG-PDMS terpolymer network are concerns since the overall wt% of PEG and PDMS in this network is much greater than in any of the previous networks that have been generated in our laboratory. Therefore, it was of our interest to investigate the crosslinking efficiency and stability of

the terpolymer network. A series of experiments was designed in which the HBFP-PEG-PDMS terpolymer networks were immersed in synthetic seawater for 0 d (dry), 1 d and 1 wk and were characterized by AFM, ATR-FTIR and tensiometer and the results were compared. The data from 0 d immersion and 1 d immersion would give information of any dynamic reorganization occurring during the one day synthetic sea water immersion and allow for chemicals such as DIPEA to leach out of the coating while the data from 1 wk immersion would provide preliminary data on the change in surface over a function of time.

AFM was used to investigate the surfaces of dry, 1 d immersed, 1 wk immersed, and Interseal® 670 HS epoxy-based undercoat (**Figure 2.4**). The Interseal® 670 HS epoxy-based undercoat prepared on a microscope glass slide by draw down method resulted in a surface with R_{rms} roughness of 110 nm. As the HBFP-PEG-PDMS terpolymer formulation was deposited on the Interseal® 670 HS epoxy-based undercoat, distinctive topographical features were apparent and the R_{rms} roughness was increased. The terpolymer coatings displayed a slight increase in R_{rms} roughness when immersed in synthetic water for 1 d and a slightly higher increase in R_{rms} roughness when immersed in synthetic seawater for 1 wk. Overall, the slight increase in R_{rms} roughness was insignificant and the increase in R_{rms} roughness could be due to remaining salt residues from the synthetic seawater.

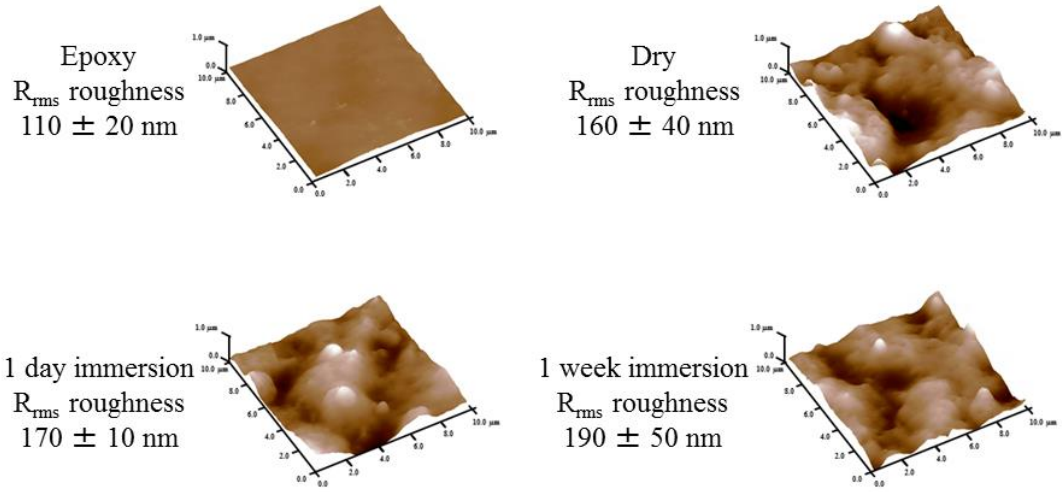

Figure 2.4. AFM images for Interseal® 670 HS epoxy-base undercoat (top left) and HBFP-PEG-PDMS terpolymer networks that were immersed in synthetic seawater for 0 d (top right), 1 d (bottom left), and 1 wk (bottom right). The average R_{rms} of three regions were reported with each image. Field of view for AFM renderings is 100 μm^2 with a 100 nm z-scale.

The terpolymer surfaces were analyzed with ATR-FTIR and the IR spectra of coatings when immersed in 0 d, 1 d, and 1 wk showed little to no changes in the functional groups of the coatings (**Figure 2.5**). The static water contact angle of coatings when immersed in 0 d, 1 d, and 1 wk also remained constant at approximately 105°. The minimal change in IR spectra and static water contact angle suggests that the coatings were stable for at least a week.

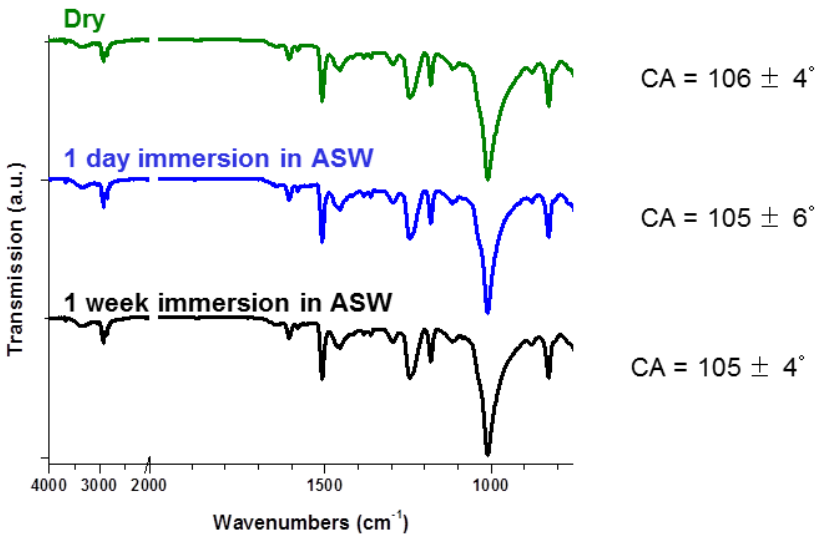

Figure 2.5. IR spectra of HBFP-PEG-PDMS terpolymer networks that were immersed in synthetic seawater for 0 d (top), 1 d (middle), and 1 wk (bottom). The average static water contact angles of nine regions per sample were also reported.

Soxhlet extraction using THF as solvent was also performed on the terpolymer coatings when immersed in 0 d, 1 d, and 1 wk to probe the stability and crosslinking of the terpolymer coatings (**Figure 2.6**). It is noted that the Interseal® 670 HS epoxy-base undercoat delaminates off the microscope glass slides and breaks into smaller pieces when immersed in THF. Therefore, the terpolymer coatings were prepared by drop cast method of the terpolymer formulation on microscope glass slides. The terpolymer was peeled off the microscope glass slides and cut into 1 cm x 1 cm pieces, weighed and subjected to Soxhlet extraction in THF. All coatings were still intact and resulted in a 10% mass loss after Soxhlet extraction. The solution containing the extracted contents was evaporated and the extracted contents were analyzed by ^{1}H NMR spectroscopy. There was no presence of HBFP, PEG, or PDMS in the extracted contents which

suggests that the polymers have had either formed a crosslinked network or have strong interactions with one another. A majority of extracted contents was identified to be butylated hydroxytoluene (BHT) which was an inhibitor included in the bottle of PFS. It was possible that BHT was trapped in the terpolymer network because of its low solubility in water, and it was only extracted during Soxhlet extraction in THF.[61]

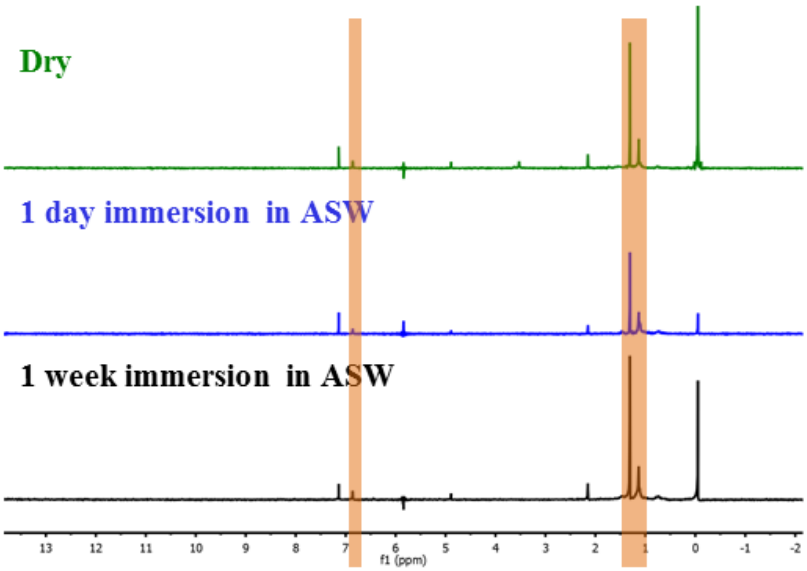

Figure 2.6. ^{1}H NMR spectra of extracted contents from Soxhlet extraction of HBFP-PEG-PDMS terpolymer networks that were immersed in synthetic seawater for 0 d (top), 1 d (middle), and 1 wk (bottom).

2.4 Conclusions

In order to further improve the anti-fouling properties of the HBFP-PEG-PDMS terpolymer coatings by increasing the amount of each polymer component or adding new polymer components, the stability and crosslinking efficiency of the higher

crosslinked HBFP-PEG-PDMS terpolymer coatings must be investigated. Experiments were designed to test for the stability and crosslinking efficiency of the HBFP-PEG-PDMS terpolymer coatings. HBFP was synthesized by ATR-SCVCP to afford bromoalkyl end groups that can be crosslinked with PEG and PDMS to produce HBFP-PEG-PDMS terpolymer coatings. The HBFP-PEG-PDMS terpolymer coating with the formulation of HBFP, PEG (200 wt% relative to HBFP), and PDMS (50 wt% relative to HBFP) was prepared on an Interseal® 670 HS epoxy-base undercoat to prevent delamination of the terpolymer coating from the microscope glass slide when immersed in water. The airbrush application allows for rapid preparation of minimal materials needed to coat the slide.

Stability of the HBFP-PEG-PDMS terpolymer coatings that were immersed in synthetic seawater for 0 d, 1 d, and 1 wk were investigated using AFM, ATR-FTIR and tensiometer and the data suggest that the terpolymer coatings were still stable after a week of immersion in synthetic seawater. Soxhlet extraction of the HBFP-PEG-PDMS terpolymer coatings that were immersed in synthetic seawater for 0 d, 1 d, and 1 wk confirmed that the coatings were stable after a week of immersion in synthetic seawater. The coatings that were immersed in synthetic seawater for 0 d, 1 d, and 1 wk were still intact after being subjected to Soxhlet extraction experiment with only 10% mass loss in which the majority of the mass loss was attributed to the loss of BHT.

The investigations in the crosslinking efficiency and stability of the HBFP-PEG-PDMS terpolymer coating with the formulation of HBFP, PEG (200 wt% relative to HBFP), and PDMS (50 wt% relative to HBFP) has confirmed that the coating is stable

with the increased linear polymer contents. This confirmation allows for more future modifications in the terpolymer formulation in order to improve the anti-fouling properties of the system.

CHAPTER III

CHARACTERIZATION AND ANTI-FOULING PERFORMANCES OF CROSSLINKED, FLUORINATED-ZWITTERIONIC-SILSESQUIOXANE TERNARY COATINGS[†]

3.1 Introduction

The majority of current anti-fouling treatments on ship hulls consists of the utilization of biocide formulations, in which copper oxide was chosen predominantly as the biocide.[62-64] However, the choice of using copper oxide as the biocide has been heavily criticized for posing detrimental effects similar to the recently banned TBT AF paints.[41,63-67] Instead of incorporating biocides in anti-fouling formulations to form ablative coatings, considerable efforts have been spent in investigating in non-ablative anti-biofouling coatings as an environmentally-benign ship hull coating.[14,38,68] In particular, amphiphilic polymeric systems that present a variation of chemical complexities, roughness, and energy on the surface have been explored and shown to prevent the settlement on marine organisms.[14,50,69-73]

Some of the most commonly used materials in amphiphilic systems include fluorinated polymers, siloxanes polymers, zwitterionic polymers, and PEG.[3,14,45,68,69,74-78] Our laboratory had well documented a highly complexed binary coating formed by

---

[†] In collaboration with Kevin A. Pollack,[‡] Eric D. Vavra,[‡] Samantha L. Kristufek,[‡] John Finlay,[†] Sofia C. Franco,[†] Nick Aldred,[†] Anthony S. Clare,[†] Karen L. Wooley,[‡] [†]School of Marine Science & Technology, Newcastle University, [‡]Departments of Chemistry, Chemical Engineering and Materials Science & Engineering, Texas A&M University

crosslinking hyperbranched fluoropolymer with PEG, in which the resultant HBFP-PEG coating undergoes dynamic reorganization when immersed in water presenting chemically complex composition and roughness on the surface.[46,48,57-60,79] To further increase the complexity in the system, a third component PDMS has been added into the binary system to form a terpolymer AF system of HBFP-PEG-PDMS.[50] Although the HBFP-PEG-PDMS terpolymer system has been shown to have great initial anti-fouling performances in both laboratory and field testing, the synthesis of HBFP involves multiple steps.[43] Therefore, there is a desire to explore other methods and chemistries to generate amphiphilic systems.

Thiol-ene click chemistry has been employed by many researchers as a robust and efficient method to couple materials together.[80-84] As amphiphilic zwitterionic surfaces have shown to have great anti-fouling performances, a novel amphiphilic ternary system consisting of silsesquioxane (POSS), amphiphilic fluorinated small molecule (AFSM) and zwitterionic small molecules (ZSM) has been designed.[43,85,86] The design involves utilizing thiol-ene click chemistry to form amphiphilic zwitterionic ternary networks with multi-functional thiol POSS and varying stoichiometric molar ratios of AFSM that possesses two alkene end groups and varying stoichiometric molar ratios of ZSM that has one alkene end group. Herein, we used thiol-ene click chemistry to form networks that combines the merits of both zwitterionic and amphiphilic properties. Previous studies were performed on a series of ternary coatings with different molar ratio of POSS, AFSM and ZSM prepared by drop cast method.[43] The studies provided information that increasing the amounts of zwitterions in the system

decreases the static water contact angle and compressive module value of the coatings. Previous in-house anti-fouling experiments with *Ulva* have also shown that the ternary coatings have potential for anti-fouling applications. Therefore, it is of our interest to be able to generate the coatings rapidly in a larger scale and study the anti-fouling properties against a wider range of marine organisms. The same series of ternary coatings were prepared by airbrush application and sent to collaborators at Newcastle University to probe the anti-fouling performances with *Ulva linza*, diatoms and barnacle cyprids.

3.2 Experimental Section

Materials

All chemicals and reagents were purchased from Sigma-Aldrich (St. Louis, MO) and used without further purification unless otherwise noted. PFS was purchased from Oakwood Chemical (West Columbia, SC) and filtered through neutral alumina to remove inhibitor prior to use. Thiopropyl T8/T10 silsesquioxane was purchased as a 1:1 mixture of isomers from Mayaterials Inc (Ann Arbor, MI). Microscope glass slides (75 mm x 25 mm x 1 mm) were purchased from VWR (Radnor, PA). Synthetic seawater was purchased from Ricca Chemical Company (Arlington, TX). Central Pneumatic mini air compressor with airbrush and hose (120 VAC/ 60 Hz, 1/5 HP, 1750 RPM, 30 PSI Working Air Pressure, Air Outlet: 1/8" – 27 NPT, Item 95830) were purchased from Harbor Freight Tools (Los Angeles, CA). Glascribe tungsten carbide tipped pen was purchased from Ted Pella, Inc (Redding, CA).

Nuclear Magnetic Resonance Spectroscopy

^{1}H NMR, ^{13}C NMR NMR and ^{19}F NMR spectra were recorded on a Varian Inova 300 (Varian Inc., Palo Alto, CA) interfaced to a UNIX computer using VnmrJ software. ^{1}H NMR and ^{13}C NMR were analyzed using the solvent signal as an internal reference.

High-resolution Mass Spectrometry

HRMS for the monomers was conducted on an Applied Biosystems PE SCIEX QSTAR.

Attenuated Total Reflectance-Flourier Transform Infrared Spectroscopy

ATR-FTIR spectra were recorded using an IR Prestige 21 system (Shimadzu Corp., Kyoto, Japan) attached with PIKE MIRacle™ ATR and diamond crystal and analysis was performed using IRsolution v. 1.40 software.

Scanning Electron Microscopy

SEM images were imaged using TESCAN VEGA3 SEM. All samples were sputter coated with either a 20 nm layer of gold or a 5 nm layer of 80% platinum/20% palladium. Samples were mounted perpendicular to the secondary electron detector using conductive carbon tape. Six replicates were imaged for each sample and the average and standard deviation of the thickness of the coating were reported.

Static Surface Water Contact Angle

Static contact angle of nanopure water was measured on nine areas per sample using the sessile drop technique on an Attension Theta optical tensiometer (Biolin Scientific, Stockholm, Sweden) and analysis was performed by fitting drops with a Young-Laplace formula using the Theta Software to calculate the average static contact

angles. Three replicate measurements were acquired for each sample and the average and standard deviation of the static water contact angle were reported.

Synthesis of 1,2-Bis(2-(2,3,5,6-tetrafluoro-4-vinylphenoxy)ethoxy)ethane

To a 500 mL three-necked round-bottom flask equipped with a magnetic stir bar was added 60 wt% sodium hydride dispersion in oil (2.66 g, 66.6 mmol). The flask was purged with N_2 and lowered into an ice bath. Into the flask was added dropwise THF (200 mL), followed by addition of a solution of triethylene glycol (4.00 g, 26.6 mmol) in THF (50 mL). PFS (15.5 g, 79.8 mmol) was then added dropwise into the solution. The solution was allowed to warm to room temperature and stirred for 16 h. The solution was concentrated *in vacuo* and the resulting oil was dissolved in dichloromethane (100 mL) before being washed with brine (3 x 100 mL). The organic fraction was dried with anhydrous $MgSO_4$, filtered and concentrated *in vacuo*. The product was isolated using flash chromatography with 10% methanol in dicloromethane as the eluent (yield: 65.7%). ^{1}H NMR (300 MHz, $CDCl_3$, ppm,): δ 6.62 (dd, *J* = 18 Hz and 12 Hz, 2H, ***H***(H)C=CH-R (*cis*)) , 6.03 (d, *J* = 18 Hz, 2H, H_2C=C***H***-R), 5.63 (d, *J* = 12Hz, 2H, ***H***(H)C=CH-R (*trans*)), 4.37 (t, *J* = 5 Hz, 4H, TFSOC***H₂***CH_2O), 3.83 (t, *J* = 5 Hz, 4H, TFSOCH_2C***H₂***O), 3.70 (s, *J* = 5 Hz, 4H, TFSOCH_2CH_2OOC***H₂***). ^{13}C NMR (75 MHz, $CDCl_3$, ppm): δ 146.1, 144.0, 142.1, 140.2, 136.5, 122.1, 110.7, 74.2, 71.0, 70.3. ^{19}F NMR (282 MHz, $CDCl_3$, ppm): δ -147 (m, Ar ortho- ***Fs***), -159 (m, Ar meta- ***Fs***). HRMS (m/z): calculated for $C_{22}H_{18}F_8O_4$ $[M+H]^+$ 499.11; found 499.1135. FTIR (cm^{-1}): 2941, 2875, 1869, 1739, 1697, 1647, 1485, 1454, 1427, 1406, 1365, 1354, 1330, 1290, 1246, 1151, 1118, 1078, 1030, 1018, 966, 931, 856, 783, 753, 711.

Synthesis of 3-(Dimethyl(vinyl)ammonio)propane-1-sulfonate

To a dry 250 mL round-bottom flask was added *N*,*N*-dimethylallylamine (10.0 g, 115 mmol), 1,3-propane sultone (17.2 g, 138 mmol) and acetone (100 mL). The solution was stirred for 14 h overnight. The product was collected by centrifugation and washed with acetone (100 mL). The product was dried *in vacuo* to afford a white powder (yield: 94%). ^{1}H NMR (300 MHz, $CDCl_3$, ppm,): δ 5.92 (dd, 1H, ***H***(H)C=CH-R (*cis*)), 5.62 (d, 2H, H_2C=C***H***-R, ***H***(H)C=CH-R (*trans*)), 3.92 (d, *J* = 7 Hz, 2H, CH_2=CHC***H₂***N), 3.34 (m, 2H, NC***H₂***CH_2CH_2S), 2.95 (s, 6H, (C***H₃***)$_2$-N), 2.83 (t, *J* = 7 Hz, 2H, CH_2C***H₂***S), 2.15 (m, 2H, NCH_2C***H₂***CH_2S). ^{13}C NMR (75 MHz, $CDCl_3$, ppm): δ 129.3, 124.2, 66.4, 62.0, 50.0, 47.3, 18.2. HRMS (m/z): calculated for $C_8H_{17}NO_3S$ $[M+H]^+$ 208.10; found, 208.0994. FTIR (cm^{-1}): 3030, 3010, 2970, 2230, 1649, 1485, 1465, 1448, 1431, 1419, 1398, 1348, 1321, 1292, 1238, 1203, 1180, 1134, 1111, 1064, 1033, 1006, 958, 933, 908, 844, 794, 763, 750, 655.

Silanization of Microscope Glass Slides

Microscope glass slides were cleaned in an ultraviolet (UV) ozone cleaner for 20 min. The slides were then soaked in a solution of allyltrimethylsilane (0.5 wt%) in 300 mL ethanol. The slides were then taken out of the solution and cured in an oven at 120 ºC for 18 h.

General Procedure for Application of Ternary Coating Formulation onto Silanized Microscope Glass Slides

To a 40 mL scintillation vial was added POSS (100 mg, 0.079 mmol), 1,2-bis(2-(2,3,5,6-tetrafluoro-4-vinylphenoxy)ethoxy)ethane (157 mg, 0.32 mmol), 3-

(dimethyl(vinyl)ammonio)propane-1-sulfonate (16 mg, 0.077 mmol), 2,2-dimethoxy-2-phenylacetophenone (DMPA) (54 mg, 0.21 mmol) 1,4-dioxane (9 mL) and water (1 mL). The mixture was vortexed for 1 min until all contents were dissolved. Double-sided tape was used to adhere silanized microscope glass slides on a piece of card board. The coating formulation was applied on the silanized microscope glass slides using an airbrush applicator with an application pressure of 50 psi from a distance of approximately 15 cm. Multiple airbrush passes were made over the slides with the applicator with a 1 min rest between every two passes until the solvent has evaporated. The coatings were then cured in a UV chamber at 365 nm for 3 h.

SEM Sample Preparation of Ternary Coatings on a Silanized Microscope Glass Slide to Measure Thickness of Coating

The coated slide of interest was submerged in liquid nitrogen until boiling was no longer observed. The sample was then rapidly removed from the liquid nitrogen with a pair of tweezers and sandwiched perpendicularly between two glass slides with the coated side of the sample facing the bottom glass slide. A Glascribe® tungsten carbide tipped pen was used to score the back of the coated slide using the top glass slide as a straight edge. A large pair of tweezers was used to gently tap and cleave the scored-off portion of the coated slide from the bulk coated slide. The previous process to this point was repeated until a sample of approximately 1cm x 1cm was obtained. The sample was placed in a light N_2 stream to remove any glass dust and particulates. All samples were sputter coated with either a 20 nm layer of gold or a 5 nm layer of 80% platinum/20% palladium. Samples were mounted perpendicularly to the secondary electron detector

using conductive carbon tape. The thickness of the each coating was measured at six different areas and the average and standard deviation were reported.

Biofilm Development to Study the Attachment of the Green Alga *Ulva linza* to Pristine and Biofilmed Coatings

Biofilms were cultured and visualized using similar methods as reported in the literature.[87] Pristine coatings were equilibrated for 2 h in 0.22 μm filtered artificial seawater immediately prior to testing while biofilmed coatings were immersed in natural seawater for 3 weeks during biofilm development. In order to develop biofilm on coatings, the coated glass slides were placed in clean glass dishes (10 per dish) and filled with course filtered natural seawater (200 mL). The dishes were incubated at room temperature on an orbital shaker at 50 rpm. The seawater was refreshed every 2 d over a three-week period. Bacterial cells were visualized by staining with the fluorescent stain Syto 13 (5 μM). Cell counts were made for 30 fields of view (each 0.15 mm^2) on each of three replicate slides.

Settlement of *Ulva linza* Zoospores

Zoospores were obtained from mature plants of *Ulva linza* by the standard method.[88] A suspension of zoospores (10 mL; $1x10^6$ spores mL^{-1}) was added to individual compartments of quadriPERM dishes containing the samples. After 45 min in darkness at 20 °C, the slides were washed by passing 10 times through a beaker of seawater to remove unsettled (*i.e.* swimming) spores. Slides were fixed using 2.5% glutaraldehyde solution in seawater. The density of zoospores attached to the surface was counted on each of the three replicate slides using an image analysis system attached

to a fluorescence microscope. Spores were visualized by autofluorescence of chlorophyll. Counts were made for 30 fields of view (each 0.15 mm^2) on each slide.

Growth of *Ulva Linza* Sporelings

Spores were allowed to settle on the coatings for 45 minutes and then washed by passing 10 times through a beaker of seawater to remove unsettled (i.e. swimming) spores. The spores were cultured using supplemented seawater medium for 7 d to produce sporelings (young plants) on 6 replicate slides of each treatment. Sporeling growth medium was refreshed every 48 h. Sporeling biomass was determined *in situ* by measuring the fluorescence of the chlorophyll contained within the sporelings in a Tecan fluorescence plate reader. Using this method the biomass was quantified in terms of relative fluorescence units (RFU). The RFU value for each slide is the mean of 70 point fluorescence readings taken from the central portion. The sporeling growth data are expressed as the mean RFU of 6 replicate slides; bars show standard error of the mean.

Strength of Attachment of *Ulva Linza* Sporelings

Strength of attachment of sporelings was assessed using an impact pressure of 175 kPa from a water jet sprayed across the central area of each slide. Sporeling biomass was determined *in situ* by measuring the fluorescence of the chlorophyll contained within the sporelings in a Tecan fluorescence plate reader. Using this method the biomass was quantified in terms of RFU. The RFU value for each slide is the mean of 70 point fluorescence readings taken from the central portion. The sporeling growth data are expressed as the mean RFU of 6 replicate slides; bars show standard error of the

mean. The percentage removal was calculated from readings taken before and after exposure to the water jet.

Biofilm Development to Study the Attachment of *Navicula Incerta* and *Balanus Amphitrite* to Pristine and Biofilmed Coatings

Biofilms were cultured and visualized using similar methods as reported in the literature.[87] Pristine coatings were equilibrated for 2 h in 0.22 μm filtered artificial seawater immediately prior to testing while biofilmed coatings were immersed in natural seawater for 3 weeks during biofilm development. In order to develop biofilm on coatings, coated glass slides were placed in clean glass dishes (10 per dish) and filled with course filtered natural seawater (200 mL). The dishes were incubated at room temperature on an orbital shaker at 50 rpm. The seawater was refreshed every 2 d over a three-week period. Bacterial cells were visualized by staining with the fluorescent stain Syto 13 (5 mM). Cell counts were made for 30 fields of view (each 0.15 mm^2) on each of 3 replicate slides.

Initial Attachment of Diatoms

Navicula incerta cells were cultured in F/2 medium contained in 250 mL conical flasks. After 3 d the cells were in log phase growth. Cells were washed 3 times in fresh medium before harvesting and diluted to give a suspension with a chlorophyll *a* content of approximately 0.25 μg/ml. Cells were settled on three pristine and three biofilmed coated slides of each sample in individual dishes containing 10 mL of suspension at ~20 $^{\circ}C$ on the laboratory bench. After 2 h the slides were exposed to 5 min of shaking on an orbital shaker (80 rpm) followed by a submerged wash in seawater to remove cells which

had not attached. Samples were fixed in 2.5% glutaraldehyde solution, air dried and the density of cells attached to the surface was counted on each slide using an image analysis system attached to a fluorescence microscope. Counts were made for 30 fields of view (each 0.15 mm^2) on each slide.

Strength of Attachment of Diatoms

Navicula incerta cells were cultured in F/2 medium contained in 250 mL conical flasks. After 3 d the cells were in log phase growth. Cells were washed 3 times in fresh medium before harvesting and diluted to give a suspension with a chlorophyll *a* content of approximately 0.25 μg/ml. Cells were settled on three pristine and three biofilmed coated slides of each sample in individual dishes containing 10 mL of suspension at ~20 $^{\circ}C$ on the laboratory bench. After 2 h the slides were exposed to 5 min of shaking on an orbital shaker (80 rpm) followed by a submerged wash in seawater to remove cells which had not attached. Slides with attached cells were exposed to a shear stress of 25 Pa in a water channel. Samples were fixed in 2.5% glutaraldehyde solution, air dried and the density of cells attached to the surface was counted on each slide using an image analysis system attached to a fluorescence microscope. Counts were made for 30 fields of view (each 0.15 mm^2) on each slide.

Barnacle Culture for Assays

Larvae were obtained from laboratory cultures of *Balanus amphitrite* (=*Amphibalanus amphitrite*). *B. amphitrite* adults were shipped from the Duke University Marine Laboratory at Beaufort, North Carolina and kept in aerated aquaria in full salinity (35 ppt) artificial seawater (Tropic Marin), filtered to 10 μm and UV-

sterilized. They were fed daily with *Artemia* sp. and *ad libitum* with the chlorophyte *Tetraselmis suecica*. To collect larvae, barnacles were removed from water overnight. On re-immersion, they released stage 1 nauplius larvae into the water and these were collected by attraction to a point light source. Larvae were removed in batches to temporary storage in a solution of *T. suecica*. Once 10, 000 larvae had been collected, they were transferred into 10 L buckets containing aerated artificial seawater. *B. amphitrite* larvae were fed throughout with *T. suecica* and took between 4-5 d to metamorphose into cyprids, at which point they were filtered through a 250 μm mesh and stored for 3 d at 6 °C prior to use in assays.

Barnacle Settlement Assays

Surfaces in Quadriperm plates were allowed to air dry briefly prior to the assay, in order to allow deposition of a water droplet onto each surface. A 1 mL drop of 0.22 μm-filtered artificial seawater was applied to each slide and 20 3-day-old larvae were introduced. Once all surfaces had larvae applied, the plates were closed and moved into a 28 ºC incubator. Cyprids were allowed to settle for 48 h in the dark before the assay was removed and numbers of settled larvae were counted under a light microscope. For analysis of settlement, numbers of settled larvae were expressed as a percentage of the total larvae per surface.

3.3 Results and Discussion

The ternary coatings were designed to be a three-component system consisting of POSS, AFSM, and ZSM. POSS was explored as the added hydrophobic component in order to enhance the mechanical robustness of the resulting ternary coating. POSS used

in this system was Thiopropyl T8/T10 silsesquioxane, which was a multifunctional resin containing an average of 9 thiol groups. The strategy here is to utilize thiol-ene click chemistry to covalently attach other alkene-containing compounds to the thiol groups of POSS efficiently under UV light (**Figure 3.1**). The AFSM and ZSM chosen for this ternary system were 1,2-bis(2-(2,3,5,6-tetrafluoro-4-vinylphenoxy)ethoxy)ethane and (Dimethyl(vinyl)ammonio)propane-1-sulfonate, respectively. Besides being an AFSM that contains both oligoethylene oxides and fluorines, 1,2-bis(2-(2,3,5,6-tetrafluoro-4-vinylphenoxy)ethoxy)ethane was selected because it possesses 2 alkene groups which allows for crosslinking with POSS to form a network. Furthermore, 1,2-bis(2-(2,3,5,6-tetrafluoro-4-vinylphenoxy)ethoxy)ethane was also a byproduct generated during the synthesis of HBFP as described in Chapter 2. The ZSM (dimethyl(vinyl)ammonio)propane-1-sulfonate increases the hydrophilicity of the ternary coatings and water bound on the zwitterionic units may deter settlement of marine organisms. Nucleophilic aromatic substitution was used to synthesize 1,2-bis(2-(2,3,5,6-tetrafluoro-4-vinylphenoxy)ethoxy)ethane from PFS and TrEG (**Figure 3.1-A**) while ring-opening of sultone was used to synthesize dimethyl(vinyl)ammonio)propane-1-sulfonate readily (**Figure 3.1-B**).

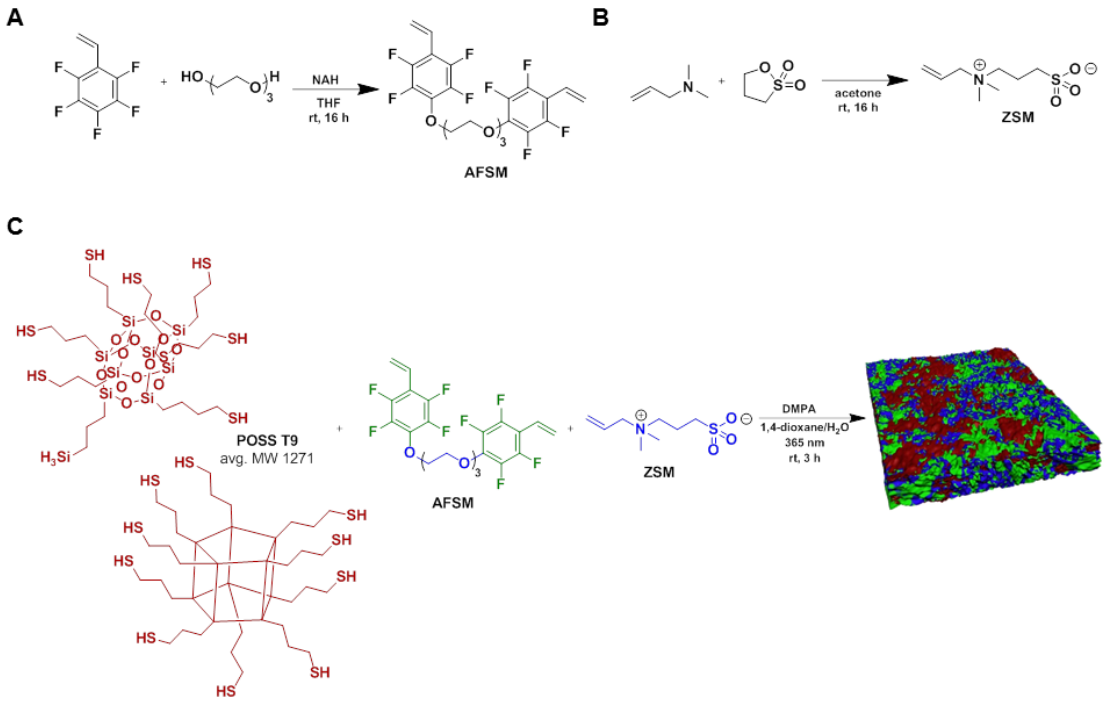

Figure 3.1. (A) Synthesis of AFSM. (B) Synthesis of ZSM. (C) Preparation of fluorinated-zwitterionic-silsesquioxane ternary coatings.

Four different types of coatings (A, B, C, D) with varying stoichiometric molar ratios (**Table 3.1**) of AFSM and ZSM were generated by airbrush application on alkene-silanized microscope glass slides. POSS was held constant while varying the molar ratio of AFSM and ZSM to POSS. Hypothetically, each AFSM molecule will covalently attach to 2 thiol groups *via* thiol-ene click chemistry. Thus the formulation to generate coating A, which contains no ZSM, consists of 4.5 molar equivalences of AFSM per molar equivalence of POSS. As the molar equivalences of ZSM increase as shown

going down **Table 3.1** from Coating A through D, the molar equivalences of AFSM also decrease.

Table 3.1. Molar equivalences of each component in the ternary coatings.

Coating	POSS (eq)	AFSM (eq)	ZSM (eq)
A	1	4.5	0
B	1	4	1
C	1	3.5	2
D	1	3	3

The deposition of the ternary coatings by airbrush application resulted in a thin layer of the coatings. Although the coatings were visible to the naked eye, it was difficult to assess the thickness of the coatings. Therefore, SEM was used to image the cross section of the ternary coatings and the thicknesses of the coatings were measured using the SEM images (**Figure 3.2**). The thicknesses of the coatings range from 0.2 μm to 1.3 μm, with Coating A having the thinnest coating and Coatings B, C, and D having similar thicknesses (**Table 3.2**). The thin coatings generated from Formulation A could attributed to Formulation A having the most AFSM and the increased crosslinking within the coating forming tighter, thinner coatings. The presence of zwitterionic moieties in Coatings B, C and D also allows for water molecules to be trapped within the networks, thus increasing the thicknesses of the coatings.

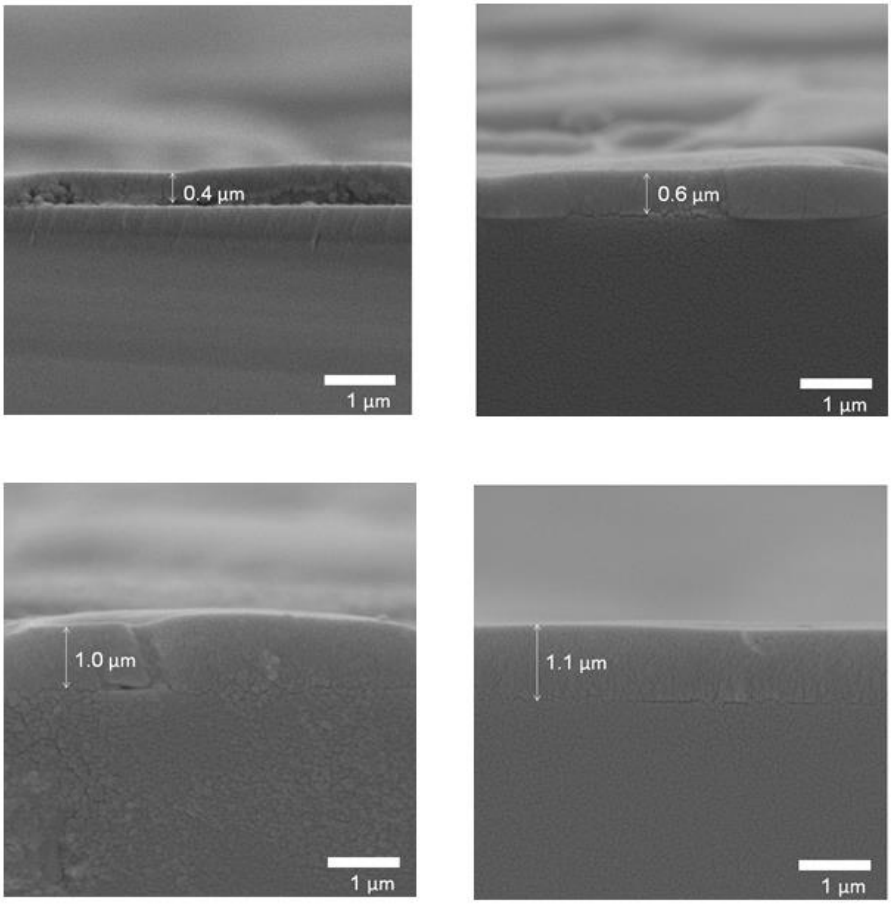

Figure 3.2. SEM images of ternary coatings A (top left), B (top right), C (bottom left) and D (bottom right). Double headed arrows on images were used to measure the thicknesses of coatings.

Table 3.2. Thicknesses of ternary coatings measured using SEM images.

Coatings	Thickness (µm)
A	0.5 ± 0.2
B	0.8 ± 0.1
C	1.0 ± 0.2
D	0.8 ± 0.2

Static water contact angle experiment was performed pre-water immersion and post-water immersion of the coatings to determine the wettability of the coatings (**Table 3.3**). Interestingly, while the water contact angles of the pre-immersed coatings followed an increasing trend as the amount of ZSM increased from Coatings A-C, Coating D had the highest water contact angle. No specific trend in water contact angle of the post-water immersed coatings was observed. Coatings A and B also showed minimal change while Coatings C and D exhibited a change in static water contact angle between the dry and water-swollen states. The increase in zwitterionic moieties in the coatings could attribute to this observation as the zwitterionic moieties could attract water molecules within the coatings causing dynamic surface reorganization.

Table 3.3. Summary of static water contact angle data for all coatings pre-water and post-water immersion. Nine areas per coating were measured.

Coating	Pre-Water Immersion	Post-Water Immersion
A	64 ± 4º	64 ± 8º
B	57 ± 7º	57 ± 7º
C	54 ± 8º	62 ± 5º
D	76 ± 9º	70 ± 5º

The anti-fouling and fouling release performances of the ternary coatings were investigated with the following three marine organisms: *Ulva linza*, *Navicula incerta*, and *Balanus amphitrite*. Colonization of a new surface has been reported to occur in 4

phases over an overlapping time sequence: biochemical conditioning, bacterial colonization, unicellular and, finally, multicellular eukaryont fouling.[30] Bacteria and their biofilms can also influence fouling in various ways, in which some will enhance settlement, some will inhibit settlement and some will have no effect.[89] With a mixed biofilm, the tendency is towards increasing settlement with increasing biofilm content. Therefore, it was in our interest to investigate how the presence of a biofilm on the ternary coatings influences the settlement and adhesion of fouling organisms on the ternary coatings.

Biofilms were developed on ternary coatings in order to study the fouling behavior of *Ulva* on biofilmed *vs.* pristine ternary coatings. The cell density of biofilms on the ternary coatings could not be evaluated due to autofluorescence of the ternary coatings. Cell counts made on the glass slides indicated a bacterial density of 2466 cells / mm^2 (standard error 88 cells / mm^2). Biofilms were composed mostly of single cells interspersed with small colonies.

Spore settlement density of *Ulva linza* was increased on all coatings by the presence of bacteria and the conditioning layer that had developed on their surfaces (**Figure 3.3**). Spore settlement density on the ternary coatings was lower than on silanized glass and unmodified glass surfaces. This indicates that the bacteria and conditioning film that developed on the glass surfaces were highly attractive to the spores. On the ternary coatings, either the type of bacteria/conditioning film or the density of the layer was not sufficient to show this effect. Either way, the implication is that the ternary coatings were more resistant to the effects of the biofilm than the

silanized glass and unmodified glass surfaces. Biomass generation (**Figure 3.4**) on all coatings broadly reflected the spore settlement densities described above (**Figure 3.3**). Sporeling growth appeared normal on all coatings with no signs of toxicity (**Figure 3.5**).

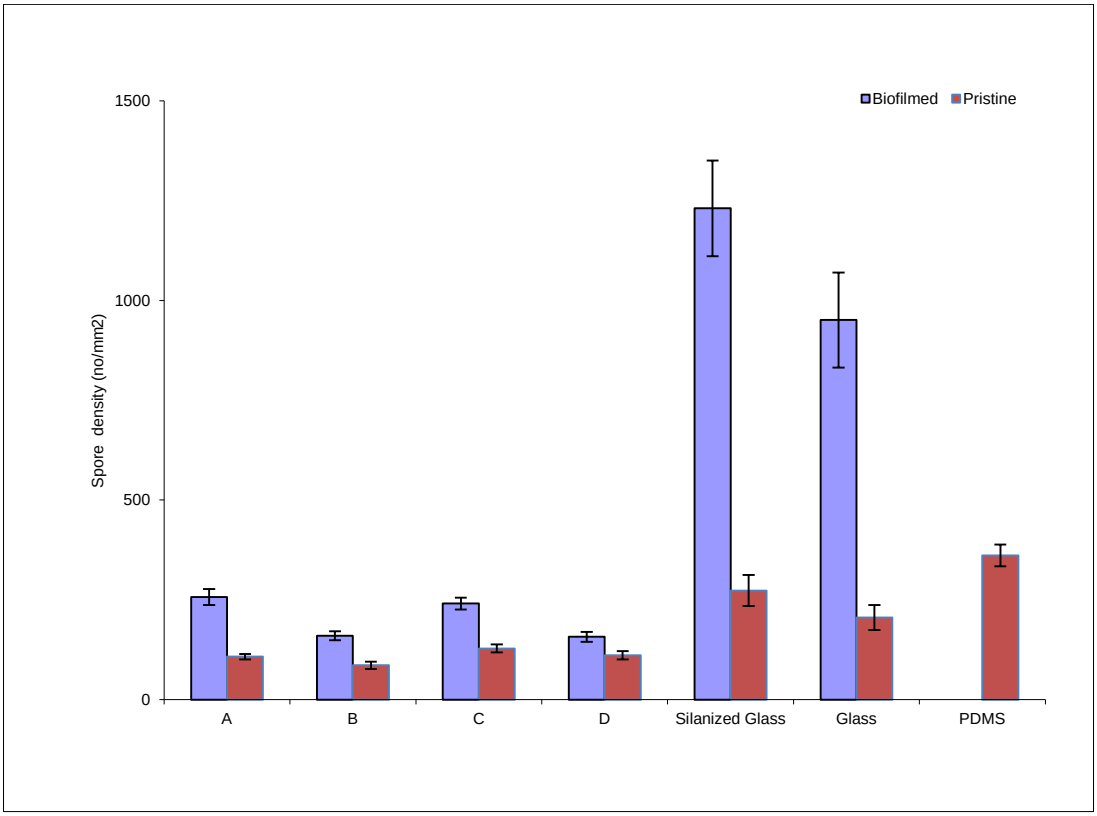

Figure 3.3. The densities of attached spores on biofilmed and pristine ternary coatings after 45 minute settlement. Each point is the mean from 90 counts on 3 replicate slides. Bars show 95% confidence limits.

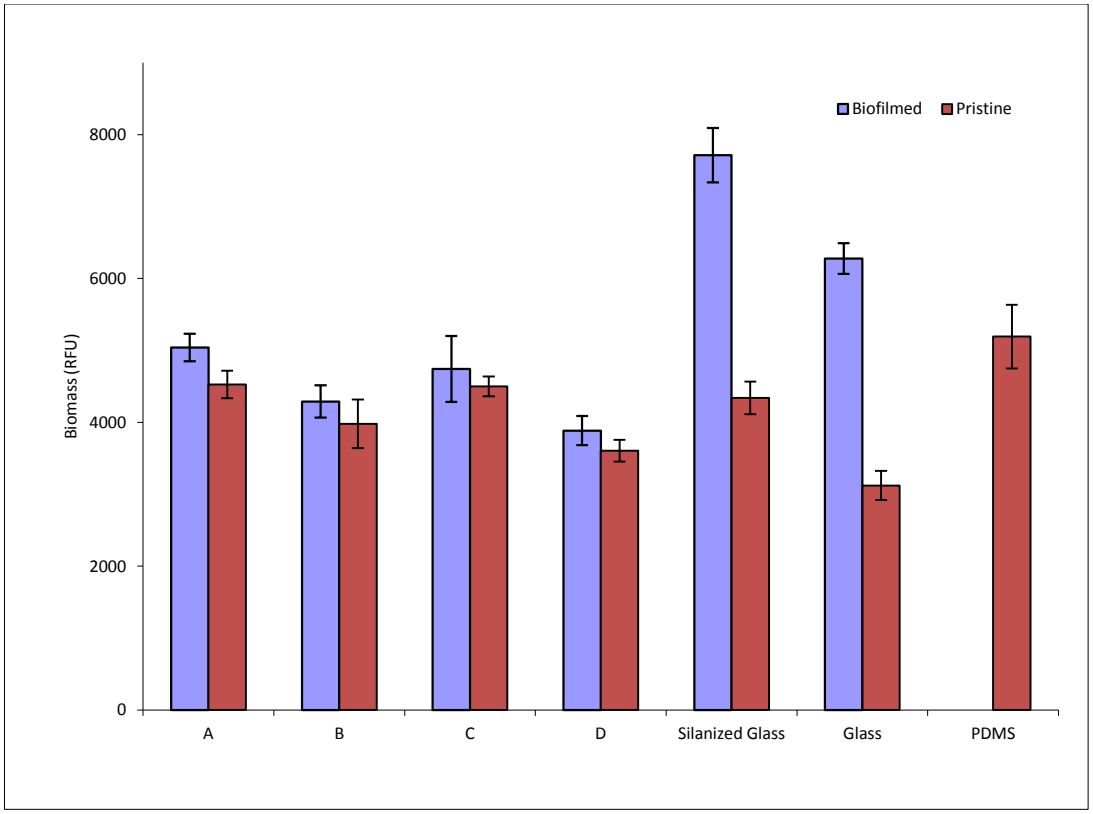

Figure 3.4. The biomass of sporelings cultured on biofilmed and pristine ternary coatings after 7 days. Each point is the mean biomass from 6 replicate slides measured using a fluorescence plate reader. Bars show standard error of the mean.

Figure 3.5. Image showing typical growth of *U. linza* sporelings on ternary coatings after 7 days. Top row biofilmed; Bottom row pristine. From left: A, B, C, D, E, Glass, PDMS.

Sporelings were strongly attached to all the ternary coatings and a water jet impact pressure of 175 kPa was required to remove approximately 50% of them. In comparison, removal of sporelings from the PDMS was near total at this pressure and the same level of removal would likely have been achieved at a lower impact pressure (typical impact pressure to remove sporelings from PDMS would be 50 kPa).[87] The percentage removal of sporelings was broadly similar among all the biofilmed ternary coatings (**Figure 3.6**). However, on the pristine surfaces removal was greater in the A and B coatings than the C and D coatings. On coating D, there was greater removal from the biofilmed coating than from the pristine coating, suggesting that the presence of bacteria and conditioning film were enhancing release from this surface. Sporeling removal from the glass and silanized glass was generally lower than from the ternary

coatings. The quantity of biomass remaining on the biofilmed glass and silanized glass was considerably higher than on the pristine surfaces (**Figure 3.7** and **Figure 3.8**). The results suggest that the settlement and adhesion strength of *Ulva linza* on the biofilmed ternary coatings is lower than that of biofilmed glass. Although removal of sporelings was not performed on biofilmed PDMS, Miezakin and coworkers have reported that the % removal of pristine PDMS is at least 4 times greater than of biofilmed PDMS.[87]

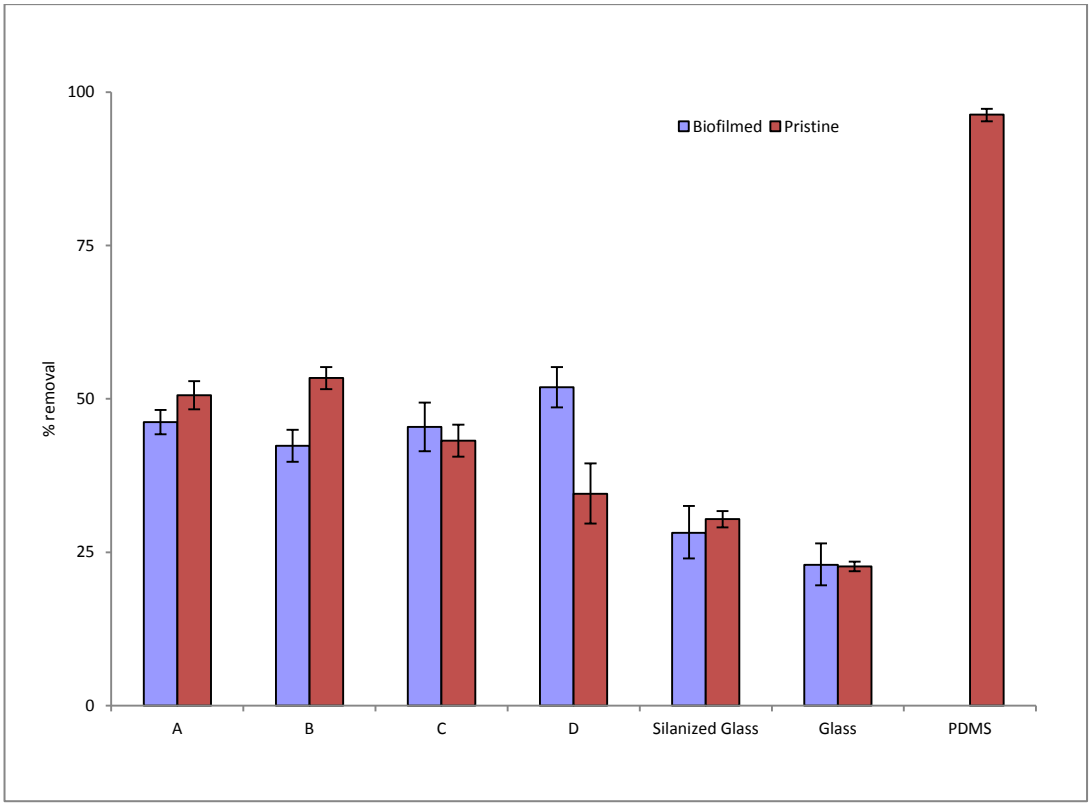

Figure 3.6. Percent removal of 7 day old sporelings from biofilmed and pristine ternary coatings due to an impact pressure of 175 kPa. Each point is the mean removal of biomass from 6 replicate slides measured using a fluorescence plate reader. Bars show standard error of the mean derived from arc-sine transformed data.

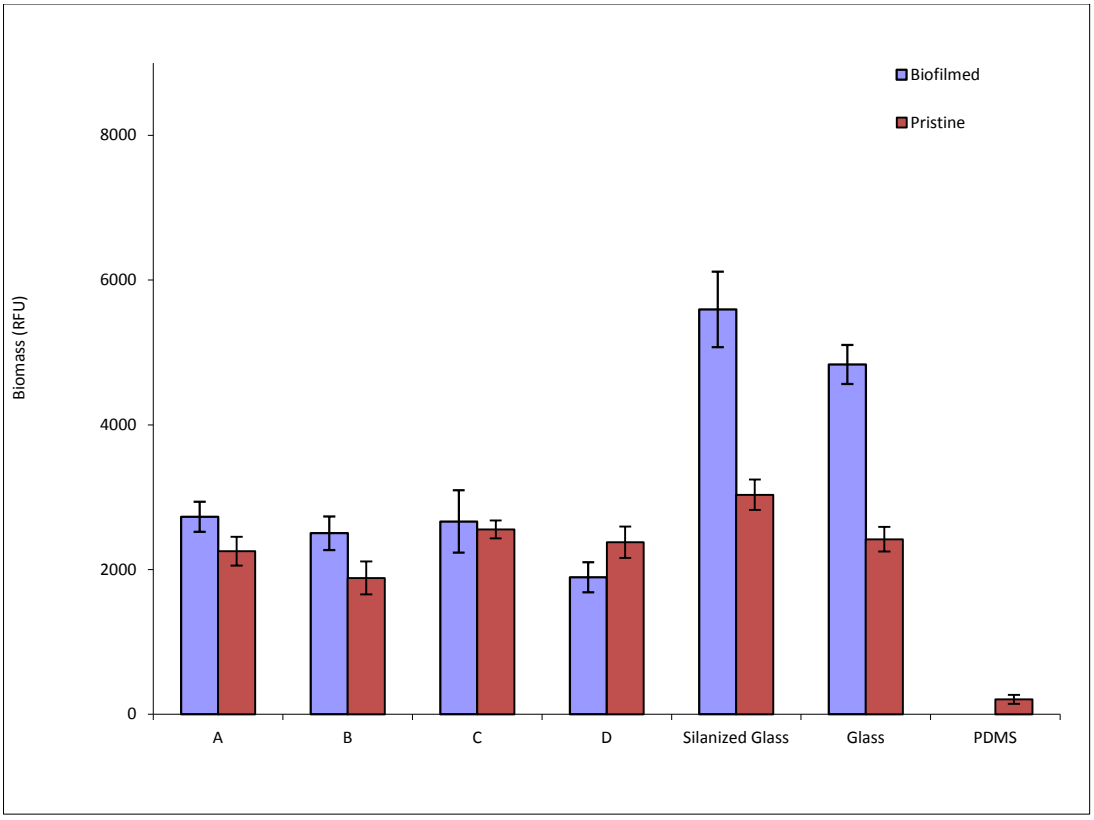

Figure 3.7. The biomass of sporelings remaining on biofilmed and pristine ternary coatings due to an impact pressure of 175 kPa. Each point is the mean biomass from 6 replicate slides measured using a fluorescence plate reader. Bars show standard error of the mean.

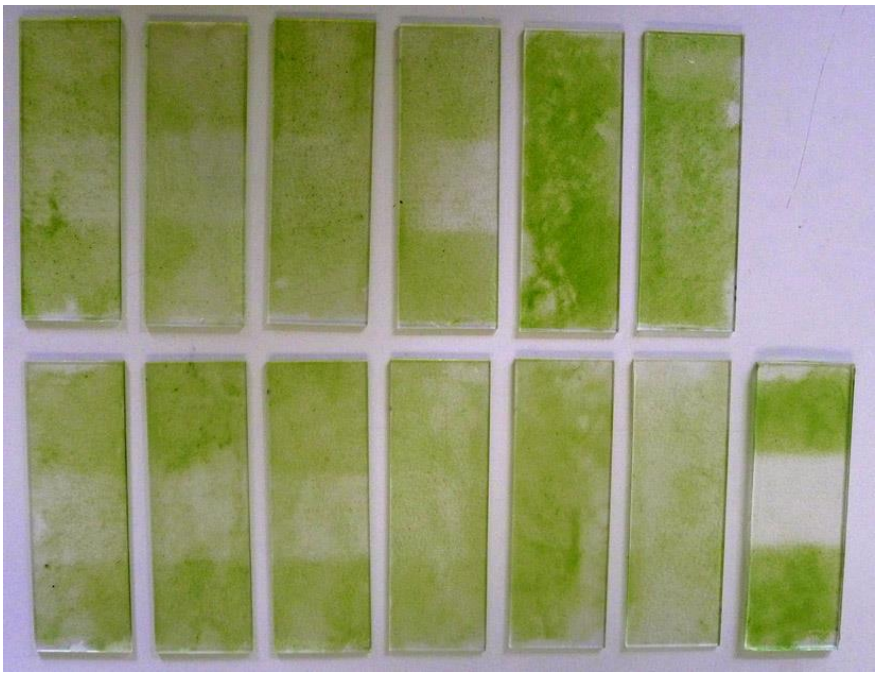

Figure 3.8. Image showing typical removal of *U. linza* sporelings from ternary coatings after exposure to a water jet inpact pressure of 175 kPa. Top row biofilmed; Bottom row pristine. From left: A, B, C, D, E, Glass, PDMS.

Biofilms were developed on ternary coatings in order to study the fouling behavior of diatoms and barnacle cyprids on biofilmed *vs.* pristine ternary coatings. The cell density of biofilms on the ternary coatings could not be evaluated due to autofluorescence of the ternary coatings. Cell counts made on the glass slides indicated a bacterial density of 12298 cells / mm^2 (standard error 391 cells / mm^2). Biofilms were composed mostly of single cells interspersed with small colonies.

Diatoms sink in the water column and land on the coating surfaces by gravity. Therefore, before washing, the cell densities on all the test surfaces are the same, irrespective of chemistry. The process of washing removes unattached and weakly attached cells; and thus, differences in initial attachment density reflect differences in the

ability of cells to attach firmly to the surfaces and resist the hydrodynamic forces of washing. The initial attachment densities of diatoms were similar on all test coatings (**Figure 3.9**).

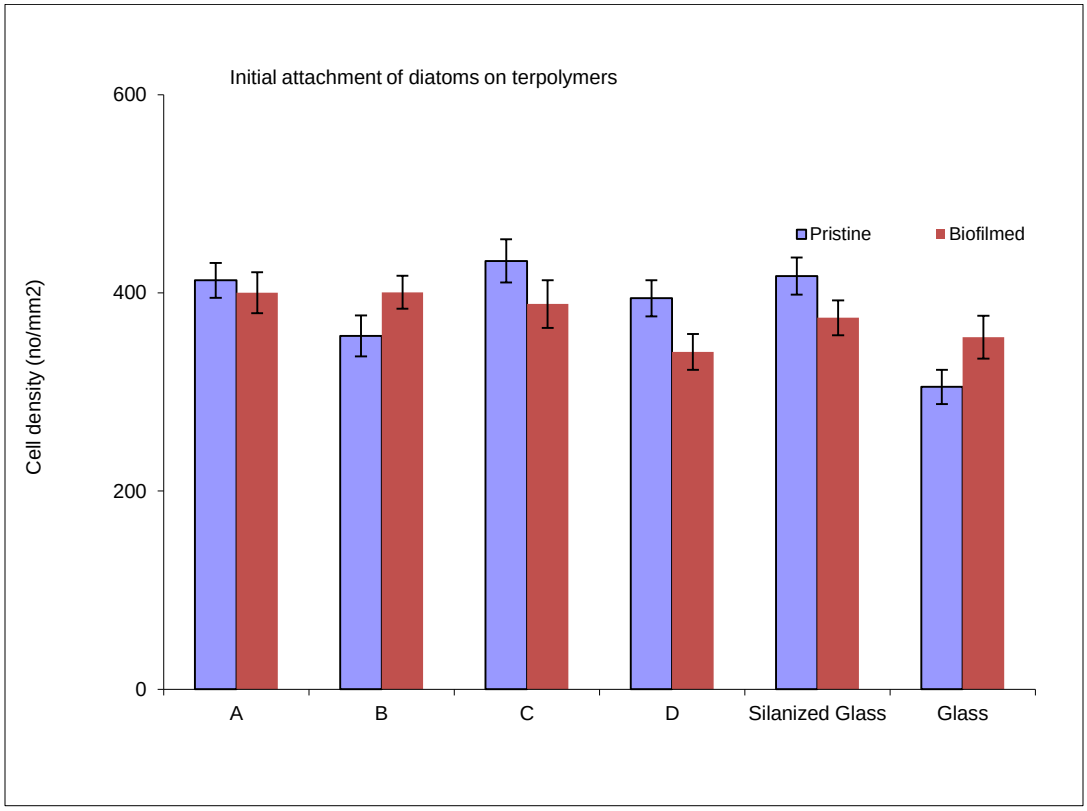

Figure 3.9. The densities of attached *N. incerta* on the test coatings after washing i.e. initial attachment densities. Each point is the mean from 90 counts on 3 replicate slides. (Except for biofilmed C which was 60 counts from 2 slides). Bars show 95% confidence limits.

Diatom removal due to a shear stress of 25 Pa did not vary greatly (36-54%) between ternary coatings irrespective of biofilm presence (**Figure 3.10**). Removal was of a similar magnitude to that of the glass standard. On the pristine surfaces a trend in

removal, increasing from A-C, was observed. On the silanized glass, removal was much lower (6%) from the pristine surface than from the biofilmed surface (64%). The density of diatoms remaining on the ternary coatings is shown in **Figure 3.11**. Cell densities were broadly similar among all coatings except for the pristine silanized glass slide, on which the diatom density was higher.

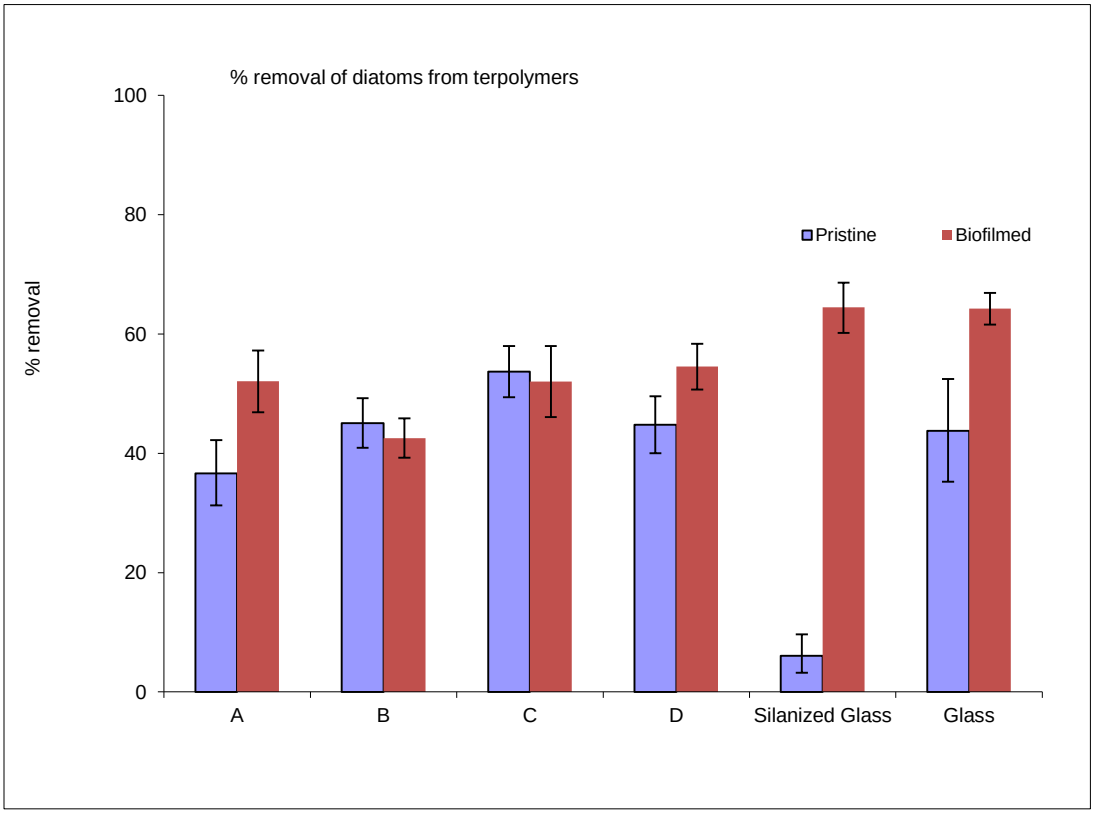

Figure 3.10. The removal of *N. incerta* from the test coatings due to exposure to a shear stress of 25 Pa. Each point is the mean from 90 counts on 3 replicate slides. Bars show 95% confidence limits derived from arc-sine transformed data.

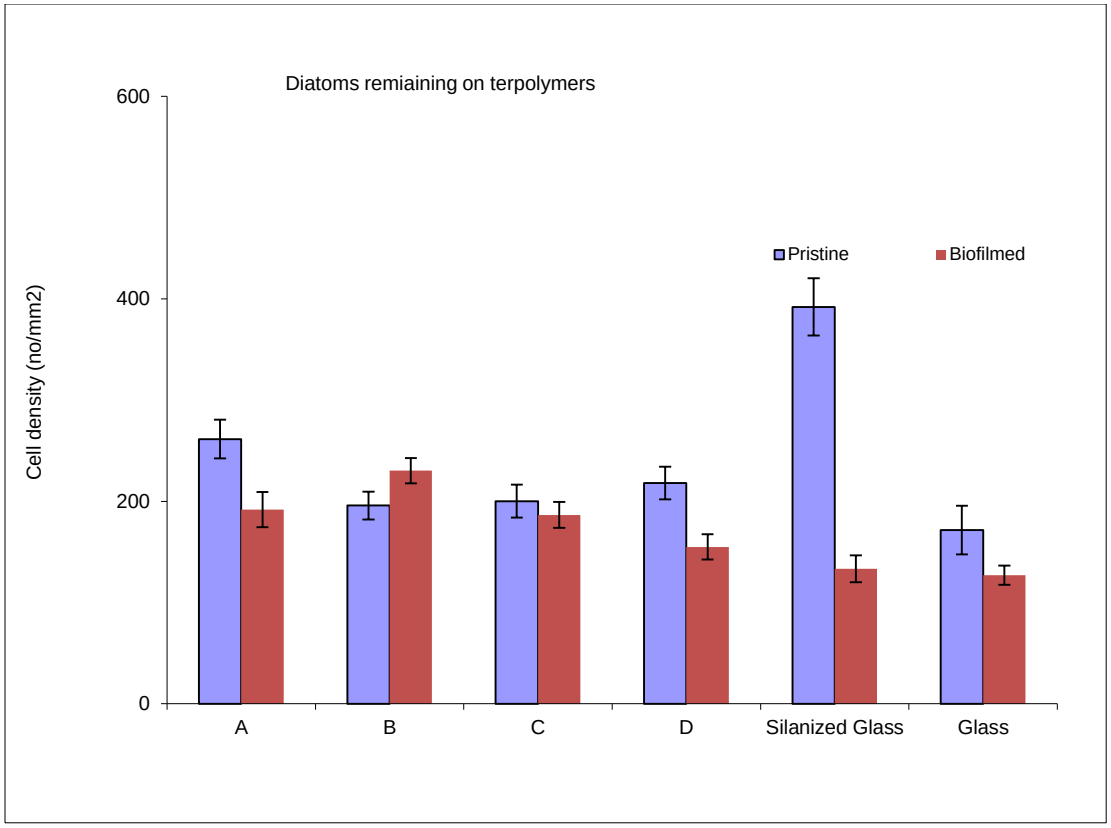

Figure 3.11. Final densities of attached *N. incerta* on the test coatings after washing and exposure to a shear stress of 25Pa. Each point is the mean of 90 counts on 3 replicate slides. Bars show 95% confidence limits.

As for barnacle assay, barnacle settlement was uniformly high across the range of ternary coatings with no effect of differing composition within the range tested (**Figure 3.12**). All ternary coatings received higher settlement than the silanized glass control in both the pristine and biofilmed condition. The presence of a biofilm on the surface did not, therefore, affect the settlement of this species of barnacle.

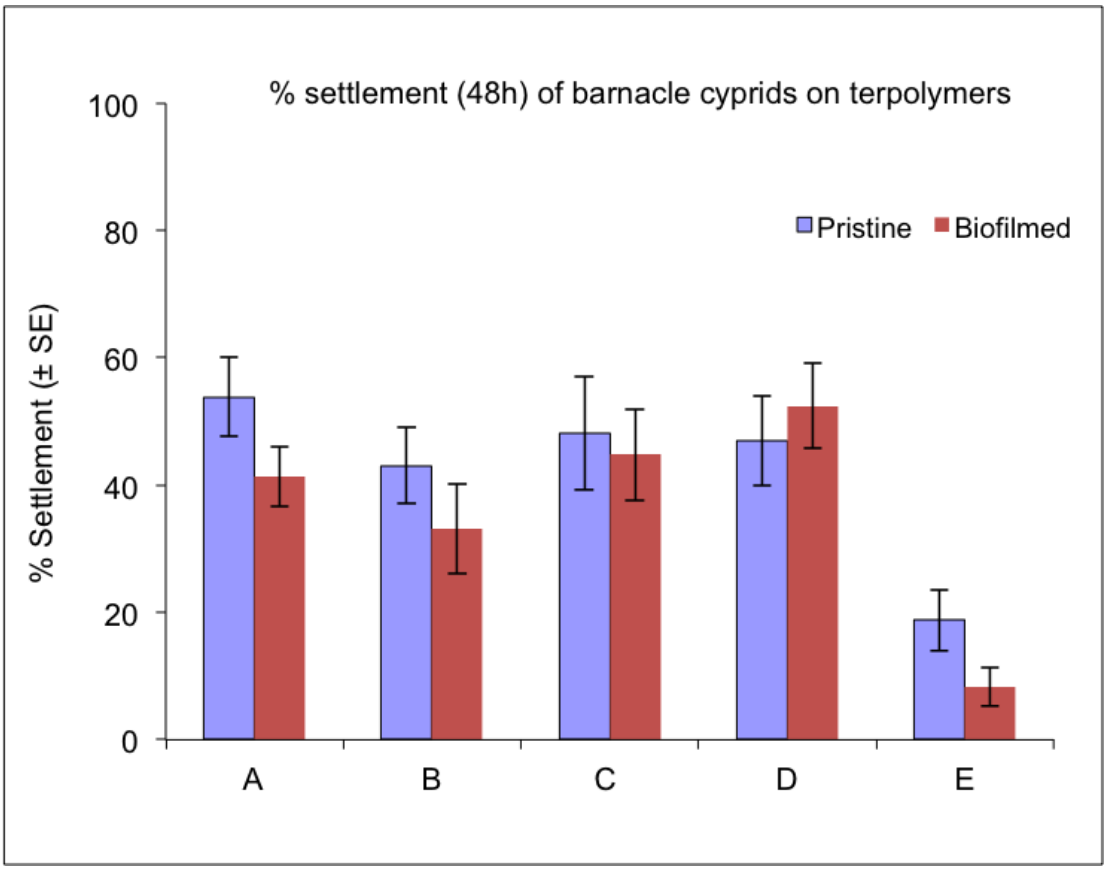

Figure 3.12. 48 h settlement of *B. amphitrite* cyprids on ternary coatings (A-D) and the silanized glass (E) control (n = 10).

3.4 Conclusions

Thiol-ene click chemistry, a simple and efficient chemistry, has been employed to generate a series of amphiphilic zwitterionic ternary coatings with different molar equivalences of AFSM and ZSM components. Airbrush applicator was used to deposit the formulations on silanized microscope glass slides rapidly with less materials being used than if the coatings were prepared by drop cast method. Coatings were cured under UV light without having to use elevated temperatures in order for crosslinking to take

place. The thicknesses of the coatings were measured to be in a range of 0.5 to 1.0 μm with Coating A being the thinnest coating.

Spore settlement density of *Ulva linza* was increased on all coatings with the presence of the biofilm. Spore settlement density on the ternary coatings was lower than on silanised glass and unmodified glass surfaces. Sporeling adhesion strength was high on all the pristine ternary coatings compared to that on the pristine PDMS standard coating. However, no such conclusion could be made on the biofilmed surfaces. Sporeling removal from the ternary coatings was not greatly affected by the presence of the biofilm.

Diatom removal from the ternary coatings was not greatly affected by the presence of the biofilm. Diatom removal from the ternary coatings was similar to that from the glass standard, while diatom removal from the silanised glass was higher from the biofilmed surface than on the pristine surface. Barnacle cyprid settlement density on the ternary coatings (A-D) was not affected by the presence of the biofilm. Barnacle cyprid settlement density on the silanised glass (E) was lower than on the ternary coatings (A-D). Overall the experiment did not show any major differences in the ternary coating performance with either diatoms or barnacle cypris larvae. Furthermore, the anti-fouling studies against all the fouling organisms demonstrated that the biofilm or conditioning layer makes a huge difference in the anti-fouling performance of the amphiphilic zwitterionic ternary coatings. Future anti-fouling assays should definitely be performed on both biofilmed and pristine coatings in order to understand how the coatings performed in a "real world" *vs.* laboratory environment.

Although the amphiphilic zwitterionic ternary systems do not display enhanced anti-fouling performances against the tested organisms, the coatings could still be used against other fouling organisms that have not been tested or even in other anti-fouling applications. The coatings could also be improved by varying the molar equivalences or even the chemical identity of each component in the system. Our studies show that there is still significant work to do to improve the amphiphilic zwitterionic ternary system.

CHAPTER IV

FACILE SYNTHESIS OF A PHOSPHORYLCHOLINE-BASED ZWITTERIONIC AMPHIPHILIC COPOLYMER FOR ANTI-BIOFOULING COATINGS[‡]

4.1 Introduction

Biofouling is a persistent global problem detrimental to the shipping industry from both economical and environmental standpoints.[90,91 92] The U.S. Navy alone, which accounts for less than half a percent of the world's shipping industry, spends $180M-$260M USD per year in fuel and hull cleaning costs due to fouling.[22] Additionally, fouling poses a significant threat to the environment as invasive organisms on ship hulls are transported into foreign waters creating ecological imbalances.[34] In the 1960s, marine paints containing TBT were used to combat biofouling through leaching of the TBT from the paint.[37] Although the strategy to incorporate organotin additives into marine paints was highly effective in resisting biofoulers, it has also been extremely harmful to the marine wildlife.[93] Cuprous oxides have also been used as an anti-biofouling agent but still pose similar detrimental effects to the marine environment.[41] The introduction of toxic agents into marine paints has led to criticisms of the usage of biocide additives and has resulted in the eventual banning of TBT by the IMO.[39] The

---

[‡] "Reprinted with permission from "Facile Synthesis of a Phosphorylcholine-based Zwitterionic Amphiphilic Copolymer for Anti-biofouling Coatings" by Kellie Seetho, Shiyi Zhang, Kevin A. Pollack, Jiong Zou, Jeffery E. Raymond, Edgar Martinez, Karen L. Wooley. *ACS Macro Letters*, **2015**, *4*, 505-510, DOI: 10.1021/mz500818c. Copyright 2015 by The American Chemical Society."

lack of non-toxic and effective alternatives to these toxic organotin and cuprous oxides calls for immediate attention, targeting more efficient and environmentally-benign solutions to combat biofouling.

Polymeric materials have been investigated heavily as environmentally-benign anti-biofouling replacements for ship hull coatings to reduce fuel consumption, hull cleaning costs, and the invasion of non-indigenous species.[3,17,23,94] A number of polymers has been explored as anti-biofouling coatings including hydrophobic polymers, such as silicone elastomers[23] and fluoropolymers,[94] hydrophilic polymers, such as PEG[17] and zwitterionic polymers.[3] Although the various polymers display anti-biofouling characteristics, with silicone elastomers and fluoropolymers already commercialized as non-toxic anti-biofouling coatings, there remains a drawback using single component systems as many biofoulers release glycoprotein adhesives that have a higher affinity to either a hydrophobic or hydrophilic surface.[14,43] Hence, amphiphilic polymer coatings with optimal nanoscale heterogeneity of hydrophilic domains, usually PEG, and hydrophobic domains have been investigated and demonstrated by several groups in the field to be more effective anti-biofouling coatings than only a single polymeric component.[14,50,95-97] Furthermore, zwitterionic polymer coatings have shown promising anti-biofouling characteristics due to a hydration layer formed around the zwitterionic polymers through electrostatic interactions and hydrogen bonding that are both energetically and kinetically unfavorable for proteins to disrupt.[3,4,98-100] Although several amphiphilic and zwitterionic systems are currently being investigated as nontoxic anti-biofouling coating replacements, individually, few systems incorporate

zwitterions as the hydrophilic component in an amphiphilic design.[100,101] Herein, we present a novel strategy that utilizes simple chemistry to modify a commercially-available polymer and then grafts it onto a substrate to form an amphiphilic polymer coating, in which the hydrophilic component is composed of zwitterionic units.

4.2 Experimental Section

Materials

(*N*,*N*-Dimethylaminopropyl)trimethoxysilane (96%), poly(styrene-*co*-allyl alcohol) (SAA) (M_w ~2,200 Da, M_n ~1,200 Da, allyl alcohol 40 mol% as labeled), trimethylamine (99%), triethylamine (TEA) (99%), glutaraldehyde solution (25%) were used as received from Sigma-Aldrich Company (St. Louis, MO). Tetrahydrofuran (THF) and *N*,*N*-dimethylformamide (DMF) were purchased from Sigma-Aldrich Company (St. Louis, Mo) and dried through a column purification system (J.C. Meyer Solvent Systems, Inc.) before use. *N,N,N',N'*-Tetramethyl-1,4-butanediamine and chloro-2-oxo-1,3,2-dioxaphospholane (COP) (95%) were used as received from TCI America (Portland, OR). Microscope glass slides (75 mm x 25 mm x 1 mm), petri dishes, and disposable polymethyl methacrylate (PMMA) cuvettes were purchased from VWR (Radnor, PA). Nanopure water (18 MΩ·cm) was acquired by means of a Milli-Q water filtration system, Millipore Corp. (St. Charles, MO). Sylgard® 184 silicone elastomer kit was purchased from Dow Corning (Midland, MI). Albumin from bovine serum (BSA), Alexa Fluor® 488 conjugate was purchased and used as received from Life Technologies Corp. (Carlsbad, CA). Phosphate buffered saline (PBS) (1X, 0.0067M (PO_4)) solution was used as received from Thermo Scientific (Waltham, MA).

Alga-Gro seawater medium was received and used as from Carolina Biological Supply Company (Burlington, NC). High 1-bulb output fluorescent grow light fixture (ViaVolt, 2 ft.) was purchased from Home Depot (Atlanta, GA). *Ulva* was purchased from Gray St. Aquatics (Tampa, FL) and allowed to grow in Alga-Gro seawater medium under the fluorescence grow light fixture with a schedule of 16:8 h light to dark cycle. Nylon net filters (20 μm) were purchased from EMD Millipore Corporation (Billerica, MA). Synthetic seawater was purchased from Ricca Chemical Company (Arlington, TX) and filtered through a 20 μm nylon net filter.

Nuclear Magnetic Resonance Spectroscopy

^{1}H NMR, ^{13}C NMR and ^{31}P NMR spectra were recorded on a Varian Inova 300 or Mercury 300 spectrometer (Varian Inc., Palo Alto, CA) interfaced to a UNIX computer using VnmrJ software. Chemical shifts were referenced to the solvent resonance signals.

Thermal Analysis

TGA was performed under Ar atmosphere using a Mettler-Toledo model TGA/DSC1 Star^{e} system (Mettler-Toledo, Inc., Columbus, OH), with a heating rate of 10 °C/min. Measurements were analyzed by using Mettler-Toledo STAR^{e} v. 7.01 software. Glass transition temperatures (T_g) were measured by DSC on a Mettler-Toledo DSC822^{e} (Mettler-Toledo, Inc., Columbus, OH), with cooling and heating rates of 10 °C/min. Measurements were analyzed using Mettler-Toledo STAR^{e} v. 7.01 software. The T_g was taken as the midpoint of the inflection tangent, upon the second heating scan.

Attenuated Total Reflectance-Flourier Transform Infrared Spectroscopy

ATR-FTIR spectra were recorded using an IR Prestige 21 system (Shimadzu Corp., Kyoto, Japan) attached with PIKE MIRacle™ ATR and diamond crystal and analysis was performed using IRsolution v. 1.40 software.

X-ray Photoelectron Spectroscopy

XPS spectra were recorded on a Kratos Axis Ultra imaging XPS system with a monochromatic aluminum X-ray source that has 10 mA current, 12 kV voltage. Three replicate measurements were acquired for each sample and the average and standard deviation of the elemental composition on the surface were reported.

Film Thickness

Duratool digital caliper was used to measure the thickness of glass and the thickness of glass with coatings attached at three different regions. Film thickness was calculated by subtracting the measurement of glass from the measurement of glass with coatings and the average was reported. Three replicate measurements were acquired for each sample and the average and standard deviation of the thicknesses of the coatings were reported.

Surface Zeta Potential

Surface zeta potential analysis was completed using Beckman Coulter Delsa^{TM}Nano C that uses Doppler Electrophoretic Light Scattering Analysis (DELSA) and the Flat Surface Zeta Potential sample cell. Specially engineered beads suspended in 10 mM NaCl were used to monitor their mobility under an electric field of 60 V and influenced by the surface charge of the samples. Three replicate measurements were

acquired for each sample and the average and standard deviation of the zeta potential were reported.

Static Surface Water Contact Angle

Static contact angles of nanopure water droplets were measured on 3 areas per sample using the sessile drop technique on an Attension Theta optical tensiometer (Biolin Scientific, Stockholm, Sweden) and analysis was performed by fitting drops with a Young-Laplace formula using the Theta Software to calculate the average static contact angle. Nine replicate measurements were acquired for each sample and the average and standard deviation of the static water contact angle on the surface were reported.

Atomic Force Microscopy

AFM images were taken with MFP-3D-BIO system (Asylum Research, Santa Barbara, CA) under ambient conditions in air using standard silicon tips (VISTA probes, T190 - 25, resonance constant: 190 kHz, tip radius: ~ 10 nm, spring constant: 48 N/m). Three replicates were imaged for each sample and the average and standard deviation of R_{rms} roughness and ΔA^2 were reported.

Ultraviolet-visible Spectroscopy

Ultraviolet-visible (UV-vis) absorption measurement was performed using a UV-2550 system (Shimadzu Corp., Kyoto, Japan). Measurements were performed in synthetic seawater in PMMA cuvettes with path lengths of 1 cm.

Fluorescence Imaging

Fluorescence imaging was performed through a 10× objective on an Olympus IX70 inverted microscope equipped with a mercury arc lamp and an Olympus DP72 digital camera. All fluorescence imaging was performed with the same optics set (Olympus U-MNIBA3 filter cube with excitation: 470-495 nm and emission: 510-550 nm), collection time and CCD gain in order to compare from frame-to-frame.

Confocal Imaging

Confocal imaging was performed on an Olympus FV 1000 system laser scanning confocal microscope operating with a 10× objective and a 635 nm excitation source. Fluorescence collection occurred under identical excitation/collection regimes, with a 640 nm clean-up long pass filter and a 655-755 nm band pass filter (B-band chlorophyll emission). To account for topographic features of both the surfaces and the organisms, identical z-stacks over a 150 μm depth were averaged for each sample. Relative fouling extent was determined by average pixel intensity, referenced to an unfouled surface.

Silanization of Glass Substrates

Microscope glass slides were cut into 1 cm × 1 cm substrates with a glass cutter. The glass substrates were immersed into 20 wt% sodium hydroxide (NaOH) solution for 12 h, washed with nanopure water and then ethanol and dried with N_2. The substrates were cleaned under UV/ozone for 20 minutes, washed with nanopure water and ethanol, and dried under inert atmosphere. The cleaned substrates were submerged in a 5 wt% solution of (*N*,*N*-dimethylaminopropyl)trimethoxysilane in ethanol for 3 h, washed with ethanol, dried with N_2 and stored *in vacuo* at 100 °C for 12 h.

Synthesis of Poly(styrene-*co*-allyl phospholane) (SAP)

A solution of 2-chloro-2-oxo-1,3,2-dioxaphospholane (COP) (2.72 g, 9.09 mmol) in THF (30 mL) was added dropwise to a stirring solution of poly(styrene-*co*-allyl alcohol) (SAA) (2.00 g, 0.17 mmol) and TEA (0.70 mL, 1.2 mmol) in THF (10 mL) at 4 °C. The reaction mixture was allowed to stir for 1 h at 4 °C before filtration. The filtrate was washed saturated sodium bicarbonate solution (3 x 10 mL) and precipitated in anhydrous diethyl ether (3 x 50 mL). The precipitate was collected and dried *in vacuo* at room temperature (yield: 93%). The resulting solid was stored in a desiccator under vacuum until further use. ^{1}H NMR (300 MHz, $CDCl_3$, ppm,): δ 7.41-6.48 (b, styrenyl ***Hs***), 5.39-3.55 (b, $CH_2C\boldsymbol{H_2}OP$, $OC\boldsymbol{H_2}C\boldsymbol{H_2}O$), 2.52-0.52 (br, $C\boldsymbol{H_2}C\boldsymbol{H}R$ aliphatic backbone ***Hs***). ^{13}C NMR (75 MHz, $CDCl_3$, ppm,): δ 145.8, 128.6, 126.3, 69.3, 68.2, 66.2, 40.6, 34.3, 25.9, 15.7. ^{31}P NMR (121 MHz, $CDCl_3$, ppm, δ): 17. FTIR (cm^{-1}): 3150-2850, 1600, 1493, 1286, 1024, 928, 864, 839, 758, 700. DSC: T_g = 58 °C. TGA in Ar: 30-200 °C, 0% mass loss; 200-300 °C, 14% mass loss; 300-400 °C, 55% mass loss; 400-500 °C, 62% mass loss; 38% mass remaining above 500°C.

General Procedure for Preparation of Amphiphilic Zwitterionic Coatings on Silanized Glass Substrates

N,N,N',N'-tetramethyl-1,4-butanediamine (TMBD) (0 mmol, 0.021 mmol and 0.041 mmol for nominally 0%, 25%, and 50% crosslinked coatings, respectively) was mixed with a solution of poly(styrene-*co*-allyl phospholane) (SAP) (50 mg, 0.028 mmol) in DMF (1 mL) and vortexed for 30 s. 80 µL of the vortexed mixture was drop casted onto silanized glass slides and placed in an oven at 70 °C under N_2 for 4 h. The slides

were lightly rinsed with DMF before being immersed in a solution of DMF containing excess trimethylamine at 70 °C for 24 h. The slides were then rinsed in DMF and dried *in vacuo* at 70 °C for 12 h.

Preparation of Sylgard® 184 on Glass Substrates

Sylgard® 184 elastomer kit comes in 2 components: base and curing agent. The 2 components were mixed slowly in a 10:1 volume ratio of base to curing agent without bubble formation. The mixed formulation (0.2 mL) was dropped at the center of a clean glass substrate. The mixed formulation was applied onto the glass substrate by spin coating at 4000 rpm for 60 s. The substrates were then cured at 100 °C for 35 min.

Adsorption of Biomacromolecules

All substrates were equilibrated in PBS solution for 12 h and dried under N_2. The freshly equilibrated surfaces were imaged in fifteen different areas by wide field fluorescence microscopy to generate intensity histograms of the fluorescence background. The surfaces were then covered in a 0.5 mg/mL solution of BSA, Alexa Fluor® 488 conjugate in PBS for 1 h in the dark before being lightly rinsed and dried in the dark under a light flow of N_2. The same areas were imaged again by wide field fluorescence microscopy under identical imaging settings pre-exposure to BSA to measure the fluorescence of the post-BSA-incubated substrates. The changes in emission intensities of the surfaces pre- and post-BSA-incubation were calculated by converting all compiled pixels of the images into intensity histograms.

Ulva Zoospores Settlement

Ulva alga was dried with paper towels and allowed to stand overnight in the dark at 4 °C to promote the release of zoospores. The *Ulva* zoospores were then suspended into synthetic seawater by submerging the *Ulva* alga in synthetic seawater. The synthetic seawater containing both the *Ulva* alga and zoospores was then pass through 20 µm nylon net filters to filter out *Ulva* alga. The filtrate consisting of the zoospores was collected and further diluted with synthetic seawater to an OD_{600} of 0.24. All substrates were equilibrated in synthetic seawater for 12 h and dried under N_2. For each type of substrate, three replicates were equilibrated in synthetic seawater for 12 h. Z-stacked confocal fluorescence images were taken in five different regions of three replicates per sample to generate intensity histograms of the fluorescence background. The substrates were placed in a polystyrene petri dish and 7 mL of the prepared zoospores suspension was added into each petri dish. All substrates were incubated in the zoospores suspension for 3 h in the dark before being rinsed lightly with synthetic seawater. The replicates fixed with 2.5% glutaraldehyde solution and rinsed lightly with nanopure water. Z-stacked confocal fluorescence images were taken of the exposed zoospore surfaces under identical imaging settings as pre-incubation in zoospores suspension and the resultant intensity histograms were compiled together and used for quantification of the autofluorescence of chlorophyll present in the zoospores.

Ulva Zoospores Growth

Ulva alga was dried with paper towels and allowed to stand overnight in the dark at 4 °C to promote the release of zoospores. The *Ulva* zoospores were then suspended

into synthetic seawater by submerging the *Ulva* alga in synthetic seawater. The synthetic seawater containing both the *Ulva* alga and zoospores was then pass through 20 µm nylon net filters to filter out *Ulva* alga. The filtrate consisting of the zoospores was collected and further diluted with synthetic seawater to an OD_{600} of 0.24. All substrates were equilibrated in synthetic seawater for 12 h and dried under N_2. For each type of substrate, three replicates were equilibrated in synthetic seawater for 12 h. The substrates were placed in a polystyrene petri dish and 7 mL of the prepared zoospores suspension was added into each petri dish. All substrates were incubated in the zoospores suspension for 3 h in the dark too let zoospores settle on the substrates before being rinsed lightly with synthetic seawater. The three replicates of each substrate were then incubated in Alga-Gro seawater medium for 5 d with a light to dark cycle of 16:8 h and a change in Alga-Gro seawater medium every 2 d.

4.3 Results and Discussion

Our strategy to develop a simple chemical approach to produce an amphiphilic zwitterionic polymer coating from a commercially-available polymer employed poly(styrene-*co*-allyl alcohol) (SAA) copolymer, which is widely used in inks and paints, and involved the installation of reactive cyclic phosphotriester functionalities to allow for incorporation of zwitterionic groups, covalent attachment to a substrate and crosslinking reactions (**Figure 4.1-C**). Even when purchased in small research quantities, this functional copolymer is relatively inexpensive, <$200/kg. The randomly-distributed reactive hydroxyl groups on SAA were allowed to undergo reaction with 2-chloro-2-oxo-1,3,2-dioxaphospholane (COP) (**Figure 4.1-A)** under basic conditions to

form poly(styrene-co-allyl phospholane) (SAP) copolymer, while the hydrophobic styrenyl groups were left unmodified to be used to create hydrophobic domains on the surfaces of the coatings. The highly-reactive phosphotriester is able to react readily with tertiary amines to form phosphorylcholine (**Figure 4.1-B**), which was deliberately chosen in our system because phosphorylcholine mimics the chemical structure of the outer cell membrane and has been shown to resist protein adhesion more readily than other zwitterions, such as sulfobetaines.[19,102-106] This chemistry permits the covalent incorporation of various functionalities or enhancement of crosslinking through the modification of the R group on the tertiary amine. Similarly, substrates functionalized with tertiary amine can also allow the attachment of the polymer onto the substrate without the use of adhesives.

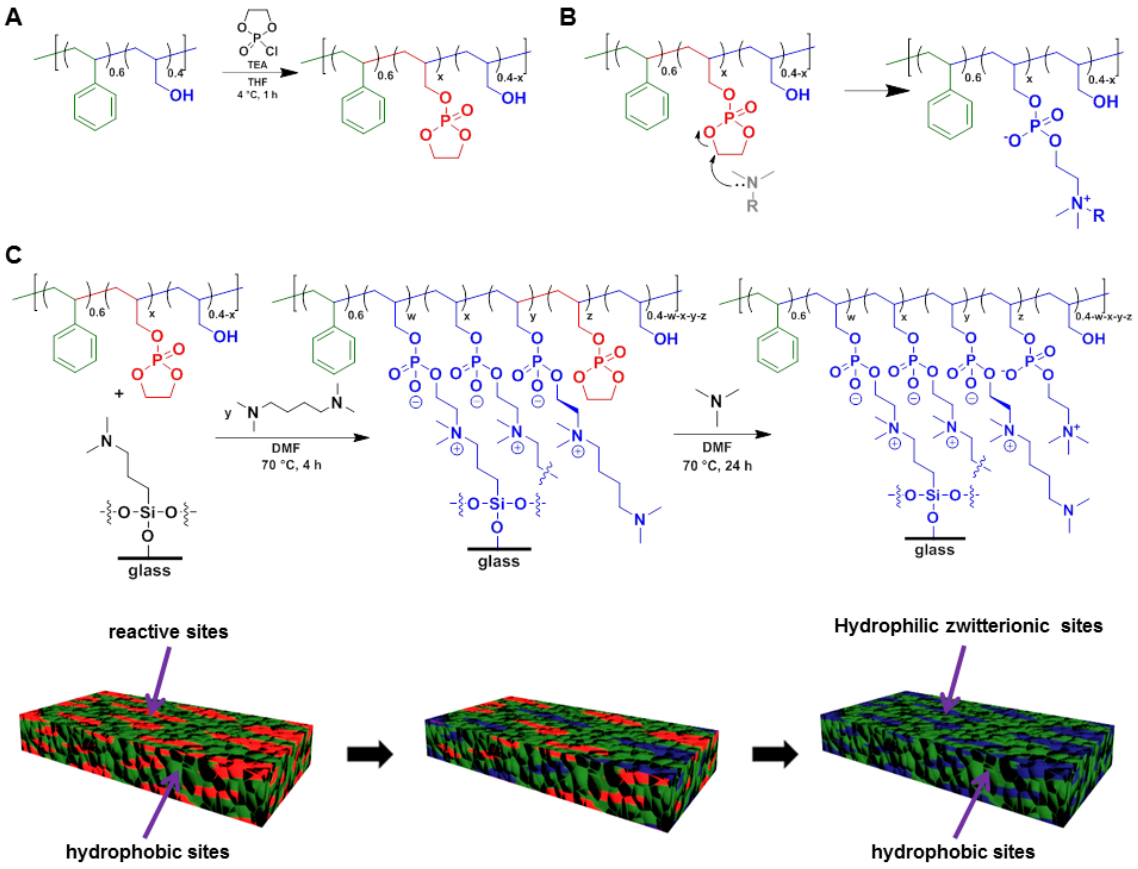

Figure 4.1. (A) Synthesis of SAP from SAA. (B) Mechanism for the ring opening of the phosphotriester units upon attack by a tertiary amine. (C) Schematic illustration of the preparation of different extents of crosslinked amphiphilic anti-biofouling coatings on silanized substrates that present sterically non-hindered tertiary amines on the surface.

Silanization of microscope glass slides was performed by first basifying the slides with sodium hydroxide solution, followed by silanization of the slides with (*N*,*N*-dimethylaminopropyl)trimethoxysilane. The silanization of the glass slides was confirmed by the change in static water contact angle of the surface of the slides at each step of the silanization process. The average static water contact angle of the surface

decreased from 45 ± 2° to <10° upon basification and increased to 58 ± 1° after silanization (**Figure 4.2**).

Figure 4.2. Static water contact angle of regular glass slide (left), basified glass slides (center), and silanized glass slide (right). (i) indicates the process of being immersed in 20 wt% NaOH solution and (ii) indicates the process of being silanized.

SAA was converted into SAP with high yield through a one-step esterification reaction with COP in the presence of TEA (**Figure 4.1-A**), followed by simple filtration and washing. The resonance frequencies of the methylene protons of the hydroxymethyl functionalities shifted downfield upon formation of the cyclic phosphotriester side chain functionalities, however, there was significant overlap overlap with the proton signals of the five-membered rings, which prevented quantitative determination of the extent of reaction by ^{1}H NMR spectroscopy (**Figure 4.3**). ^{13}C NMR spectroscopy allowed for confirmation that the reaction had proceeded, by having some level of distinction of the downfield-shifted methylene carbon signals, resonating broadly at 69-70 and 70-74 ppm), relative to the five-membered ring carbons (61-68 ppm), however, the starting hydroxymethyl methylene carbon signals overlapped (62-64 and 64-69 ppm), again, preventing quantitative determination of the extent of conversion of the hydroxyl methyl groups to cyclic phosphotriester moieties (**Figure 4.4**). Although ^{1}H and ^{13}C NMR

spectra could not be used to ascertain complete conversion of the alcohol units in SAA to phosphotriester units in SAP, the disappearance of the infrared absorbance band associated with the hydroxyl stretch at 3100-3500 cm^{-1} in SAP suggested that most of the alcohols were converted to phosphotriester units (**Figure 4.5**). ^{31}P NMR spectra shows the appearance of one 1 peak at 16.7 ppm for the SAP which was assigned to the phosphorous on the cyclic phosphotriester sidechain. The presence of only one peak also indicated that the cyclic phosphotriester is stable under ambient conditions and that any side products containing phosphorous formed from the reaction has been removed from the product during purification (**Figure 4.6**).

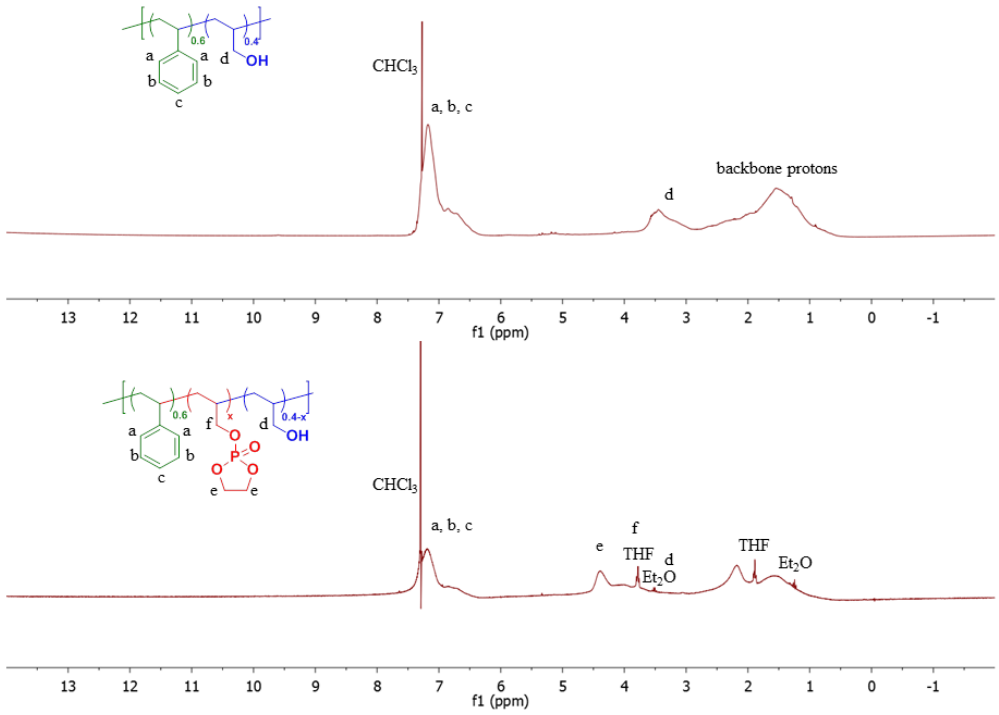

Figure 4.3. ^{1}H NMR spectra (300 MHz) of SAA (top) and SAP (bottom) in $CDCl_3$ (ppm).

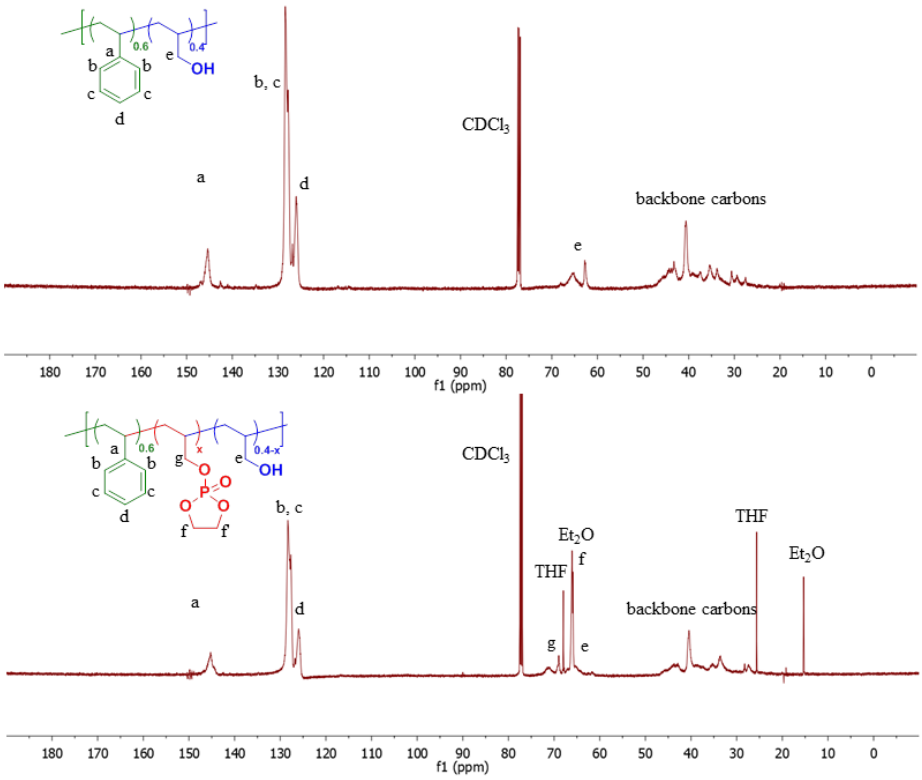

Figure 4.4. ^{13}C NMR spectra (75 MHz) of SAA (top) and SAP (bottom) in $CDCl_3$ (ppm).

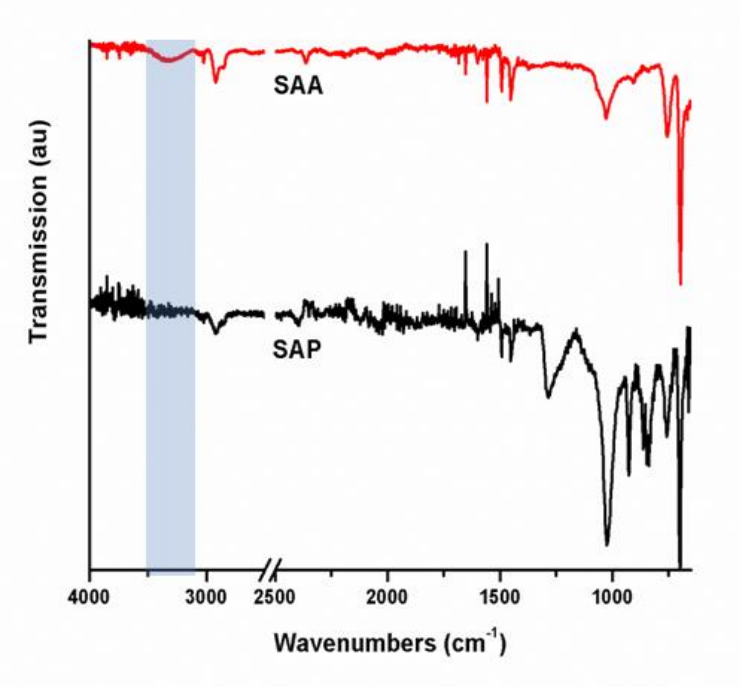

Figure 4.5. IR spectra of SAA and SAP. The blue shaded region suggested the disappearance of the peak associated with hydroxyl stretch from SAA to SAP.

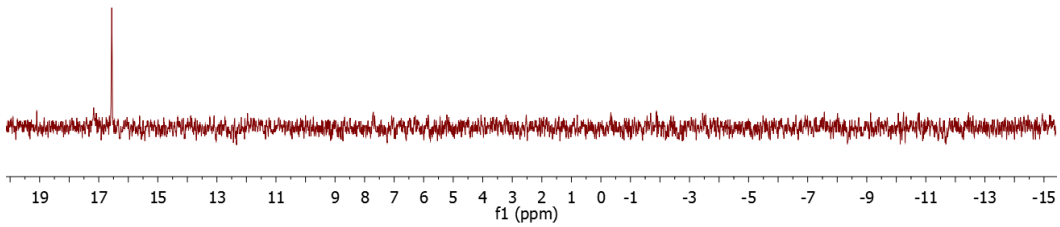

Figure 4.6. ^{31}P NMR spectrum (300 MHz) of SAP in $CDCl_3$ (ppm).

SAP was then mixed with a difunctional tertiary amine, TMBD, to form nominally 0%, 25%, and 50% crosslinked amphiphilic zwitterionic coatings, which refers to the maximum amount of crosslinking between the amines and phosphotriester units based upon their stoichiometries. The coatings were prepared by a solution deposition method on silanized glass substrates that presented tertiary amines on the surface, followed by treatment with trimethylamine to convert the remaining phosphotriester units into phosphorylcholine units (**Figure 4.1-C**).

The thicknesses of the 0%, 25%, and 50% crosslinked amphiphilic zwitterionic coatings were measured by calipers to be *ca.* 33 ± 1 μm, 43 ± 1 μm and 46 ± 1 μm, respectively (**Table 4.1**). As expected, the thickness increased with the presence of the TMBD crosslinker, likely due to a combination of the increased total mass of material and the more effective covalent attachment of SAP polymers within the networks and with connectivity to the substrate.

Table 4.1. Thicknesses of 0%, 25% and 50% crosslinked amphiphilic zwitterionic polymer surfaces measured by calipers.

Coatings	Thickness (μm)
0% crosslinked	33 ± 1
25% crosslinked	43 ± 1
50% crosslinked	46 ± 1

The coatings were characterized by XPS to study the surface chemical compositions. In the scenario of full conversion of phosphotriester units into

phosphorylcholine units, the nitrogen to phosphorous N/P ratio would be 1:1, due to a mechanism in which one lone pair on the nitrogen atom opens one phosphotriester five-membered ring. The 0% crosslinked coating resulted in a calculated N/P ratio of 0.8 indicating *ca*. 80% conversion efficiency (**Table 4.2**). Upon diamino-based crosslinking, the expected N/P ratio was observed, in which the 25% and 50% crosslinked coatings had N/P ratios of 1.0 and 1.1, respectively. The N/P value greater than 1 may be attributed to an increasing number of residual dangling amines from TMBD that did not react with the phosphotriester units. Thus, the N/P ratio of the higher crosslinked coatings would be able to exceed 1, due to TMBD molecules being attached onto the coating only from one single terminus. The N/P ratios close to the theoretical 1.0, suggest that the installation of the zwitterionic features on the modified surfaces was successful.

Table 4.2. Surface chemical compositions of 0%, 25% and 50% crosslinked amphiphilic zwitterionic polymer surfaces calculated from XPS spectra.

Coatings	O (%)	N (%)	C (%)	P (%)	N/P
0% crosslinked	18.2 ± 0.1	1.3 ± 0.1	78.8 ± 0.1	1.7 ± 0.1	0.8
25% crosslinked	14.4 ± 0.7	2.3 ± 0.5	81.1 ± 0.2	2.2 ± 0.02	1.0
50% crosslinked	11.7 ± 0.7	1.8 ± 0.8	84.8 ± 2	1.6 ± 0.1	1.1

AFM was used to investigate the surfaces of the coatings in both the dry and water-swollen states (**Figure 4.7**). In the dry state, all coatings presented rough surfaces with randomly distributed topographical features. The 0% crosslinked coatings

exhibited surfaces with the lowest R_{rms} and change in surface area (ΔA^2), generating the smoothest surfaces out of the three coatings, and they were also the thinnest, qualitatively, due to the reliance only on substrate conjugation for connection to the substrate. The 50% crosslinked coatings generated the next smoothest surface while the 25% crosslinked coatings were the roughest surfaces. The addition of TMBD into the formulations allowed for multi-layer crosslinking coincident with covalent attachment to the substrate to afford the 25% and 50% crosslinked networks. It is hypothesized that the lower degree of crosslinking gave a dynamic, loosely-crosslinked network that could undergo surface-buckling and display greater nanoscopic and microscopic roughnesses, resulting in an increased R_{rms} and ΔA^2 than the 0% or 50% crosslinked coatings. Recognizing that further studies were needed to probe the composition, structure, property behaviors, the coatings were then immersed in nanopure water for 12 h to provide for images in the water-swollen state. Overall, the water-swollen coatings displayed a lower R_{rms} and decrease in surface area, resulting in a smoother surface than their dry counterparts. The decreases in R_{rms} and ΔA^2 indicate that dynamic surface reorganization or increased water hydration had occurred on the surface of and possibly throughout the films.

The wettability of the coatings was studied by measuring the static water contact angle (**Figure 4.7**). All coatings exhibited relatively low static water contact angles (< 25°) pre-water immersion, which is indicative of their zwitterionic nature and affinity to water. Upon water immersion, an increase in static water contact angle of all the coatings was observed compared to their dry counter parts. The observation of the

contraphilic effect displayed on all surfaces can most likely be attributed to a saturation of water in the film allowing zwitterions in the surface-water interface to also be able to bury within the film.[107] The trend of higher crosslinked films exhibiting higher static water contact angle was still observed with post water immersion films. The increase in static water contact angles for networks with a greater percentage of crosslinking could be attributed to the increase in hydrodynamic response to residual tertiary amine end groups that did not react with phosphotriester moieties on the surface. The trends observed by both AFM imaging and static water contact angle measurements suggested an ability to control the surface properties by modulating TMBD incorporation.

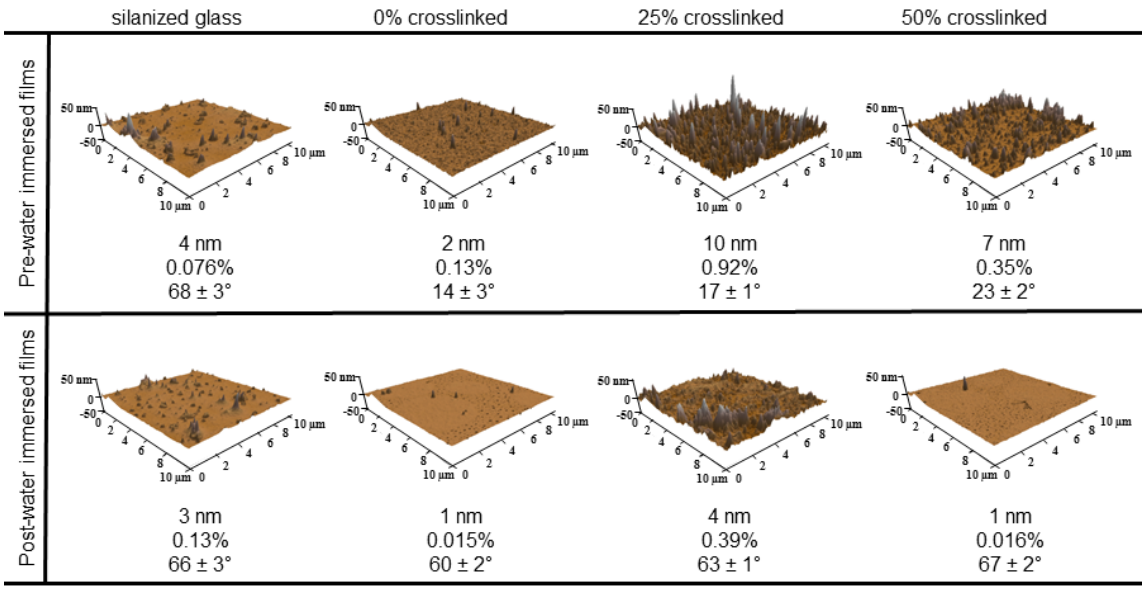

Figure 4.7. AFM images for amphiphilic zwitterionic coatings for both pre-water and post-water swollen states with R_{rms}, ΔA^2, and static water contact angle values reported, respectively, with each image. Field of view for AFM renderings is 100 μm^2 with a 100 nm z-scale.

After the demonstration of their zwitterionic and amphiphilic features, the coatings were incubated with a non-specific protein, BSA conjugated with Alexa Fluor 488 dye, to examine anti-biofouling performance. By wide field fluorescence microscopy under identical imaging conditions, the histograms for the fluorescence intensities of the coatings before and after incubation for 1 h in BSA solution were obtained and compared to the controls: glass, silanized glass and glass coated with a commercially-available silicone elastomer model Sylgard® 184 (**Figure 4.8**). The average changes in relative Alexa Fluor 488 intensities between pre- and post-BSA-exposed surfaces were calculated and presented along with the histograms. As more BSA was bound, a larger change in relative Alexa Fluor 488 intensity was expected. The histograms demonstrated that the amphiphilic zwitterionic coatings had changes in intensities no more than 2 a.u. while the changes in intensities for controls were $\geq$ 6 a.u. The results indicated that amphiphilic zwitterionic coatings have a higher resistance to the adsorption of BSA than the controls (glass, silanized glass and Sylgard® 184). The 0% and 50% crosslinked coatings both displayed slightly better anti-biofouling resistances towards BSA adsorption (1 a.u.) than the 25% crosslinked coating (2 a.u.). The slightly higher resistance to BSA adsorption behavior for both the 0% and 50% crosslinked coatings could be accredited to the overall lower R_{rms} and ΔA^2 of the coatings in comparison to the 25% crosslinked coatings, a finding that was also observed by other groups.[108,109] In addition to a higher R_{rms} and surface area, the residual unreacted tertiary amines from TMBD in the 25% and 50% crosslinked coatings may also play a factor in the effectiveness of resistance to BSA adsorption.

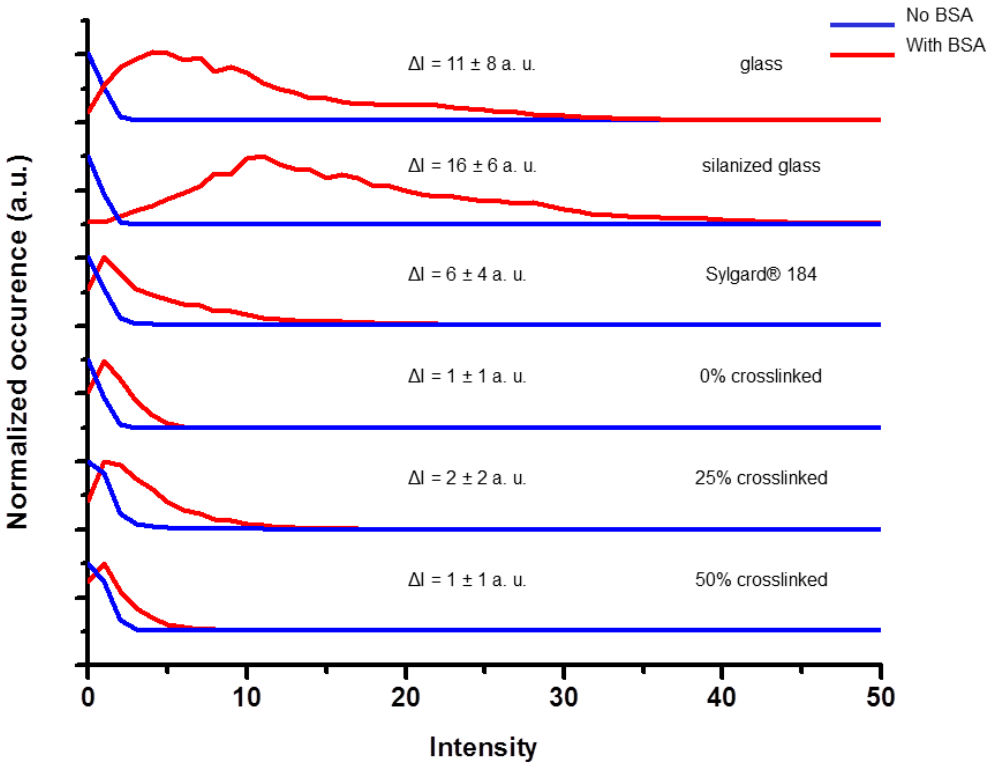

Figure 4.8. Histograms of fluorescence intensities of coatings/substrates before (blue curve) and after (red curve) BSA incubation, and calculated relative changes in fluorescence intensities.

With respect to the application of these amphiphilic zwitterionic coatings for anti-biofouling applications in the marine environment, the abilities of the coatings to prevent settlement of *Ulva*, the most widespread hull fouling alga,[110] was tested by submerging the surfaces in an *Ulva* zoospore solution. Confocal microscopy was used to measure autofluorescence of chlorophyll present in zoospores that settled on the surfaces. The changes in relative fluorescence intensities between the coatings before and after zoospore settlement on the amphiphilic zwitterionic coatings were below 51

a.u., while the average changes for the controls were all above 190 a.u. (**Figure 4.9-A**). Although there was only a slight distinction among the fluorescence images of the amphiphilic zwitterionic coatings and the controls (**Figure 4.9**), the calculated change in fluorescence intensities before and after zoospore settlement indicated that the amphiphilic zwitterionic coatings performed significantly better at resisting zoospore settlement than did the controls, including the PDMS elastomer coatings (**Figure 4.9-A** and **Figure 4.9-B**), with all amphiphilic zwitterionic coatings having a 70% less susceptibility to *Ulva* fouling compared to the controls. The 0% crosslinked coatings were observed to be the most effective at preventing the settlement of zoospores among all coatings, with an average relative fluorescence intensity at approximately 30 a.u. Meanwhile, the average relative fluorescence intensity for 25% and 50% crosslinked coatings were calculated to be similar at approximately 50 a.u. The 0% crosslinked coating was able to resist the most zoospores, possibly due to its surface having the highest wettability among all coatings as illustrated by static water contact angle measurements. The zoospores that had settled on the coatings/substrates were also allowed to grow for qualitative measurements of *Ulva* fouling (**Figure 4.9-C**) and the controls can be visually observed to be more fouled than were the amphiphilic zwitterionic coatings. In addition, the growth of the zoospores on the amphiphilic zwitterionic coatings also implied that our coatings are non-toxic.

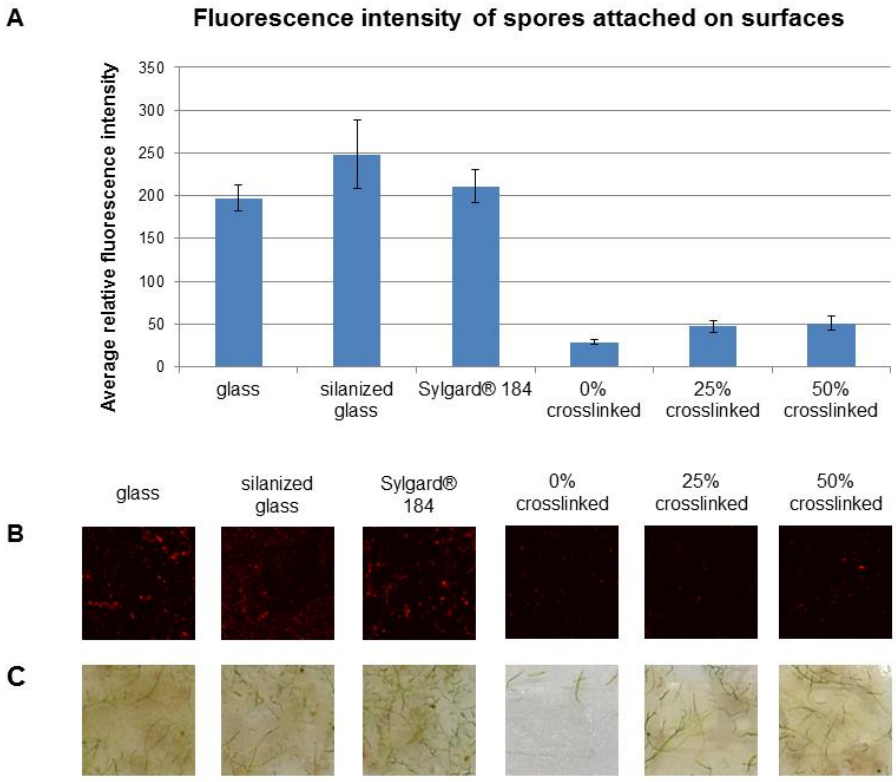

Figure 4.9. (A) Average relative chlorophyll fluorescence intensity results for tested coatings/substrates regarding settlement of *Ulva* zoospores. Bars show standard error of the mean. (B) Fluorescence images of the settlement of zoospores onto substrates. (C) Qualitative images *Ulva* growth on substrates after five days. Size of each substrate is 1 cm^2.

The surface zeta potential of 0%, 25% and 50% crosslinked coatings were measured to be -32.47 mV, -22.50 mV and -54.39 mV, respectively (**Table 4.3**). The negatively charged characteristic of the coatings could be in accordance to the ring opening of any remaining unreacted cyclic phosphotriester which did not react with an amine. Nanomaterials with phosphotriester moieties have also shown to exhibit negative characteristics.[111-113] Although the coatings showed negatively charged characteristics, it

is hypothesized that the zwitterionic characteristics of the phosphorylcholine in the coating decrease protein adsorption and microorganism adhesion.

Table 4.3. Surface Zeta Potentials of 0%, 25% and 50% crosslinked amphiphilic zwitterionic polymer surfaces.

Coatings	Zeta potential (mV)
0% crosslinked	-32.47
25% crosslinked	-22.50
50% crosslinked	-54.39

4.4 Conclusions

A new facile strategy to achieve amphiphilic zwitterionic coatings has been developed, which starts from a commercially-available relatively inexpensive polymer and allows for easy functionalization and crosslinking reactions. The wettabilities of the zwitterionic polymeric networks were controlled by varying the extent of crosslinking in the networks, which influenced the compositional profiles. AFM characterization suggested that the surface properties of our amphiphilic zwitterionic coatings could also be adjusted by tuning crosslinking extents. The amphiphilic zwitterionic coatings displayed superior anti-biofouling performance at resisting both protein (BSA) and whole marine organism (*Ulva* zoospore) fouling, compared to glass substrates and commercialized anti-biofouling silicone-based coatings.

With these promising initial anti-biofouling results obtained for materials prepared by a straightforward synthetic approach, future directions will further explore

the applicability of the current coatings, while also expanding the compositions, structures and properties. In particular, we are interested in controlled, quantitative laboratory and field tests of fouling performance, conducted against diverse types of marine organisms, with evaluation of the coatings surface characteristics before and after fouling has occurred to better map out the composition-structure-property-performance relationships. In addition, we are investigating expansion of the compositions, with inclusion of mixtures of amino components, coating thicknesses, while also probing the durability and longevity under challenging conditions, including those resembling a marine environment.

CHAPTER V

DETERMINING THE EXTENT OF INTERACTIONS OF ZWITTERIONIC VS. BLENDED IONIC POLYMERS *VIA* THERMAL AND MECHANICAL CHARACTERIZATIONS[§]

5.1 Introduction

Zwitterionic polymers have garnered an increasing amount of attention due their excellent anti-fouling properties which can be used in various applications such as medical implants, biosensors, water purification systems and ship hulls.[3,20,77,85,114-118] Their unique structures that have the same number of anionic and cationic moieties on the same pendant side chain of zwitterionic polymers help create a hydration layer through electrostatic interactions and hydrogen bonds around the surface which requires disruption from proteins that is both energetically and kinetically unfavorable.[119-121] In addition to providing great anti-fouling properties, zwitterionic polymers could also be developed as smart materials that respond to a stimulus such as change in pH or salt concentration.[122-125]

Mixed charged polymers with either positive or negative moieties on a pendant side chain that have a neutral net charge have also been explored for anti-fouling

---

[§] In collaboration with Nathaniel A. Lynd,[†] Kevin A. Pollack,[‡] Jeffery E. Raymond,[‡] Craig J. Hawker,[†] Karen L. Wooley,[‡] [†]Departments of Chemistry and Biochemistry and Materials, University of California, Santa Barbara, [‡]Departments of Chemistry, Chemical Engineering and Materials Science & Engineering, Texas A&M University

purposes.[126,127] For example, Mi and coworker also reported a tunable mixed-charge copolymer surface containing positively charged quaternary amine monomers ([2-(acryloyloxy)ethyl] trimethylammonium chloride, TMA) and negatively-charged carboxylic acid monomers (2-carboxy ethyl acrylate, CAA) that is resistant to bacteria adhesion.[127] Furthermore, Chang and coworkers synthesized poly(TMA-*co*-SA), which bears positively charged trimethylammonium chloride and negatively charged sulfonate groups, to show that the closer the mixed charged polymer reaches charge neutrality, the more resistant the polymer is to nonspecific protein adsorption.[126] Due to excellent anti-fouling properties displayed by both zwitterionic and mixed charged polymers, understanding the difference in properties between both zwitterionic and mixed charged polymers has become of great importance for the selection of polymers in anti-fouling applications.[128,129]

With anti-fouling applications on substrates ranging from ship hulls to ultrafiltration membranes, it is significant to select a neutral charged polymer, whether it is zwitterionic or mixed charged polymers, with appropriate thermal and mechanical properties for the application.[130,131] The zwitterion, sulfobetaine, in particular, has received significant attention due to its high dipole moment, stability over a wide range of temperatures and permanent neutral charge over a wide pH range.[132,133] Our work describes the synthesis of different charged polymers bearing either positively charged trimethylammonium chloride units (cationic), negatively charged sodium sulfonate units (anionic) and neutral charged sulfobetaine units (zwitterionic) side chains from P(AGE-*b*-EG-*b*-AGE) *via* thiol-ene click chemistry. The post-functionalization of P(AGE-*b*-

EG-*b*-AGE) to different charged polymers allow for all the charged polymers to have the same number of charged functional groups in the polymer. Equimolar amounts of polymers with positive charged side chains and negative charged side chains were then mixed together and compared to polymers with zwitterionic side chains which possess similar charge densities. The thermal and mechanical properties of the zwitterionic polymers *vs.* blended cationic/anionic polymers were reported.

5.2 Experimental Section

Materials

All chemicals and reagents were purchased from Sigma-Aldrich (St. Louis, MO) and used without further purification unless otherwise noted. Custom Delrin® molds were fabricated at the Texas A&M University machine shop (College Station, TX). The Spectra/Por Dialysis Membranes (MWCO 6,000 to 8,000 Da) were purchased from Spectrum Laboratories, Inc (Rancho Dominguez, CA). Nanopure water (18 MΩ•cm) was acquired by means of a Milli-Q water filtration system, Millipore Corp. (Bedford, MA).

Nuclear Magnetic Resonance Spectroscopy

^{1}H NMR and ^{13}C NMR NMR spectra were recorded on a Varian Inova 300 (Varian Inc., Palo Alto, CA) interfaced to a UNIX computer using VnmrJ software. ^{1}H NMR and ^{13}C NMR were analyzed using the solvent signal as an internal reference.

High-resolution Mass Spectrometry

HRMS for the monomers was conducted on an Applied Biosystems PE SCIEX QSTAR.

Thermal Analysis

TGA was performed under argon atmosphere using a Mettler-Toledo model TGA/DSC1 Star^{e} system (Mettler-Toledo, Inc., Columbus, OH), with a heating rate of 10 °C/min. Measurements were analyzed by using Mettler-Toledo STAR^{e} v. 7.01 software. Thermal properties were measured by DSC on a Mettler-Toledo DSC822^{e} (Mettler-Toledo, Inc., Columbus, OH), with cooling and heating rates of 10 °C/min. Measurements were analyzed using Mettler-Toledo STAR^{e} v. 7.01 software. The third heating and second cooling scans were presented.

Dynamic Mechanical Thermal Analysis

DMTA was performed on a Mettler Toledo TT-DMA system. DMTA was performed in compression mode over a temperature range of -75 °C to 75 °C with a ramp rate 1 °C/min and 0.03 mm displacement at a frequency of 1 Hz.

Synthesis of 2-Mercapto-*N,N,N*-trimethylethan-1-aminium chloride

In a 100 mL round-bottom flask equipped with a stir bar was added acetylthiocholine iodide (5.00g, 16.9 mmol) and 6 M HCl (34 mL). The mixture was stirred at 80 °C for 1 h before being concentrated *in vacuo* to remove acetic acid and water. The resulting solid was washed with acetone and dried under vacuum (yield: 95). ^{1}H NMR (300 MHz, D_2O, ppm): δ 3.45 (t, *J* = 7 Hz, 2H, $SCH_2C\boldsymbol{H_2}$), 3.25 (s, 9H, $N^{+}(C\boldsymbol{H_3})_3$), 2.77 (t, *J* = 7 Hz, $SC\boldsymbol{H_2}CH_2$). ^{13}C NMR (75 MHz, D_2O, ppm): δ 70.3, 53.5, 17.2. HRMS (m/z): calculated for $C_5H_{14}NSCl$ $[M+H]^{+}$ 156.05; found, 156.1129. FTIR (cm^{-1}): 2955, 2864, 1685, 1466, 1405, 1400, 1377, 1367, 1342, 1267, 1262, 1136, 1106, 1051, 1016, 964, 851, 806.

Synthesis of S-(2-(Dimethylamino)ethyl) ethanethioate

In a 1 L round-bottom flask was added 2-(dimethylamino)ethanethiol hydrochloride (25.0 g, 167 mmol), acetyl chloride (15.0 g, 187 mmol), triethylamine (36.0 g, 335 mmol) and dichloromethane (100 mL). The reaction mixture was heated at 40 °C for 24 h and then filtered to remove triethylammonium salts. The solution was concentrated *in vacuo* to yield yellow oil. The crude product was purified by dissolving in diethyl ether and washing with 1 M HCl solution (3 x 100 mL), sodium bicarbonate solution (3 x 100 mL), and brine (100 mL). The organic solution was then collected and dried over magnesium sulfate and concentrated *in vacuo* to afford light yellow oil (yield: 55%). ^{1}H NMR (300 MHz, $CDCl_3$, ppm): δ 2.94 (t, *J* = 7 Hz, 2H, $SCH_2C\boldsymbol{H_2}N$), 2.41 (t, *J* = 7 Hz, 2H, $SC\boldsymbol{H_2}CH_2N$), 2.27 (s, $C\boldsymbol{H_3}S$), 2.20 (s, $N^+(C\boldsymbol{H_3})_2$). ^{13}C NMR (75 MHz, $CDCl_3$, ppm): δ 199.5, 57.8, 45.3, 31.2, 23.1. HRMS (m/z): calculated for $C_6H_{13}NOS$ $[M+H]^+$ 149.09; found, 149.2571. FTIR (cm^{-1}): 1715, 1470, 1443, 1379, 1322, 1246, 1236, 1171, 1138, 1066, 1061, 1038, 1009, 968, 934, 824.

Synthesis of 3-((2-(Acetylthio)ethyl)dimethylammonio)propane-1-sulfonate

In a 250 mL round-bottom flask equipped with a stir bar was added *s*-(2-(dimethylamino)ethyl) ethanethioate (10.0 g, 68.0 mmol), 1, 3-propanesultone (17.0 g, 136 mmol) and acetone (80 mL). The reaction mixture was allowed to stir for 24 h. The precipitate was filtered and washed with acetone before drying under vacuum (yield: 99%). ^{1}H NMR (300 MHz, D_2O, ppm): δ 3.51 (t, *J* = 7 Hz, 2H, $SCH_2C\boldsymbol{H_2}$), 3.48 (t, *J* = 7Hz, 2H, $N^+(CH_3)_3C\boldsymbol{H_2}CH_2CH_2$), 3.27 (t, *J* = 7 Hz, 2H, $CH_3COSC\boldsymbol{H_2}$), 3.18 (s, 6H, $N^+(C\boldsymbol{H_3})_3$), 3.00 (t, *J* = 7 Hz, 2H, $C\boldsymbol{H_2}SO_3^-$), 2.30 (t, *J* = 7 Hz, 2H, $CH_2C\boldsymbol{H_2}CH_2$), 2.23 (s,

3H, C***H₃***CO). ^{13}C NMR (75 MHz, D_2O, ppm): δ 199.1, 65.4, 62.1, 50.1, 47.1, 31.0, 23.1, 18.2. HRMS (m/z): calculated for $C_9H_{19}NO_4S_2$ $[M+H]^+$ 270.08; found, 270.2151. FTIR (cm^{-1}): 2235, 1713, 1483, 1455, 1385, 1350, 1322, 1247, 1216, 1175, 1136, 1112, 1066, 1061, 1035, 1008, 960, 934, 850, 824, 790.

Synthesis of 3-((2-(Acetylthio)ethyl)dimethylammonio)propane-1-sulfonate

In a 250 mL round-bottom flask equipped with a stir bar was added 3-((2-(acetylthio)ethyl)dimethylammonio)propane-1-sulfonate (18.0 g, 66.9 mmol) and 6 M HCl (80 mL). The mixture was allowed to stir for 1 h at 80 °C. The solution was concentrated *in vacuo*. The white solid was washed with diethyl ether (3 x 100 mL) and dried under vacuum for 24 h (yield: 95%). ^{1}H NMR (300 MHz, D_2O, ppm): 3.49 (m, 4H, C***H₂***N$(CH_3)_2$)C***H₂***), 3.10 (s, 6H, N(C***H₃***)$_2$), 2.93 (m, 4H, HSC***H₂***CH_2, C***H₂***SO_3^-), 2.19 (m, *J* = 7 Hz, 2H, CH_2C***H₂***CH_2). ^{13}C NMR (75 MHz, D_2O, ppm): δ 70.3, 65.4, 50.2, 47.2, 18.1, 17.5. HRMS (m/z): calculated for $C_7H_{17}NO_3S_2$ $[M+H]^+$ 228.06; found, 228.1121. FTIR (cm^{-1}): 2945, 2862, 2235, 1685, 1481, 1453, 1381, 1355, 1245, 1215, 1170, 1110, 1061, 1030, 1018, 965, 931, 847, 790.

Synthesis of P(AGE-*b*-EG-*b*-AGE)

P(AGE-*b*-EG-*b*-AGE) (M_w^{NMR}: PEG midblock = 10,000 Da, PAGE endblock M_w = 4,100 Da) was synthesized as reported in literature.[134]

Synthesis of P(AGE-*b*-EG-*b*-AGE) with cationic functionalities (anionic polymers)

In a 20 mL scintillation vial was added P(AGE-*b*-EG-*b*-AGE) (50.0 mg, 2.75 μmol), 2-mercapto-*N*,*N*,*N*-trimethylethanaminium chloride, (290 mg, 1.92 mmol), 2, 2'-dimethoxy-2-phenylacetophenone (148 mg, 0.576 mmol) and methanol (5 mL). The

mixture was purged with N_2 for 30 min, then reacted under UV light (365 nm) for 3 h to completion. The mixture was then dialyzed in dialysis bag (MWCO 6,000 to 8,000 Da) in nanopure water. The dialyzed solution was lyophilized resulting in a white solid that was kept under vacuum until use (yield: 95%). ^{1}H NMR (300 MHz, D_2O, ppm): 3.76-3.34 (m, OEG ***Hs***), 3.14-3.00 (s, $N^+(CH_3)_3$), 2.99-2.83 (br, S SCH_2CH_2N), 2.70-2.52 (br, $OCH_2CH_2CH_2S$), 1.91-1.72 (br, $OCH_2CH_2CH_2S$). ^{13}C NMR (75 MHz, D_2O, ppm): δ 78.3, 69.7, 65.6, 53.0, 40.0, 31.7, 31.2, 28.7, 28.1, 23.7, 22.7, 18.9. TGA in Ar: 30-200 °C, 3% mass loss; 200-300 °C, 22% mass loss; 300-400 °C, 90% mass loss; 400-500 °C, 95% mass loss; 5% mass remaining above 500°C.

Synthesis of P(AGE-*b*-EG-*b*-AGE) with Anionic Functionalities (Anionic Polymers)

In a 20 mL scintillation vial was added P(AGE-*b*-EG-*b*-AGE) (50.0 mg, 2.75 μmol), sodium-3-mercapto-1-propanesulfonate (340 mg, 1.92 mmol), 2, 2'-dimethoxy-2-phenylacetophenone (148 mg, 0.576 mmol), methanol (2.5 mL) and water (2.5 mL). The mixture was purged with N_2 for 30 min, then reacted under UV light (365 nm) for 3 h to completion. The mixture was then dialyzed in dialysis bag (MWCO 6,000 to 8,000 Da) in nanopure water. The dialyzed solution was lyophilized resulting in a white solid that was kept under vacuum until use (yield: 97%). ^{1}H NMR (300 MHz, D_2O, ppm): 3.80-3.33 (m, OEG ***Hs***), 2.95-2.82 (br, $CH_2SO_3^-$), 2.72-2.47 (m, CH_2SCH_2), 2.00-1.85 (m, $OCH_2CH_2CH_2S$), 1.85-1.71 (br, $SCH_2CH_2CH_2S$). ^{13}C NMR (75 MHz, D_2O, ppm): δ 78.2, 68.6, 49.9, 39.0, 29.8, 28.7, 27.6, 24.7, 24.2, 21.2, 17.8. TGA in Ar: 30-200 °C, 3% mass loss; 200-300 °C, 8% mass loss; 300-400 °C, 60% mass loss; 400-500 °C, 64% mass loss; 36% mass remaining above 500°C.

Synthesis of P(AGE-*b*-EG-*b*-AGE) with Zwitterionic Functionalities (Zwitterionic Polymers)

In a 20 mL scintillation vial was added P(AGE-*b*-EG-*b*-AGE) (50.0 mg, 2.75 μmol), 3-((2-(acetylthio)ethyl)dimethylammonio)propane-1-sulfonate (430 mg, 1.92 mmol), 2, 2'-dimethoxy-2-phenylacetophenone (148 mg, 0.576 mmol) and methanol (5 mL). The mixture was purged with N_2 for 30 min, then reacted under UV light (365 nm) for 3 h to completion. The mixture was then dialyzed in dialysis bag (MWCO 6,000 to 8,000 Da) in nanopure water. The dialyzed solution was lyophilized resulting in a white solid that was kept under vacuum until use (yield: 93%). ^{1}H NMR (300 MHz, D_2O, ppm): 3.76-3.31 (m, OEG ***Hs***, C***H₂***$N^+(CH_3)_3$C***H₂***), 3.14-3.00 (br, CH_2N^+(C***H₃***)$_3CH_2$), 2.94-2.78 (br, NCH_2C***H₂***S, C***H₂***SO_3^-), 2.68-2.58 (br, OCH_2CH_2C***H₂***S), 2.23-2.02 (br, C***H₂***$CH_2SO_3^-$), 1.87-1.21(br, OCH_2C***H₂***CH_2S). ^{13}C NMR (75 MHz, D_2O, ppm): δ. 69.3, 63.3, 62.0, 50.8, 47.2, 45.1, 38.9, 28.0, 26.3, 18.1. TGA in Ar: 30-200 °C, 2% mass loss; 200-300 °C, 8% mass loss; 300-400 °C, 83% mass loss; 400-500 °C, 88% mass loss; 12% mass remaining above 500°C.

Preparation of Blended Cationic/anionic Polymers

In a 20 mL scintillation vial equipped with a stir bar was added a solution of cationic polymers (500 mg, 17.1 μmol) in nanopure water (5 mL) and a solution of anionic polymers (528 mg, 17.1 μmol) in nanopure water (5 mL). The solution was stirred at room temperature for 1 h, dialyzed in dialysis bag (MWCO 6,000 to 8,000 Da) in nanopure water and lyophilized to form a white solid that was kept under vacuum until use (yield: 98%).

Disc Preparations for DMTA

Polymers were loaded and packed into custom Delrin® molds. The molds containing the polymer were placed in an oven under vacuum at 50 °C for 24 h. The resulting disc with a thickness of 3 mm and 5 mm diameter was removed from the mold and placed under vacuum until use.

5.3 Results and Discussion

Herein, an ABA triblock copolymer, poly(allyl glycidyl ether-*block*-ethylene glycol-*block*-allyl glycidyl ether) (P(AGE-*b*-EG-*b*-AGE)), in which the P(AGE) endblocks contain alkene units allows for facile direct functionalization of the P(AGE) endblocks with cationic or anionic moieties without the use of protecting groups in quantitative yields (**Figure 5.1**). P(AGE-*b*-EG-*b*-AGE) (M_w^{NMR}: PEG midblock = 10,000 Da, PAGE endblock M_w = 4,100 Da) was synthesized by oxyanionic ring-opening polymerization using PEG (M_w: 10,000 Da) as an initiator. Thiols bearing cationic or zwitterionic moieties were synthesized *via* protection and deprotection of thiolacetyl protecting groups (**Figure 5.2**). Direct functionalization of the P(AGE) endblocks was performed by reacting P(AGE-*b*-EG-*b*-AGE) with cationic, anionic, or zwitterionic thiol compounds under UV (365 nm) light to yield cationic, anionic or zwitterionic polymers, respectively. Complete functionalization was confirmed by ^{1}H NMR with the disappearance of peaks at 5.10 to 6.10 ppm that correspond to the alkene protons. A minimum of three times excess of charged thiols was required to convert all alkenes into thiol ester units.

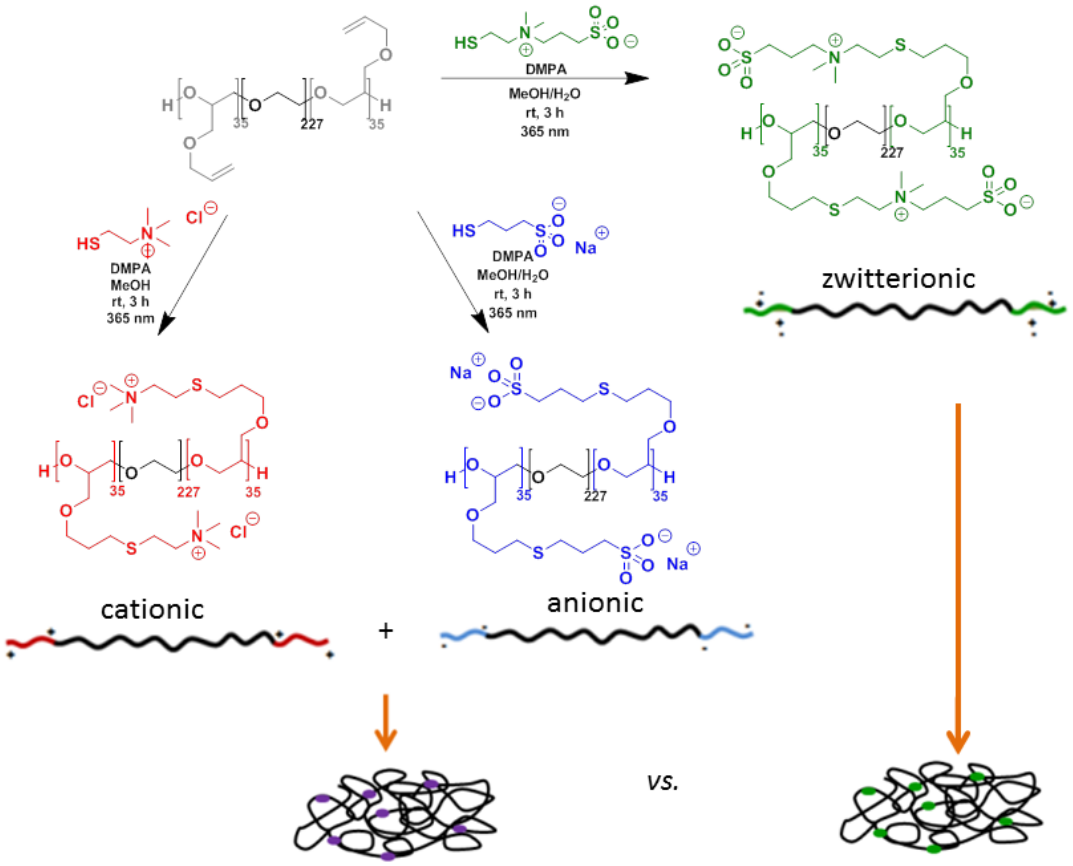

Figure 5.1. General macromolecular design for charged triblock copolymers derived from a common triblock copolymer precursor. Mixture of cationic and anionic blended polymer was compared to zwitterionic polymer.

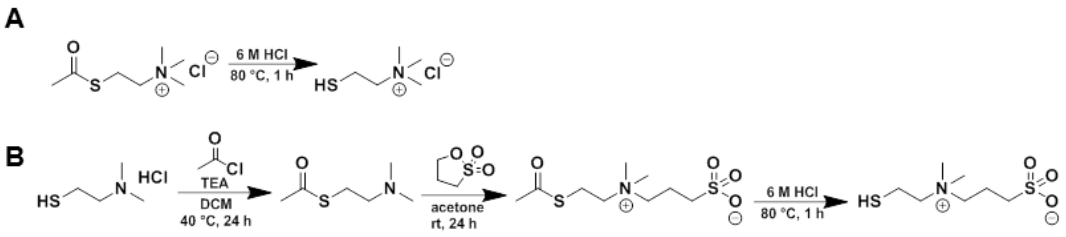

Figure 5.2. (A) Synthesis of cationic thiol compound. (B) Synthesis of anionic thiol compound.

The charged polymers were investigated by TGA to determine the thermal stability of each charged polymer (**Figure 5.3**). From ambient temperature to 130 °C, 2 to 3% mass loss was observed in all polymers which could be attributed to the loss of water molecules from the hygroscopic polymers. Interestingly, two degradation events were observed in the cationic polymers, the first occurring from 180 °C to *ca.* 300 °C, and the second from 270 °C to *ca.* 400 °C. Two degradation events were also observed in the blended cationic/anionic polymers, with the first occurring at from 230 °C to *ca.* 280 °C, and the second from 280 °C to *ca.* 400 °C. The two degradation events correspond to the degradation of cationic polymer portion in the blend while the increase in degradation temperature was contributed by thermal properties of the anionic polymer. The degradation events for the anionic and zwitterionic polymers were observed to occur at *ca.* 300 °C. Interestingly, the blended cationic/anionic polymer has retained more mass than zwitterionic polymer upon heating above *ca.* 350 °C.

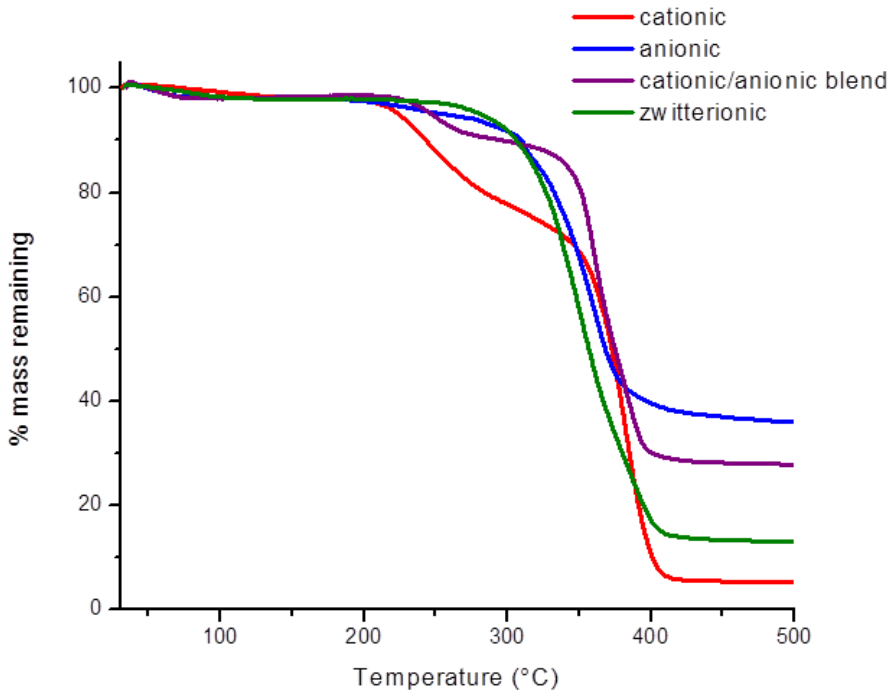

Figure 5.3. TGA traces of charged polymers.

DSC was used to probe the phase transitions present in the charged polymers (**Figure 5.4**). The DSC samples were prepared in an argon filled glove box to prevent any moisture from affecting the phase transition temperatures. Upon heating, a T_c and a T_m were observed for all polymers. Although all the polymers have the same backbone, there is a huge discrepancy in the T_c of the polymers while the T_m of the polymer ranges from 44 to 45 °C. Meanwhile the T_c of the cationic and anionic polymers were observed to be -25 and 31 °C, respectively. The T_c of the blended cationic/anionic polymer shifted to 22 °C which was in between the T_c of the individual cationic and anionic polymers, indicating the existence of strong interactions between the cationic and

anionic polymers in the blended cationic/anionic polymer. The zwitterionic polymer exhibits lower crystallinity than the blended cationic/anionic polymer due to its lower T_c at -27 °C.

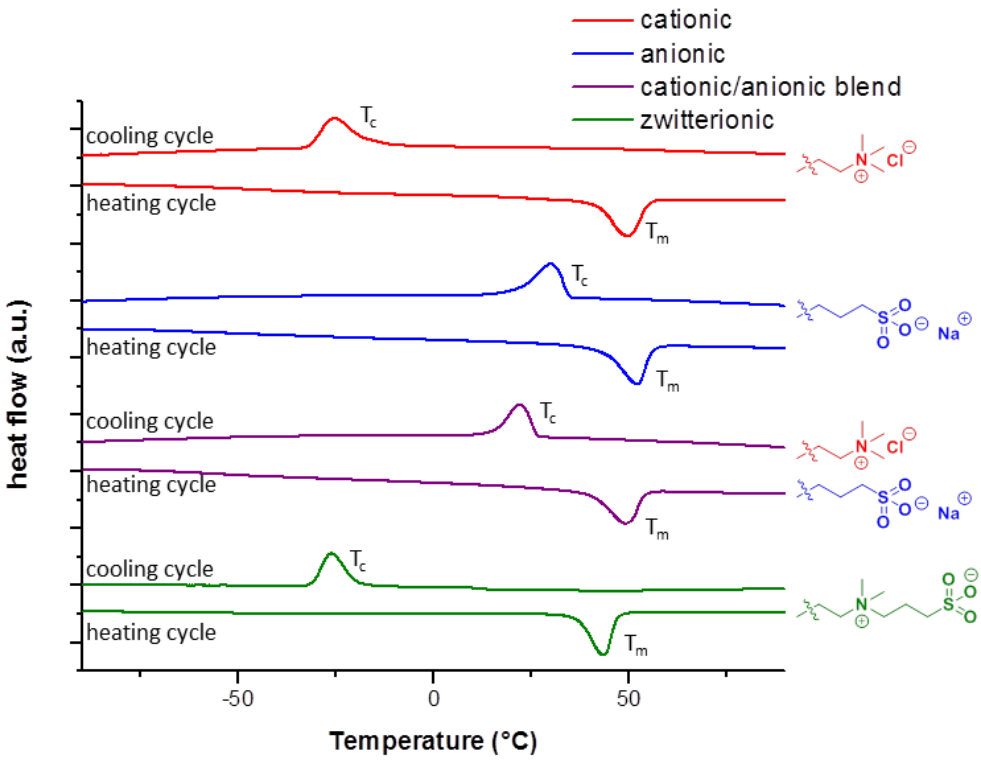

Figure 5.4. Normalized DSC traces of charged polymers on heating (lower) and cooling (upper).

Charged polymeric discs were prepared by filling a custom Delrin® mold with the charged polymers and pressing the polymers into a disc with the mold. The mechanical properties of the charged polymers discs were investigated with a DMTA and the storage moduli of were plotted against temperature (**Figure 5.5**). The anionic

polymer was observed to have a higher storage modulus than the cationic polymer at throughout the temperature ramp. The storage modulus of the cationic/anionic blended polymer was similar to the storage modulus of anionic polymer at low temperatures. However, as the temperature increased past -20 °C, the storage modulus of the cationic/anionic blended polymer has dropped to lower than the storage modulus of the anionic polymer. The zwitterionic polymer was observed to display a significantly higher storage modulus than the cationic/anionic blended polymer at low temperatures while displaying a lower storage modulus than the cationic/anionic blended polymers above its T_c. The DMTA curves indicated that the zwitterionic polymer interact differently than the cationic/anionic blended polymer and that the zwitterionic polymer displayed lower storage modulus than the cationic/anionic blended polymer at relevant aquatic temperatures.

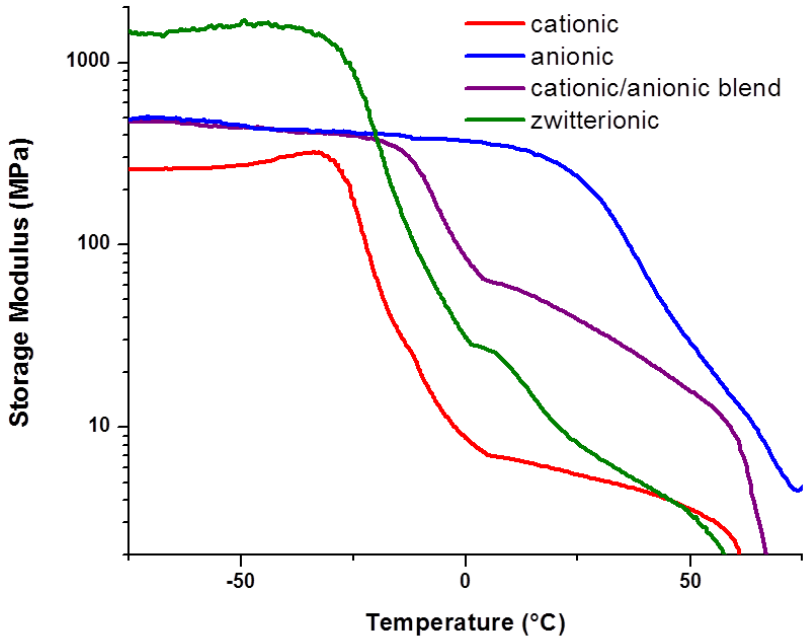

Figure 5.5. Storage modulus measurements by DMTA of charged polymers as a function of temperature.

5.4 Conclusions

The synthesis of various charged polymers was completed by an efficient post-functionalization method using thiol-ene click chemistry to click various charged moieties onto P(AGE-*b*-EG-*b*-AGE), which bears alkene functionalities on P(AGE) endblocks. This method allows for the preparation of different charged polymers with similar repeat units. Three different types of polymers (cationic, anionic and zwitterionic) were synthesized while an additional cationic/anionic polymer was prepared by mixing an equimolar ratio of cationic and anionic polymers together.

The thermal properties of the polymers were investigated and zwitterionic polymers were observed to be more stable than blended cationic/anionic polymer at up to 350 °C and less stable as the temperature increases above 350 °C. All polymers have a similar T_m values while the T_c of blended cationic/anionic polymer was significantly higher than that of zwitterionic polymer. Strong interactions were observed between the cationic and anionic moieties within the blended cationic/anionic blended polymer as suggested by the discrepancy of the DMTA curve between the zwitterionic polymer and the cationic/anionic blended polymer. Electrostatic interactions of polymers with zwitterionic side chains are found to be weaker than electrostatic interactions of equimolar blends of cationic and anionic polymers at temperatures above the T_c of the zwitterionic polymer.

CHAPTER VI

CONCLUSIONS

6.1 Conclusions

This dissertation has expanded on the development of new methodologies to synthesize and characterize polymeric networks that have advanced the development of anti-fouling coatings. Specifically, multi-component polymeric systems are the focus as the systems combine the unique properties of each component, which can therefore be tuned and optimized for used in specific anti-fouling applications. Amphiphilic networks of HBFP crosslinked with PEG display chemical heterogeneities, topographical and topological features and have shown resistance to the attachment of biomacromolecules and marine organisms of both hydrophobic or hydrophilic nature. The incorporation of PDMS into HBFP-PEG shows greater chemical heterogeneities on the surface and improved fouling release than the HBFP-PEG system. New methodologies and experiments have been developed to probe the stability and crosslinking efficiency of the HBFP-PEG-PDMS terpolymer network in order to investigate the maximum wt% of PEG and PDMS that can be added into the terpolymer network before hitting the threshold of having excess non-crosslinked PEG and/or PDMS leaching off the network. Amphiphilic networks that combine silsesquioxanes, fluoro- and oligo(ethylene oxide) compounds, and sulfobetaine were also generated efficiently *via* thiol-ene click chemistry for anti-fouling applications and their anti-fouling performances were tested against various marine organisms. Furthermore,

chemical modifications were performed on commercially available polymers and crosslinked to form amphiphilic zwitterionic crosslinked ant-fouling networks. Lastly, the thermal and mechanical properties of net neutral charged (zwitterionic *vs.* mixed cationic/anionic neutral charged) polymers were investigated as the properties will play an important role when selecting a net neutral charged polymer for an anti-fouling application.

Chapter 2 introduced the methods used to investigate the stability and crosslinking efficiency of HBFP-PEG-PDMS terpolymer systems. Calculations were performed to determine that the number of crosslinking sites of PEG and PDMS does not surpass the number of bromoalkyl end groups of HBFP by 10% for HBFP-PEG-PDMS networks with HBFP, PEG (200 wt% relative to HBFP) and PDMS (50 wt% relative to HBFP). The HBFP-PEG-PDMS terpolymer networks were prepared on Interseal® 670 HS epoxy-base undercoat covered microscope glass slides by airbrush application. Although SEM images of the cross sections showed subtle differences in the visualization of the Interseal® 670 HS epoxy-base undercoat layer and the HBFP-PEG-PDMS terpolymer network layer, the presence of a thin layer of HBFP-PEG-PDMS terpolymer network on top of the Interseal® 670 HS epoxy-base undercoat was still confirmed. The water contact angles, IR spectra and AFM images of the HBFP-PEG-PDMS terpolymer network showed minimal change in the dry and water-swollen states, indicating that dynamic surface reorganization was probably not occurring when the networks were immersed in water, which could be attributed to the bottom layer of the HBFP-PEG-PDMS terpolymer network lacking the freedom and mobility to move to

the surface as it was covalently attached to the Interseal® 670 HS epoxy-base undercoat. The HBFP-PEG-PDMS terpolymer network produced by airbrush application was also much thinner than those produced by drop cast method (1 μm *vs.* 300 μm). Therefore, there are significantly fewer materials between the bottom layer that is covalently attached to the epoxy and the surface to be able to reorganize to the surface. The HBFP-PEG-PDMS terpolymer networks were also confirmed to be stable when immersed in synthetic seawater for at least a week. Soxhlet extraction experiments were performed on the HBFP-PEG-PDMS terpolymer networks and the results indicated that the terpolymer networks were stable. This indication suggests that future modifications in the terpolymer formulation can be performed while maintaining a stable network as long as the number of crosslinking sites of the linear polymers does not surpass the number of bromoalkyl end groups in HBFP by 10%.

Chapter 3 maintained the concept of using a three-component system for anti-fouling applications through a UV-cured crosslinked system using the simple and efficient thiol-ene click chemistry. A series of amphiphilic zwitterionic ternary coatings with different molar equivalences of POSS, AFSM and ZSM have been prepared on silanized microscope glass slides with an airbrush applicator. Coatings were cured under UV light without having to use elevated temperatures in order for crosslinking to take place. Anti-fouling experiments using various marine organisms were performed on pristine and biofilmed ternary coatings to understand the fouling behavior of these organisms in both a laboratory and "real world" environment. The biofilm was observed to increase the settlement of the sporelings while displaying no difference in the

settlement of diatoms and barnacle cyprids. The ternary networks also failed to exhibit significant improvement in resisting the settlement of the tested marine organisms. Future directions of these ternary coatings will involve tuning the ratio of each component or even changing one or more components in the system.

Chapter 4 explored the development of a new facile strategy to achieve amphiphilic zwitterionic coatings from a commercially-available polymer. The starting polymer contains both nonreactive hydrophobic and alcohol groups. The alcohol groups allow for easy functionalization to form cyclic phosphotriester units that can then be converted to phosphorylcholine units. The wettabilities and surface properties of the amphiphilic zwitterionic polymeric networks could be controlled by varying the extent of crosslinking in the networks, which influenced the compositional profiles. The amphiphilic zwitterionic coatings displayed superior anti-biofouling performance at resisting both protein (BSA) and whole marine organism (*Ulva* zoospore) fouling.

The thermal and mechanical properties of zwitterionic *vs.* net neutral mixed charged polymers were investigated in Chapter 5. Three charged (cationic, anionic and zwitterionic) polymers were prepared by an efficient post-functionalization method using thiol-ene click chemistry to click various charged moieties onto P(AGE-*b*-EG-*b*-AGE), which bears alkene functionalities on P(AGE) endblocks. An additional cationic/anionic polymer was prepared by mixing an equimolar ratio of cationic and anionic polymers together to form the net neutral mixed charged polymers. TGA suggested that zwitterionic polymers were more stable than blended cationic/anionic polymer at up to 350 °C and less stable as the temperature increased above 350 °C.

Higher crystallinity was observed in the blended cationic/anionic polymer than in the zwitteronic polymer as indicated by the measured T_c. Electrostatic interactions of polymers with zwitterionic side chains were found to be weaker than the electrostatic interactions of equimolar blends of cationic and anionic polymers at temperatures above -27 °C as indicated by the storage modulus curves measured from DMTA.

This dissertation has contributed to the understanding of the surface properties, stabilities and antifouling properties of various amphiphilic crosslinked systems to help with the further advancement of amphiphilic anti-fouling coatings. The ability to test for the stabilities of the HBFP-PEG-PDMS terpolymer networks has allowed for increased wt% of linear polymers or even small molecules to be incorporated into the formulation while maintaining a stable network. Furthermore, the stabilities of the HBFP-PEG-PDMS terpolymer networks in seawater overtime can be studied to provide insight on the longevity of the coatings. Although the Soxhlet extraction experiment does not confirm that crosslinking of the HBFP with PEG and PDMS has in fact taken place, the experiment still suggests that the polymers are either crosslinked or interacting strongly, forming a stable network. Soxhlet extraction experiments can also be performed on coatings that are prepared without the use of DIPEA, where crosslinking can occur. This experiment, however, will not help determine the extent of crosslinking within the network. The extent of crosslinking may be determined by XPS as the binding energy of primary amine groups of the linear polymers when not crosslinked would differ from the binding energy of secondary amine groups formed when the linear polymers are crosslinked.

The use of thiol-ene click chemistry to form UV-cured crosslink networks has eliminated the use of elevated temperatures for curing. However, shining UV light to cure the networks may not be necessarily feasible on ship hulls. Other chemistries that do not require elevated temperatures or UV light should be explored to form amphiphilic crosslinked networks. Ternary crosslinked networks generated from various amounts of silsesquioxanes, amphiphilic small molecules and zwitterionic small molecules *via* thiol-ene click chemistry were shown to not display improved anti-fouling properties. There was no significant change in the anti-fouling properties of the whole series of ternary systems. The use of small molecules for crosslinking and coupling does not provide the method to change the chemical heterogeneities drastically. The small molecules may need to be replaced by polymers for the polymers to make a significant contribution to the physical and chemical properties of the ternary networks.

The amphiphilic zwitterionic coatings containing phosphorylcholine groups demonstrated that these polymers could be generated from a simple two steps modification. However, each step does not reach a 100% conversion. Any unreacted units or side product generated during the two steps could lead to unwanted properties in the coating. Therefore, there is a need to optimize the conditions for the two steps modification before introducing the amphiphilic zwitterionic coatings into the marine environment. Moreover, silanizing a ship hull may not be practical to help attach the coating on the ship. The use of the epoxy undercoat to attach the coating on a substrate or other methods may need to be explored.

In closing, biofouling is clearly a complex problem with much chemistry, physics and biology remaining to be understood. Fouling in the marine environment poses an increasing challenge due to the difference in water temperament and vast variety of species around the world. This work contributes to the platform in the current advancement of anti-fouling coatings by investigating new methodologies in the design and characterization of amphiphilic anti-fouling networks.

REFERENCES

(1) Liu, L.; Li, W.; Liu, Q. Recent Development of Antifouling Polymers: Structure, evaluation, and biomedical applications in nano/micro-structures. *Wiley Interdiscip. Rev. Nanomed. Nanobiotechnol.* **2014**, *6*, 599-614.

(2) Zhang, H.; Jackson, J. K.; Bian, C.; Burt, H. M.; Chiao, M. Enzyme-modified Hydrogel Coatings with Self-cleaning Abilities for Low Fouling PDMS Devices. *Adv. Mater. Interfaces* **2015**, *2*, [Online early access]. 10.1002/admi.201500154.201502007.201500104.201500114. Published Online: July 201500151, 201502015.

(3) Zhang, Z.; Chao, T.; Chen, S.; Jiang, S. Superlow Fouling Sulfobetaine and Carboxybetaine Polymers on Glass Slides. *Langmuir* **2006**, *22*, 10072-10077.

(4) Chen, S.; Zheng, J.; Li, L.; Jiang, S. Strong Resistance of Phosphorylcholine Self-assembled Monolayers to Protein Adsorption: Insights into nonfouling properties of zwitterionic materials. *J. Am. Chem. Soc.* **2005**, *127*, 14473-14478.

(5) Leng, C.; Buss, H. G.; Segalman, R. A.; Chen, Z. Surface Structure and Hydration of Sequence-Specific Amphiphilic Polypeptoids for Antifouling/fouling Release Applications. *Langmuir* **2015**, *31*, 9306-9311.

(6) Fujii, T. PDMS-based Microfluidic Devices for Biomedical Applications. *Microelectron. Eng.* **2002**, *61-62*, 907-914.

(7) Lee, K. K.; Bhushan, B.; Hansford, D. Nanotribological Characterization of Fluoropolymer Thin Films for Biomedical Micro/nanoelectromechanical System Applications. *J. Vac. Sci. Technol., A* **2005**, *23*, 804-810.

(8) Wentrup-Byrne, E.; Grøndahl, L.; Suzuki, S. Methacryloxyethyl Phosphate-grafted Expanded Polytetrafluoroethylene Membranes for Biomedical Applications. *Polym. Int.* **2005**, *54*, 1581-1588.

(9) Pieper, R. J.; Ekin, A.; Webster, D. C.; Cassé, F.; Callow, J. A.; Callow, M. E. Combinatorial Approach to Study the Effect of Acrylic Polyol Composition on the Properties of Crosslinked Siloxane-polyurethane Fouling-release Coatings. *J. Coat. Technol. Res.* **2007**, *4*, 453-461.

(10) Schimidt, D. L.; Coburn, C. E.; DeKoven, B. M.; Potter, G. E.; Meyers, G. F.; Fischer, D. A. Water-based Non-stick Hydrophobic Coatings. *Nature*, *368*, 39-41.

(11) Schmidt, D. L.; DeKoven, B. M.; Coburn, C. E.; Potter, G. E.; Meyers, G. F.; Fischer, D. A. Characterization of a New Family of Nonwettable, Nonstick Surfaces. *Langmuir* **1996**, *12*, 518-529.

(12) Yarbrough, J. C.; Rolland, J. P.; DeSimone, J. M.; Callow, M. E.; Finlay, J. A.; Callow, J. A. Contact Angle Analysis, Surface Dynamics, and Biofouling Characteristics of Cross-linkable, Random Perfluoropolyether-based Graft Terpolymers. *Macromolecules* **2006**, *39*, 2521-2528.

(13) Andruzzi, L.; Chiellini, E.; Galli, G.; Li, X.; Kang, S. H.; Ober, C. K. Engineering Low Surface Energy Polymers Through Molecular Design: Synthetic routes to fluorinated polystyrene-based block copolymers. *J. Mater. Chem.* **2002**, *12*, 1684-1692.

(14) Krishnan, S.; Wang, N.; Ober, C. K.; Finlay, J. A.; Callow, M. E.; Callow, J. A.; Hexemer, A.; Sohn, K. E.; Kramer, E. J.; Fischer, D. A. Comparison of the Fouling Release Properties of Hydrophobic Fluorinated and Hydrophilic PEGylated Block Copolymer Surfaces: Attachment strength of the diatom Navicula and the green alga Ulva. *Biomacromolecules* **2006**, *7*, 1449-1462.

(15) Ma, H.; Hyun, J.; Stiller, P.; Chilkoti, A. "Non-fouling" Oligo(ethylene glycol)-functionalized Polymer Brushes Synthesized by Surface-initiated Atom Transfer Radical Polymerization. *Adv. Mater.* **2004**, *16*, 338-341.

(16) Gasteier, P.; Reska, A.; Schulte, P.; Salber, J.; Offenhäusser, A.; Moeller, M.; Groll, J. Surface Grafting of PEO-based Star-shaped Molecules for Bioanalytical and Biomedical Applications. *Macromol. Biosci.* **2007**, *7*, 1010-1023.

(17) Prime, K. L.; Whitesides, G. M. Adsorption of Proteins onto Surfaces Containing End-attached Oligo(ethylene oxide): A model system using self-assembled monolayers. *J. Am. Chem. Soc.* **1993**, *115*, 10714-10721.

(18) Heuberger, M.; Drobek, T.; Vörös, J. About the Role of Water in Surface-grafted Poly(ethylene glycol) Layers. *Langmuir* **2004**, *20*, 9445-9448.

(19) Ishihara, K.; Nomura, H.; Mihara, T.; Kurita, K.; Iwasaki, Y.; Nakabayashi, N. Why Do Phospholipid Polymers Reduce Protein Adsorption? *J. Biomed. Mater. Res.* **1998**, *39*, 323-330.

(20) Ladd, J.; Zhang, Z.; Chen, S.; Hower, J. C.; Jiang, S. Zwitterionic Polymers Exhibiting High Resistance to Nonspecific Protein Adsorption from Human Serum and Plasma. *Biomacromolecules* **2008**, *9*, 1357-1361.

(21) Banerjee, I.; Pangule, R. C.; Kane, R. S. Antifouling Coatings: Recent developments in the design of surfaces that prevent fouling by proteins, bacteria, and marine organisms. *Adv. Mater.* **2011**, *23*, 690-718.

(22) Schultz, M. P.; Bendick, J. A.; Holm, E. R.; Hertel, W. M. Economic Impact of Biofouling on a Naval Surface Ship. *Biofouling* **2010**, *27*, 87-98.

(23) Schumacher, J. F.; Carman, M. L.; Estes, T. G.; Feinberg, A. W.; Wilson, L. H.; Callow, M. E.; Callow, J. A.; Finlay, J. A.; Brennan, A. B. Engineered Antifouling Microtopographies – Effect of feature size, geometry, and roughness on settlement of zoospores of the green alga Ulva. *Biofouling* **2007**, *23*, 55-62.

(24) Stein, J.; Truby, K.; Wood, C. D.; Takemori, M.; Vallance, M.; Swain, G.; Kavanagh, C.; Kovach, B.; Schultz, M.; Wiebe, D.; Holm, E.; Montemarano, J.; Wendt, D.; Smith, C.; Meyer, A. Structure-property Relationships of Silicone Biofouling-release Coatings: Effect of silicone network architecture on pseudobarnacle attachment strengths. *Biofouling* **2003**, *19*, 87-94.

(25) Hayward, J. A.; Chapman, D. Biomembrane Surfaces as Models for Polymer Design: the potential for haemocompatibility. *Biomaterials* **1984**, *5*, 135-142.

(26) Li, G.; Xue, H.; Gao, C.; Zhang, F.; Jiang, S. Nonfouling Polyampholytes from an Ion-pair Comonomer with Biomimetic Adhesive Groups. *Macromolecules* **2009**, *43*, 14-16.

(27) Li, J.; Chen, Y.; Wang, Z.; Ding, M.; Tan, H.; Fu, Q.; Jiang, X. Synthesis and Self-assembly of an Amino-functionalized Hybrid Hydrocarbon/fluorocarbon Double-chain Phospholipid. *Langmuir* **2011**, *27*, 10859-10866.

(28) Holmlin, R. E.; Chen, X.; Chapman, R. G.; Takayama, S.; Whitesides, G. M. Zwitterionic SAMs that Resist Nonspecific Adsorption of Protein from Aqueous Buffer. *Langmuir* **2001**, *17*, 2841-2850.

(29) He, Y.; Hower, J.; Chen, S.; Bernards, M. T.; Chang, Y.; Jiang, S. Molecular Simulation Studies of Protein Interactions with Zwitterionic Phosphorylcholine Self-assembled Monolayers in the Presence of Water. *Langmuir* **2008**, *24*, 10358-10364.

(30) Wahl, M. Marine Epibiosis. I. Fouling and Antifouling: some basic aspects. *Mar. Ecol. Prog. Ser.* **1989**, 175-189.

(31) S., P. E.; J., B. A. Biofouling and Climate Change. *Biofouling* **2010**, 333-347.

(32) Turner, A. Marine Pollution from Antifouling Paint Particles. *Mar. Pollut. Bull.* **2010**, *60*, 159-171.

(33) Otani, M.; Oumi, T.; Uwai, S.; Hanyuda, T.; Prabowo, R. E.; Yamaguchi, T.; Kawai, H. Occurrence and Diversity of Barnacles on International Ships Visiting Osaka Bay, Japan, and the Risk of Their Introduction. *Biofouling* **2007**, *23*, 277-286.

(34) Yamaguchi, T.; Prabowo, R. E.; Ohshiro, Y.; Shimono, T.; Jones, D.; Kawai, H.; Otani, M.; Oshino, A.; Inagawa, S.; Akaya, T.; Tamura, I. The Introduction to Japan of the Titan Barnacle, Megabalanus Coccopoma (Darwin, 1854) (Cirripedia: Balanomorpha) and the Role of Shipping in its Translocation. *Biofouling* **2009**, *25*, 325-333.

(35) Piola, R. F.; Johnston, E. L. The Potential for Translocation of Marine Species via Small-scale Disruptions to Antifouling Surfaces. *Biofouling* **2008**, *24*, 145-155.

(36) Byers, J. E. Impact of Non-indigenous Species on Natives Enhanced by Anthropogenic Alteration of Selection Regimes. *Oikos* **2002**, *97*, 449-458.

(37) Howell, D.; Behrends, B. A Review of Surface Roughness in Antifouling Coatings Illustrating the Importance of Cutoff Length. *Biofouling* **2006**, *22*, 401-410.

(38) Evans, L. V.; Clarkson, N. Antifouling Strategies in the Marine Environment. *J. Appl. Bacteriol.* **1993**, *74*, 119S-124S.

(39) Yebra, D. M.; Kiil, S.; Dam-Johansen, K. Antifouling Technology—Past, present and future steps towards efficient and environmentally friendly antifouling coatings. *Prog. Org. Coat.* **2004**, *50*, 75-104.

(40) Thomas, K.; Raymond, K.; Chadwick, J.; Waldock, M. The Effects of Short-term Changes in Environmental Parameters on the Release of Biocides from Antifouling Coatings: Cuprous oxide and tributyltin. *Appl. Organomet. Chem.* **1999**, *13*, 453-460.

(41) Omae, I. Organotin Antifouling Paints and Their Alternatives. *Appl. Organomet. Chem.* **2003**, *17*, 81-105.

(42) Callow, M. E.; Callow, J. A. Marine Biofouling: A sticky problem. *Biologist* **2002**, 1-5.

(43) Schlip, S.; Kueller, A.; Rosenhahn, A.; Grunze, M.; Pettitt, M. E.; Callow, M. E.; Callow, J. A. Settlement of Adhesion of Algal Cells to Hexa(ethylene glycol)-containing Self-assembled Monolayers with Systematically Charge Wetting Properties. *Biointerphases* **2007**, *2*, 143-150.

(44) Imbesi, P. M.; Finlay, J. A.; Aldred, N.; Eller, M. J.; Felder, S. E.; Pollack, K. A.; Lonnecker, A. T.; Raymond, J. E.; Mackay, M. E.; Schweikert, E. A.; Clare, A. S.; Callow, J. A.; Callow, M. E.; Wooley, K. L. Targeted Surface Nanocomplexity: Two-dimensional control over the composition, physical properties and anti-biofouling performance of hyperbranched fluoropolymer-poly(ethylene glycol) amphiphilic crosslinked networks. *Polym. Chem.* **2012**, *3*, 3121-3131.

(45) Martinelli, E.; Suffredini, M.; Galli, G.; Glisenti, A.; Pettitt, M. E.; Callow, M. E.; Callow, J. A.; Williams, D.; Lyall, G. Amphiphilic Block Copolymer/poly(dimethylsiloxane) (PDMS) Blends and Nanocomposites for Improved Fouling-release. *Biofouling* **2011**, *27*, 529-541.

(46) Gudipati, C. S.; Finlay, J. A.; Callow, J. A.; Callow, M. E.; Wooley, K. L. The Antifouling and Fouling-release Perfomance of Hyperbranched Fluoropolymer (HBFP)−poly(ethylene glycol) (PEG) Composite Coatings Evaluated by Adsorption of Biomacromolecules and the Green Fouling Alga Ulva. *Langmuir* **2005**, *21*, 3044-3053.

(47) Powell, K. T.; Cheng, C.; Wooley, K. L. Complex Amphiphilic Hyperbranched Fluoropolymers by Atom Transfer Radical Self-Condensing Vinyl (Co)polymerization. *Macromolecules* **2007**, *40*, 4509-4515.

(48) Gan, D.; Mueller, A.; Wooley, K. L. Amphiphilic and Hydrophobic Surface Patterns Generated from Hyperbranched Fluoropolymer/linear Polymer Networks: Minimally adhesive coatings via the crosslinking of hyperbranched fluoropolymers. *J. Polym. Sci., Part A: Polym. Chem.* **2003**, *41*, 3531-3540.

(49) Pollack, K. A. Multiply Complex, Non-toxic, Anti-fouling Surfaces Designed for Marine and Biomedical Applications. Ph.D. Dissertation, Texas A&M University, 2015.

(50) Pollack, K. A.; Imbesi, P. M.; Raymond, J. E.; Wooley, K. L. Hyperbranched Fluoropolymer-polydimethylsiloxane-poly(ethylene glycol) Cross-Linked Terpolymer Networks Designed for Marine and Biomedical Applications: heterogeneous nontoxic Antibiofouling surfaces. *ACS Appl. Mater. Interfaces* **2014**, *6*, 19265-19274.

(51) Chambers, L. D.; Stokes, K. R.; Walsh, F. C.; Wood, R. J. K. Modern Approaches to Marine Antifouling Coatings. *Surf. Coat. Technol.* **2006**, *201*, 3642-3652.

(52) Minchin, D.; Gollasch, S. Fouling and Ships' Hulls: How changing circumstances and spawning events may result in the spread of exotic species. *Biofouling* **2003**, *19*, 111-122.

(53) Rajagopal, S.; van der Velde, G.; van der Gaag, M.; Jenner, H. A. Factors Influencing the Upper Temperature Tolerances of Three Mussel Species in a Brackish Water Canal: Size, season and laboratory protocols. *Biofouling* **2005**, *21*, 87-97.

(54) Occhipinti-Ambrogi, A. Global Change and Marine Communities: alien species and climate change. *Marine Pollution Bulletin* **2007**, *55*, 342-352.

(55) Verween, A.; Vincx, M.; Degraer, S. The Effect of Temperature and Salinity on the Survival of Mytilopsis Leucophaeata Larvae (Mollusca, Bivalvia): The search for environmental limits. *Journal of Experimental Marine Biology and Ecology* **2007**, *348*, 111-120.

(56) Stachowicz, J. J. Mutualism, Facilitation, and the Structure of Ecological Communities: Positive interactions play a critical, but underappreciated, role in ecological communities by reducing physical or biotic stresses in existing habitats and by creating new habitats on which many species depend. *BioScience* **2001**, *51*, 235-246.

(57) Bartels, J. W.; Cheng, C.; Powell, K. T.; Xu, J.; Wooley, K. L. Hyperbranched Fluoropolymers and their Hybridization into Complex Amphiphilic Crosslinked Copolymer Networks. *Macromol. Chem. Phys.* **2007**, *208*, 1676-1687.

(58) Gudipati, C. S.; Greenlief, C. M.; Johnson, J. A.; Prayongpan, P.; Wooley, K. L. Hyperbranched Fluoropolymer and Linear Poly(ethylene glycol) Based Amphiphilic Crosslinked Networks as Efficient Antifouling Coatings: An insight into the surface compositions, topographies, and morphologies. *J. Polym. Sci., Part A: Polym. Chem.* **2004**, *42*, 6193-6208.

(59) Imbesi, P. M.; Gohad, N. V.; Eller, M. J.; Orihuela, B.; Rittschof, D.; Schweikert, E. A.; Mount, A. S.; Wooley, K. L. Noradrenaline-functionalized Hyperbranched Fluoropolymer–poly(ethylene glycol) Cross-linked Networks As Dual-mode, Anti-biofouling Coatings. *ACS Nano* **2012**, *6*, 1503-1512.

(60) Powell, K. T.; Cheng, C.; Wooley, K. L.; Singh, A.; Urban, M. W. Complex Amphiphilic Networks Derived from Diamine-terminated Poly(ethylene glycol) and Benzylic Chloride-functionalized Hyperbranched Fluoropolymers. *J. Polym. Sci., Part A: Polym. Chem.* **2006**, *44*, 4782-4794.

(61) Chang, S. S.; Maurey, J. R. Solubilities of BHT in Various Solvents. *J. Chem. Eng. Data* **1985**, *30*, 384-387.

(62) Thomas, K. V. The Environmental Fate and Behaviour of Antifouling Paint Booster Biocides: A review. *Biofouling* **2001**, *17*, 73-86.

(63) Thomas, K. V.; Blake, S. J.; Waldock, M. J. Antifouling Paint Booster Biocide Contamination in UK Marine Sediments. *Mar. Pollut. Bull.* **2000**, *40*, 739-745.

(64) Konstantinou, I. K.; Albanis, T. A. Worldwide Occurrence and Effects of Antifouling Paint Booster Biocides in the Aquatic Environment: A review. *Environment International* **2004**, *30*, 235-248.

(65) Ytreberg, E.; Karlsson, J.; Eklund, B. Comparison of Toxicity and Release Rates of Cu and Zn From Anti-fouling Paints Leached in Natural and Artificial Brackish Seawater. *Sci. Total Environ.* **2010**, *408*, 2459-2466.

(66) Lamoree, M. H.; Swart, C. P.; van der Horst, A.; van Hattum, B. Determination of Diuron and the Antifouling Paint Biocide Irgarol 1051 in Dutch Marinas and Coastal Waters. *J. Chromatogr. A* **2002**, *970*, 183-190.

(67) Tesler, A. B.; Kim, P.; Kolle, S.; Howell, C.; Ahanotu, O.; Aizenberg, J. Extremely Durable Biofouling-resistant Metallic Surfaces Based on Electrodeposited Nanoporous Tungstite Films on Steel. *Nat Commun* **2015**, *6*.

(68) Sundaram, H. S.; Cho, Y.; Dimitriou, M. D.; Finlay, J. A.; Cone, G.; Williams, S.; Handlin, D.; Gatto, J.; Callow, M. E.; Callow, J. A.; Kramer, E. J.; Ober, C. K. Fluorinated Amphiphilic Polymers and Their Blends for Fouling-release Applications: The benefits of a triblock copolymer surface. *ACS Appl. Mater. Interfaces* **2011**, *3*, 3366-3374.

(69) Wang, Y.; Pitet, L. M.; Finlay, J. A.; Brewer, L. H.; Cone, G.; Betts, D. E.; Callow, M. E.; Callow, J. A.; Wendt, D. E.; Hillmyer, M. A.; DeSimonea, J. M. Investigation of the Role of Hydrophilic Chain Length in Amphiphilic Perfluoropolyether/poly(ethylene glycol) Networks: Towards high-performance antifouling coatings. *Biofouling* **2011**, *27*, 1139-1150.

(70) Feng, S.; Wang, Q.; Gao, Y.; Huang, Y.; Qing, F.-L. Synthesis and Characterization of a Novel Amphiphilic Copolymer Capable as Anti-biofouling Coating Material. *J. Appl. Polym. Sci.* **2009**, *114*, 2071-2078.

(71) Brady, R. F.; Singer, I. L. Mechanical Factors Favoring Release from Fouling Release Coatings. *Biofouling* **2000**, *15*, 73-81.

(72) Genzer, J.; Efimenko, K. Recent Developments in Superhydrophobic Surfaces and their Relevance to Marine Fouling: A review. *Biofouling* **2006**, *22*, 339-360.

(73) Scardino, A. J.; Zhang, H.; Cookson, D. J.; Lamb, R. N.; Nys, R. d. The Role of Nano-roughness in Antifouling. *Biofouling* **2009**, *25*, 757-767.

(74) Chen, Y.; Liu, D.; Deng, Q.; He, X.; Wang, X. Atom Transfer Radical Polymerization Directly from Poly(vinylidene fluoride): Surface and antifouling properties. *J. Polym. Sci., Part A: Polym. Chem.* **2006**, *44*, 3434-3443.

(75) Brady Jr, R. F. A Fracture Mechanical Analysis of Fouling Release from Nontoxic Antifouling Coatings. *Prog. Org. Coat.* **2001**, *43*, 188-192.

(76) Dobretsov, S.; Thomason, J. C. The Development of Marine Biofilms on Two Commercial Non-biocidal Coatings: A comparison between silicone and fluoropolymer technologies. *Biofouling* **2011**, *27*, 869-880.

(77) Sun, Q.; Su, Y.; Ma, X.; Wang, Y.; Jiang, Z. Improved Antifouling Property of Zwitterionic Ultrafiltration Membrane Composed of Acrylonitrile and Sulfobetaine Copolymer. *J. Membr. Sci.* **2006**, *285*, 299-305.

(78) Calabrese, D.; Wenning, B.; Ober, C.: Block Copolymers as Antifouling and Fouling Resistant Coatings. In *Anionic Polymerization*; Hadjichristidis, N., Hirao, A., Eds.; Springer Japan, 2015; pp 881-924.

(79) Brown, G. O.; Bergquist, C.; Ferm, P.; Wooley, K. L. Unusual, Promoted Release of Guests from Amphiphilic Cross-linked Polymer Networks. *J. Am. Chem. Soc.* **2005**, *127*, 11238-11239.

(80) Dondoni, A. The Emergence of Thiol–ene Coupling as a Click Process for Materials and Bioorganic Chemistry. *Angew. Chem. Int. Ed.* **2008**, *47*, 8995-8997.

(81) Hoyle, C. E.; Bowman, C. N. Thiol–ene Click Chemistry. *Angew. Chem. Int. Ed.* **2010**, *49*, 1540-1573.

(82) Killops, K. L.; Campos, L. M.; Hawker, C. J. Robust, Efficient, and Orthogonal Synthesis of Dendrimers via Thiol-ene "Click" Chemistry. *J. Am. Chem. Soc.* **2008**, *130*, 5062-5064.

(83) Lowe, A. B. Thiol-ene "Click" Reactions and Recent Applications in Polymer and Materials Synthesis. *Polym. chem.* **2010**, *1*, 17-36.

(84) Kade, M. J.; Burke, D. J.; Hawker, C. J. The Power of Thiol-ene Chemistry. *J. Polym. Sci., Part A: Polym. Chem.* **2010**, *48*, 743-750.

(85) Li, J.-H.; Li, M.-Z.; Miao, J.; Wang, J.-B.; Shao, X.-S.; Zhang, Q.-Q. Improved Surface Property of PVDF Membrane with Amphiphilic Zwitterionic Copolymer as Membrane Additive. *Appl. Surf. Sci.* **2012**, *258*, 6398-6405.

(86) Seetho, K.; Zhang, S.; Pollack, K. A.; Zou, J.; Raymond, J. E.; Martinez, E.; Wooley, K. L. Facile Synthesis of a Phosphorylcholine-based Zwitterionic Amphiphilic Copolymer for Anti-biofouling Coatings. *ACS Macro Lett.* **2015**, *4*, 505-510.

(87) Mieszkin, S.; Martin-Tanchereau, P.; Callow, M. E.; Callow, J. A. Effect of Bacterial Biofilms Formed on Fouling-release Coatings from Natural Seawater and Cobetia Marina, on the Adhesion of Two Marine Algae. *Biofouling* **2012**, *28*, 953-968.

(88) Callow, M. E.; Callow, J. A.; Pickett-Heaps, J. D.; Wetherbee, R. Primary Adhesion of Enteromorpha (Chlorophyta, Ulvales) Propadules: Quantitative Settlement Studies and Video Microscopy. *J. Physcol* **1997**, *33*, 938-947.

(89) Patel, P.; Callow, M. E.; Joint, I.; Callow, J. A. Specificity in the Settlement – Modifying response of bacterial biofilms towards zoospores of the marine alga Enteromorpha. *Environ. Microbiol.* **2003**, *5*, 338-349.

(90) Xiao, L.; Li, J.; Mieszkin, S.; Di Fino, A.; Clare, A. S.; Callow, M. E.; Callow, J. A.; Grunze, M.; Rosenhahn, A.; Levkin, P. A. Slippery Liquid-infused Porous Surfaces Showing Marine Antibiofouling Properties. *ACS Appl. Mater. Interfaces* **2013**, *5*, 10074-10080.

(91) Serrano, Â.; Sterner, O.; Mieszkin, S.; Zürcher, S.; Tosatti, S.; Callow, M. E.; Callow, J. A.; Spencer, N. D. Nonfouling Response of Hydrophilic Uncharged Polymers. *Adv. Funct. Mater.* **2013**, *23*, 5706-5718.

(92) Detty, M. R.; Ciriminna, R.; Bright, F. V.; Pagliaro, M. Environmentally Benign Sol–gel Antifouling and Foul-Releasing Coatings. *Acc. Chem. Res.* **2014**, *47*, 678-687.

(93) Maguire, R. J. Environmental Aspects of Tributyltin. *Appl. Organomet. Chem.* **1987**, *1*, 475-498.

(94) Andruzzi, L.; Hexemer, A.; Li, X.; Ober, C. K.; Kramer, E. J.; Galli, G.; Chiellini, E.; Fischer, D. A. Control of Surface Properties Using Fluorinated Polymer Brushes Produced by Surface-initiated Controlled Radical Polymerization. *Langmuir* **2004**, *20*, 10498-10506.

(95) Wang, Y.; Betts, D. E.; Finlay, J. A.; Brewer, L.; Callow, M. E.; Callow, J. A.; Wendt, D. E.; DeSimone, J. M. Photocurable Amphiphilic Perfluoropolyether/poly(ethylene glycol) Networks for Fouling-release Coatings. *Macromolecules* **2011**, *44*, 878-885.

(96) Park, D.; Weinman, C. J.; Finlay, J. A.; Fletcher, B. R.; Paik, M. Y.; Sundaram, H. S.; Dimitriou, M. D.; Sohn, K. E.; Callow, M. E.; Callow, J. A.; Handlin, D. L.; Willis, C. L.; Fischer, D. A.; Kramer, E. J.; Ober, C. K. Amphiphilic Surface Active Triblock Copolymers with Mixed Hydrophobic and Hydrophilic Side Chains for Tuned Marine Fouling-release Properties. *Langmuir* **2010**, *26*, 9772-9781.

(97) van Zoelen, W.; Buss, H. G.; Ellebracht, N. C.; Lynd, N. A.; Fischer, D. A.; Finlay, J.; Hill, S.; Callow, M. E.; Callow, J. A.; Kramer, E. J.; Zuckermann, R. N.; Segalman, R. A. Sequence of Hydrophobic and Hydrophilic Residues in Amphiphilic Polymer Coatings Affects Surface Structure and Marine Antifouling/fouling Release Properties. *ACS Macro Lett.* **2014**, *3*, 364-368.

(98) Cao, Z.; Mi, L.; Mendiola, J.; Ella-Menye, J.-R.; Zhang, L.; Xue, H.; Jiang, S. Reversibly Switching the Function of a Surface between Attacking and Defending Against Bacteria. *Angew. Chem. Int. Ed.* **2012**, *51*, 2602-2605.

(99) Kyomoto, M.; Moro, T.; Yamane, S.; Watanabe, K.; Hashimoto, M.; Takatori, Y.; Tanaka, S.; Ishihara, K. Poly(2-methacryloyloxyethyl phosphorylcholine) Grafting and Vitamin E Blending for High Wear Resistance and Oxidative Stability of Orthopedic Bearings. *Biomaterials* **2014**, *35*, 6677-6686.

(100) Bodkhe, R. B.; Stafslien, S. J.; Daniels, J.; Cilz, N.; Muelhberg, A. J.; Thompson, S. E. M.; Callow, M. E.; Callow, J. A.; Webster, D. C. Zwitterionic Siloxane-polyurethane Fouling-release Coatings. *Prog. Org. Coat.* **2014**, 369-380.

(101) Epstein, A. K.; Wong, T.-S.; Belisle, R. A.; Boggs, E. M.; Aizenberg, J. Liquid-infused Structured Surfaces with Exceptional Anti-biofouling Performance. *Proc. Natl. Acad. Sci.* **2012**, *109*, 13182-13187.

(102) West, S. L.; Salvage, J. P.; Lobb, E. J.; Armes, S. P.; Billingham, N. C.; Lewis, A. L.; Hanlon, G. W.; Lloyd, A. W. The Biocompatibility of Crosslinkable Copolymer Coatings Containing Sulfobetaines and Phosphobetaines. *Biomaterials* **2004**, *25*, 1195-1204.

(103) Iwasaki, Y.; Ishihara, K. Phosphorylcholine-containing Polymers for Biomedical Applications. *Anal Bioanal Chem* **2005**, *381*, 534-546.

(104) Ishihara, K.; Ziats, N. P.; Tierney, B. P.; Nakabayashi, N.; Anderson, J. M. Protein Adsorption from Human Plasma is Reduced on Phospholipid Polymers. *J. Biomed. Mater. Res.* **1991**, *25*, 1397-1407.

(105) Ishihara, K.; Ueda, T.; Nakabayashi, N. Preparation of Phospholipid Polylners and Their Properties as Polymer Hydrogel Membranes. *Polym. J.* **1990**, *22*, 355-360.

(106) Kiritoshi, Y.; Ishihara, K. Synthesis of Hydrophilic Cross-linker Having Phosphorylcholine-like Linkage for Improvement of Hydrogel Properties. *Polymer* **2004**, *45*, 7499-7504.

(107) Lee, H.; Alcaraz, M. L.; Rubner, M. F.; Cohen, R. E. Zwitter-Wettability and Antifogging Coatings with Frost-Resisting Capabilities. *ACS Nano* **2013**, *7*, 2172-2185.

(108) Thouvenin, M.; Langlois, V.; Briandet, R.; Langlois, J. Y.; Guerin, P. H.; Peron, J. J.; Haras, D.; Vallee-Rehel, K. Study of Erodable Paint Properties Involved in Antifouling Activity. *Biofouling* **2003**, *19*, 177-186.

(109) Kerr, A.; Cowling, M. J. The Effects of Surface Topography on the Accumulation of Biofouling. *Philos. Mag.* **2003**, *83*, 2779-2795.

(110) Hayden, H. S.; Blomster, J.; Maggs, C. A.; Silva, P. C.; Stanhope, M. J.; Waaland, J. R. Linnaeus was Right All Along: Ulva and Enteromorpha are not distinct genera. *Eur. J. Phycol.* **2003**, *38*, 277-294.

(111) Zhang, S.; Zou, J.; Zhang, F.; Elsabahy, M.; Felder, S. E.; Zhu, J.; Pochan, D. J.; Wooley, K. L. Rapid and Versatile Construction of Diverse and Functional Nanostructures Derived from a Polyphosphoester-based Biomimetic Block Copolymer System. *J. Am. Chem. Soc.* **2012**, *134*, 18467-18474.

(112) Zou, J.; Zhang, F.; Zhang, S.; Pollack, S. F.; Elsabahy, M.; Fan, J.; Wooley, K. L. Poly(ethylene oxide)-block-polyphosphoester-graft-paclitaxel Conjugates with Acid-labile linkages as a pH-sensitive and Functional Nanoscopic Platform for Paclitaxel Delivery. *Adv. Healthcare Mater.* **2014**, *3*, 441-448.

(113) Xiong, M.-H.; Bao, Y.; Yang, X.-Z.; Wang, Y.-C.; Sun, B.; Wang, J. Lipase-sensitive Polymeric Triple-layered Nanogel for "On-demand" Drug Delivery. *J. Am. Chem. Soc.* **2012**, *134*, 4355-4362.

(114) Zhang, L.; Cao, Z.; Bai, T.; Carr, L.; Ella-Menye, J.-R.; Irvin, C.; Ratner, B. D.; Jiang, S. Zwitterionic Hydrogels Implanted in Mice Resist the Foreign-body Reaction. *Nat Biotech* **2013**, *31*, 553-556.

(115) Hasan, J.; Crawford, R. J.; Ivanova, E. P. Antibacterial Surfaces: The quest for a new generation of biomaterials. *Trends Biotechnol.* **2013**, *31*, 295-304.

(116) Ma, W.; Rajabzadeh, S.; Matsuyama, H. Preparation of Antifouling Poly(vinylidene fluoride) Membranes via Different Coating Methods Using a Zwitterionic Copolymer. *appl. Surf. Sci.* **2015**, *357*, 1388-1395.

(117) Shafi, H. Z.; Matin, A.; Khan, Z.; Khalil, A.; Gleason, K. K. Surface Modification of Reverse Osmosis Membranes with Zwitterionic Coatings: A potential strategy for control of biofouling. *Surf. Coat. Technol.* **2015**, *279*, 171-179.

(118) Hibbs, M. R.; Hernandez-Sanchez, B. A.; Daniels, J.; Stafslien, S. J. Polysulfone and Polyacrylate-based Zwitterionic Coatings for the Prevention and Easy Removal of Marine Biofouling. *Biofouling* **2015**, *31*, 613-624.

(119) Tegoulia, V. A.; Rao, W.; Kalambur, A. T.; Rabolt, J. F.; Cooper, S. L. Surface Properties, Fibrinogen Adsorption, and Cellular Interactions of a Novel Phosphorylcholine-containing Self-assembled Monolayer on Gold. *Langmuir* **2001**, *17*, 4396-4404.

(120) Lowe, A. B.; McCormick, C. L. Synthesis and Solution Properties of Zwitterionic Polymers. *Chem. Rev.* **2002**, *102*, 4177-4190.

(121) Xuan, F.; Liu, J. Preparation, Characterization and Application of Zwitterionic Polymers and Membranes: Current developments and perspective. *Polym. Int.* **2009**, *58*, 1350-1361.

(122) Yang, J.; Chen, H.; Xiao, S.; Shen, M.; Chen, F.; Fan, P.; Zhong, M.; Zheng, J. Salt-responsive Zwitterionic Polymer Brushes with Tunable Friction and Antifouling Properties. *Langmuir* **2015**, *31*, 9125-9133.

(123) Chang, C.-C.; Letteri, R.; Hayward, R. C.; Emrick, T. Functional Sulfobetaine Polymers: Synthesis and salt-responsive stabilization of oil-in-water droplets. *Macromolecules* **2015**.

(124) Kathmann, E. E. L.; White, L. A.; McCormick, C. L. Water-Soluble Polymers. 73. Electrolyte- and pH-Responsive Zwitterionic Copolymers of 4-[(2-Acrylamido-2-methylpropyl)- dimethylammonio]butanoate with 3-[(2-Acrylamido-2-methyl- propyl)dimethylammonio]propanesulfonate. *Macromolecules* **1997**, *30*, 5297-5304.

(125) Thomas, D. B.; Vasilieva, Y. A.; Armentrout, R. S.; McCormick, C. L. Synthesis, Characterization, and Aqueous Solution Behavior of Electrolyte- and pH-responsive Carboxybetaine-containing Cyclocopolymers†. *Macromolecules* **2003**, *36*, 9710-9715.

(126) Chang, Y.; Shu, S.-H.; Shih, Y.-J.; Chu, C.-W.; Ruaan, R.-C.; Chen, W.-Y. Hemocompatible Mixed-charge Copolymer Brushes of Pseudozwitterionic Surfaces Resistant to Nonspecific Plasma Protein Fouling. *Langmuir* **2010**, *26*, 3522-3530.

(127) Mi, L.; Bernards, M. T.; Cheng, G.; Yu, Q.; Jiang, S. pH Responsive Properties of Non-fouling Mixed-charge Polymer Brushes Based on Quaternary Amine and Carboxylic Acid Monomers. *Biomaterials* **2010**, *31*, 2919-2925.

(128) Brown, R. H.; Duncan, A. J.; Choi, J.-H.; Park, J. K.; Wu, T.; Leo, D. J.; Winey, K. I.; Moore, R. B.; Long, T. E. Effect of Ionic Liquid on Mechanical Properties and Morphology of Zwitterionic Copolymer Membranes. *Macromolecules* **2010**, *43*, 790-796.

(129) Duncan, A. J.; Leo, D. J.; Long, T. E.; Akle, B. J.; Park, J. K.; Moore, R. B. In *Tilte*2009.

(130) Rohani, M. M.; Zydney, A. L. Protein Transport Through Zwitterionic Ultrafiltration Membranes. *J. Membr. Sci.* **2012**, *397–398*, 1-8.

(131) Callow, J. A.; Callow, M. E. Trends in the Development of Environmentally Friendly Fouling-resistant Marine Coatings. *Nat. Commun.* **2011**, *2*, 244-253.

(132) Galin, M.; Chapoton, A.; Galin, J.-C. Dielectric Increments, Intercharge Distances and Conformation of Quaternary Ammonioalkylsulfonates and Alkoxydicyanoethenolates in Aqueous and TrIfluoroethanol Solutions. *J. Chem. Soc., Perkin Trans. 2* **1993**, 545-553.

(133) Wu, T.; Beyer, F. L.; Brown, R. H.; Moore, R. B.; Long, T. E. Influence of Zwitterions on Thermomechanical Properties and Morphology of Acrylic Copolymers: Implications for Electroactive Applications. *Macromolecules* **2011**, *44*, 8056-8063.

(134) Hunt, J. N.; Feldman, K. E.; Lynd, N. A.; Deek, J.; Campos, L. M.; Spruell, J. M.; Hernandez, B. M.; Kramer, E. J.; Hawker, C. J. Modular Hydrogels: Tunable, high modulus hydrogels driven by ionic coacervation. *Adv. Mater.* **2011**, *23*, 2326-2326.